

**TORQUE AND DRAG CALCULATIONS IN  
THREE-DIMENSIONAL WELLBORES**

A Dissertation

by

**RUKTAI ACE PRURAPARK**

Submitted to the Office of Graduate Studies of  
Texas A&M University  
in partial fulfillment of the requirements for the degree of

**DOCTOR OF PHILOSOPHY**

May 2009

Major Subject: Petroleum Engineering

**TORQUE AND DRAG CALCULATIONS IN  
THREE-DIMENSIONAL WELLBORES**

A Dissertation

by

**RUKTAI ACE PRURAPARK**

Submitted to the Office of Graduate Studies of  
Texas A&M University  
in partial fulfillment of the requirements for the degree of

**DOCTOR OF PHILOSOPHY**

Approved by:

Chair of Committee,	Hans Juvkam-Wold
Committee Members,	Ann Jochens
	Jerome Schubert
	Catalin Teodoriu
Head of Department,	Stephen Holditch

May 2009

Major Subject: Petroleum Engineering

**ABSTRACT**

Torque and Drag Calculations in Three-Dimensional Wellbores.

(May 2009)

Ruktai Ace Prurapark,

B.Eng., Chulalongkorn University, Bangkok, Thailand;

M.Eng., Texas A&M University

Chair of Advisory Committee: Dr. Hans C. Juvkam-Wold

Torque and drag (T&D) modeling is regarded as extremely helpful in well planning because it helps to predict and prevent drilling problems that might occur during the drilling process. Although T&D software has existed since the 1990s, some confusion still exists over the validity of the models that are used to characterize drilling operations, especially as we extend the length of modern horizontal wells.

Moreover, it seems that only minimal improvements have been made to the underlying mathematical models over the last two decades. For normal planning on extended-reach and other challenging wells, T&D modeling provides a guideline for performance. Better modeling is especially important in complex three-dimensional wellbores.

To optimize well design, T&D modeling needs to be incorporated into the planning of each well. The following factors should be evaluated:

- Optimizing the well planning design
- Adapting casing or tubular designs
- Changing annulus fluids; for example, oil-based mud lubricates are better than water-based mud
- Adjusting operating drilling processes such as reducing sliding distances or rotating to the bottom

This project develops software that will give more accurate 3D T&D calculations.

Moreover, this research is also widely beneficial in handling wellbore tortuosity which is explained in detail in the text. The new software will optimize the wellbore path and assist significantly in torque and drag calculation in well design.

## ACKNOWLEDGMENTS

I would like to give my sincere gratitude to those that have helped me through my doctoral degree studies.

I especially would like to thank my mentor, Dr. Hans C. Juvkam-Wold, for his invaluable advice, guidance, and encouragement, as well as consultation in the past four years. His philosophy and career have inspired my study as well as my ideas. His encouragement has taken me this far. I would also like to give my special thanks to Dr. Jerome J. Schubert for his thoughtfulness and kindness to me. I will always remember both of them as my own family.

I would like to express my sincere appreciation to the Committee Members, Dr. Ann E. Jochens and Dr. Catalin Teodoriu, for their most useful comments and time. Thanks to all of my friends in College Station who have supported me in every way.

My deepest gratitude goes to my wonderful parents, Udomdej and Piyatida Prurapark, and my younger sister, Kwankamol Prurapark, for their everlasting love and support, and also my wonderful aunt, Nitaya Maliwan, MD., who has supported me continuously since my B.S. four years and M.S. degrees one year. I also would like to thank the rest of my relatives and friends, who have constantly given me strength throughout my difficulties.

Last but not least, my posthumous gratitude goes to chief highway engineer, Mr. Kamol Maliwan, my grandfather, who was the first person to inspire me in the engineering profession.

## TABLE OF CONTENTS

	Page
ABSTRACT .....	iii
ACKNOWLEDGMENTS.....	v
TABLE OF CONTENTS .....	vii
LIST OF FIGURES.....	xi
LIST OF TABLES .....	xvii
 CHAPTER	
I INTRODUCTION.....	1
1.1 Literature Review .....	2
1.1.1 T&D equations for three-dimensional wellbore .....	2
1.1.2 Tortuosity effects .....	3
1.1.3 Stress concentration factor.....	4
1.1.4 Buckling.....	4
1.2 Objectives and Organization .....	5
II TORQUE AND DRAG CALCULATIONS IN THREE- DIMENSIONAL WELLBORE METHODOLOGY .....	7
2.1 Introduction .....	7
2.2 Original Concept for Calculating Normal Contact Force .....	7
2.3 Soft-string Model for Three-dimensional T&D Calculation.....	11
2.4 Lowering the Pipe into the Hole .....	13
2.4.1 Lowering the pipe into the hole in the build section.....	13
2.4.2 Lowering the pipe into the hole in the hold section.....	15
2.4.3 Lowering the pipe into the hole in the drop section .....	16
2.4.4 Lowering the pipe into the hole while the wellbore turns .....	19
2.5 Pulling the Pipe out of the Hole .....	21
2.5.1 Pulling the pipe out of the hole in the build section .....	21
2.5.2 Pulling the pipe out of the hole in the hold section .....	24
2.5.3 Pulling the pipe out of the hole in the drop section .....	25
2.5.4 Pulling the pipe out of the hole while the wellbore turns .....	28
2.6 Conclusion.....	30

CHAPTER	Page
III WELL PLANNING IN THREE-DIMENSIONAL WELLBORE .....	31
3.1 Introduction .....	31
3.2 System Modeling.....	32
3.2.1 Well-planning and math modeling between surveys .....	32
3.2.1.1 Finding minimum curvature (DLS) to intersect target.....	33
3.2.1.2 Example tie-on surveys and target directions.....	36
3.2.2 Well-planning and math modeling for build type.....	38
3.2.3 Well-planning and math modeling for build and hold type.....	39
3.2.4 Well-planning and math modeling for build hold and drop type .....	39
3.2.5 Well-planning and math modeling for horizontal well design type .....	40
IV TORTUOSITY IN THREE-DIMENSIONAL WELLBORES AND THE EFFECT OF TORTUOSITIES ON TORQUE CALCULATION .....	42
4.1 Introduction .....	42
4.2 Oscillation in the Wellbore.....	42
4.3 Borehole Oscillations .....	44
4.4 Model of Borehole Oscillations .....	48
4.5 Mathematical Model for Torque Calculations .....	50
V STRESS CONCENTRATION WITHIN TOOL JOINT .....	52
5.1 Introduction .....	52
5.2 Stress Concentration.....	52
5.3 Mathematical Model for the Stress Concentration Factor.....	55
VI BUCKLING .....	59
6.1 Introduction .....	59
6.2 System Modeling for a Deviation Wellbore.....	60
6.3 Buckling in a Vertical Well.....	61



CHAPTER	Page
VII NUMERICAL METHOD SOLVING T&D CALCULATION.....	63
7.1 Introduction .....	63
7.2 Euler's Theory.....	63
7.2.1 Euler's method.....	63
7.2.2 Geometric description.....	65
7.2.3 Step size versus error .....	66
7.2.4 Example of the step size effect in Euler's method.....	67
7.2.5 Euler's method calculated in a three-dimensional wellbore .....	68
VIII DISCUSSION OF RESULTS .....	72
8.1 Introduction .....	72
8.2 Mathematical Models for Three-dimensional Wellbores.....	72
8.2.1 Lowering the pipe into the hole .....	72
8.2.1.1 Build section .....	72
8.2.1.2 Drop section.....	73
8.2.2 Pulling the pipe out of the hole.....	74
8.2.2.1 Build section .....	74
8.2.2.2 Drop section.....	75
8.3 Soft-string Model for Three-dimensional T&D Calculations .....	76
8.4 Example and Comparison in Force Calculations .....	77
8.5 Example and Comparison in Torque Calculations.....	79
8.5.1 Example while rotating off the bottom.....	79
8.5.2 Example for survey calculations.....	84
IX CONCLUSIONS AND RECOMMENDATIONS.....	87
9.1 Conclusions .....	87
9.2 Recommendations .....	88
NOMENCLATURE.....	89
REFERENCES.....	93
APPENDIX A .....	96
APPENDIX B .....	107
APPENDIX C .....	115
APPENDIX D .....	123

	Page
APPENDIX E.....	133
APPENDIX F.....	139
VITA .....	149

## LIST OF FIGURES

FIGURE	Page
1.1 Schematic of forces acting on downhole tubular assembly .....	5
2.1 Illustration of forces in build-up section (vertical view) .....	8
2.2 Illustration of forces in inclined section (vertical view) .....	9
2.3 Illustration of forces in drop section (vertical view).....	9
2.4 Illustration of forces while the wellbore turns to the right (horizontal view) .....	10
2.5 Illustration of forces while the wellbore turns to the left (horizontal view) .....	11
2.6 Soft-string T&D model schematic .....	12
2.7 Illustration of forces in build-up section (lowering the pipe into the hole, vertical view) .....	13
2.8 Illustration of differences between positive and negative forces in build- up section (lowering the pipe into the hole, vertical view).....	14
2.9 Illustration of force in hold section (lowering the pipe into the hole, vertical view) .....	15
2.10 Illustration of forces in drop section (lowering the pipe into the hole, vertical view) .....	16
2.11 Illustration of differences between positive and negative forces in drop section (lowering the pipe into the hole, vertical view).....	18
2.12 Illustration of forces when the wellbore turns right (lowering the pipe into the hole, horizontal view) .....	19
2.13 Illustration of forces when the wellbore turns left (lowering the pipe into the hole, horizontal view) .....	20
2.14 Illustration of forces in build-up section (pulling the pipe out of the hole, vertical view) .....	21

FIGURE	Page
2.15 Illustration of differences between positive and negative forces in build-up section (pulling the pipe out of the hole, vertical view) .....	23
2.16 Illustration of forces in the hold section (pulling the pipe out of the hole, vertical view) .....	24
2.17 Illustration of forces in the drop section (pulling the pipe out of the hole, vertical view) .....	25
2.18 Illustration of differences between positive and negative forces in the drop section (pulling the pipe out of the hole, vertical view) .....	27
2.19 Illustration of forces when the wellbore turns right (pulling the pipe out of the hole, horizontal view) .....	28
2.20 Illustration of forces when the wellbore turns left (pulling the pipe out of the hole, horizontal view) .....	29
3.1 Wellbore build & hold type in three-dimensional wellbore .....	32
3.2 Horizontal view of wellbore .....	37
3.3 Vertical view of wellbore .....	37
3.4 3D wellbore path by MATLAB version 7.4.0 .....	38
3.5 Build type well design .....	38
3.6 Build and hold type well design .....	39
3.7 Build hold and drop type well design .....	40
3.8 Horizontal well design .....	41
4.1 Spiral borehole as shown in 2D (Tracks 1 and 2) and 3D images .....	44
4.2 An MWD survey tool cannot detect a tight spiral .....	45
4.3 Illustrates the evidence of profound spiraling .....	46
4.4 3D CAD model of 12-1/4" borehole .....	47
4.5 Rippling 2D oscillation .....	48

FIGURE	Page
4.6 Spiraling 3D corkscrew .....	49
4.7 Hour-glassing cyclic hole enlargement.....	49
4.8 Showing the two-dimensional schematic of the drift equation.....	50
5.1 Torque-turn curve .....	53
5.2 Representative torque-turn curve with torque ranges shown.....	54
5.3 Cross-sectional view of a typical premium connection shown.....	54
5.4 A comparison of a premium casing connection and a proprietary rotary shouldered connection .....	54
6.1 Sinusoidal buckling of the pipe in a horizontal wellbore .....	60
6.2 Helical buckling of the pipe in a horizontal wellbore.....	60
6.3 Helical buckling in vertical wellbores .....	62
7.1 Euler's approximations $y_{k-1} = y_k + h f(t_k, y_k)$ .....	65
7.2 Comparison of Euler solutions with different step sizes .....	68
7.3 Illustrates force in the build-up section (lowering the pipe into the hole, vertical view) .....	69
7.4 Illustrates the differences between positive and negative forces in the build-up section (lowering the pipe into the hole).....	70
7.5 Comparison between Wu and Juvkam-Wold's (1991) equations and numerical methods.....	71
8.1 Wellbore geometry for this example .....	77
8.2 Comparison between Wu and Juvkam-Wold's (1991) equations and numerical methods.....	78
8.3 Axial tension plot for this example using Wu and Juvkam-Wold's (1991) method.....	81

FIGURE	Page
8.4 Torque plot for this example using Wu and Juvkam-Wold's (1991) method .....	81
8.5 Axial tension plot for this example using numerical method .....	83
8.6 Torque plot for this example using numerical method .....	84
8.7 3D wellbore path by MATLAB version 7.4.0 .....	85
8.8 Normal contact force (lb/ft) versus measured depth (ft).....	86
8.9 Axial force (lb) versus measured depth (ft) .....	86
A.1 T&D calculations for 3D well planning user form .....	97
A.2 Showing enlarge picture application in 3D software .....	98
A.3 Build type user form .....	99
A.4 Build & hold type user form .....	100
A.5 Build hold & drop type user form.....	102
A.6 Horizontal wellbore user form.....	103
A.7 T&D calculation between survey user form.....	104
A.8 3D wellbore path by MATLAB version 7.4.0 .....	106
B.1 Wellbore schematic for example in Appendix B .....	108
B.2 Normal contact force (lb/ft) versus measured depth (ft) for this example using Wu and Juvkam-Wold's (1991) method .....	109
B.3 Axial tension plot for this example using Wu and Juvkam-Wold's (1991) method.....	110
B.4 User form of Appendix B example .....	111
B.5 Result user form of Appendix B example .....	112
B.6 Normal contact force (lb/ft) versus measured depth (ft).....	113

FIGURE	Page
B.7 Axial tension force (lb) versus measured depth (ft) ( $F > 0$ referred to tensile force) .....	114
C.1 Wellbore Schematic for example in Appendix C .....	116
C.2 Normal contact force (lb/ft) versus measure depth (ft) for this example using Wu and Juvkam-Wold's (1991) method .....	117
C.3 Axial tension plot for this example using Wu and Juvkam-Wold's (1991) method.....	118
C.4 User form of Appendix C example.....	119
C.5 Result user form of Appendix C example .....	120
C.6 Normal contact force (lb/ft) versus measured depth (ft).....	121
C.7 Axial force (lb) versus measured depth (ft) ( $F < 0$ referred to tensile force).....	122
D.1 Wellbore schematic for example in Appendix D.....	124
D.2 Force table for Appendix D example.....	126
D.3 Normal contact force (lb/ft) versus measure depth (ft) from Wu and Juvkam-Wold's (1991) equation .....	127
D.4 Axial tension plot for this example using Wu and Juvkam-Wold's (1991) method.....	128
D.5 User form of Appendix D example.....	129
D.6 Result user form of Appendix D example .....	130
D.7 Normal contact force (lb/ft) versus measured depth (ft).....	131
D.8 Axial force (lb) versus measured depth (ft) ( $F < 0$ referred to tensile force).....	132
E.1 Wellbore schematic for example in Appendix E .....	134
E.2 Result user form with 2D wellbore trajectory (no left/right turn) .....	135

FIGURE	Page
E.3 Axial force (lb) versus measured depth (ft) ( $F < 0$ referred to tensile force) from 2D wellbore trajectory .....	136
E.4 Result user form with 3D wellbore trajectory (10 deg/100ft left/right turn).....	137
E.5 Axial force (lb) versus measured depth (ft) ( $F < 0$ referred to tensile force) from 3D wellbore trajectory .....	138
F.1 Comparison between push-the-bit results and point-the-bit-results .....	141
F.2 The standard BHA configuration.....	143
F.3 Illustrates deflection in the bottom hole assembly.....	144



**LIST OF TABLES**

TABLE		Page
3.1	Input field data for tie-on surveys and target directions .....	36
5.1	Maximum SCF values and locations in shouldered connections .....	57
7.1	Showing parameters for build section .....	69
8.1	Showing parameters.....	78
8.2	Input field data for tie-on surveys and target directions for 3D wellbore paths .....	85
F.1	Listing of generic T&D reduction techniques .....	145
F.2	Advantages and disadvantages of T&D reduction techniques .....	146

## CHAPTER I

### INTRODUCTION

Excessive torque and drag in the design of a wellbore trajectory and drillstring configuration might cause severe damage to a device that turns the drillstring (topdrive) capacity, drillpipe strength, and available lifting capacity. It can increase pipe fatigue, casing wear, and mechanical borehole problems, such as hole enlargement and can lead to an inability to slide. Moreover, a conventional steerable assembly might increase frictional forces, which can lead to failures in the tubular from excessive wear, bucking, and collapse.

If helical bucking is unavoidable, then torque and drag (T&D) models must be more robust if they are to accurately calculate the additional drag created in the post-buckled portion of the string. This is essential to predict the loss of weight on a bit, the potential for lock-up, and the impact on fatigue (Haduch, Procter, and Samuels 1994).

According to over two decades of petroleum literature that addresses Torque and Drag (T&D) software, the basic mathematical model that underlies most T&D software has not changed significantly since its original inception. Now is the right time to reflect on the state of current models and identify the future requirements because T&D software is commonly used during planning processes (Adewuya and Pham 1998).

---

This dissertation follows the style and format of *SPE Drilling and Completion*.

A new model will help engineers identify feasible well designs and define drilling limitations for particular field development options. A reliable mathematical model is fundamental to a true understanding of the accuracy and applicability of T&D models. Software based on a more accurate T&D mathematical model for each particular well design will be highly useful in well planning design processes and will prevent the problems caused by T&D.

## **1.1 Literature Review**

T&D calculations and other information need to be changed in T&D software including T&D equations, tortuosity effects, stress concentration factor, and buckling.

### **1.1.1 T&D equations for three-dimensional wellbore**

Mason and Chen (2007) states that T&D modeling is regarded as an invaluable process in well planning for assisting and predicting, as well as preventing, drilling problems. Although T&D software has been developed for over 20 years, some confusion still exists over the validity of the models. Meanwhile, Exxon production research has developed soft string models for T&D equations. The soft string model is so called because it ignores any effects of tubular stiffness. This means the drillstring is represented as a heavy chain that transmits axial tension and torque caused by drillstring friction resulting from normal contact forces between the pipe and the wellbore. The soft string will be used in this research for T&D calculations during surveying in three-dimensional wellbores. Moreover, Mason and Chen (2007) also provide criterion for each type of buckling (sinusoidal and helical).

When discussing T&D calculations in the build section, Wu and Juvkam-Wold (1993) included three activities: rotating off bottom, running in the hole, and pulling out of the hole. His paper provides analytical solutions for T&D calculations in two-dimensional wellbore design. However, it will be most beneficial if we can develop these two-dimensional equations into three-dimensional equations. This will be of great advantage for our next generation of T&D calculations.

Aston, Hearn, and McGhee (1998) discuss techniques for solving present torque and drag problems and mention many other techniques that are widely used for reducing torque and drag problems. One of the techniques mentioned is to optimize the well profile before drilling. This means that before the drilling begins, we have already acquired the information concerning optimizing the wellbore profile. As a result, the optimization will be greatly useful in facing any difficulties in the drilling process.

### **1.1.2 Tortuosity effects**

Gaynor, Chen, Stuart, and Comeaux (2001) explain how to quantify tortuosity. Their paper discusses “micro-tortuosity,” as well as the primary cause of hole spiraling that will cause poor hole quality. Spiraling can be easily eliminated. It is desirable to reduce “micro-tortuosity,” and thus it will improve hole quality. From this paper it will be useful if T&D software programs also consider reducing this effect.

Gaynor, Halmer, Chen, and Stuart (2002) discuss the information on tortuosity versus micro-tortuosity. This information has greatly assisted eliminating excessive tortuosity,

which is regarded as a successful factor in solving extended reach drilling operation problems. This paper also provides a mathematical model of a spiral hole and gives a change in diameter in torque equations which changes the diameter of tool joint ( $D_{ij}$ ) to the average diameter that has been used in torque equations ( $D_{drift}$ ).

### **1.1.3 Stress concentration factor**

Tang, Muradov, Chandler, Jellison, Prideco, Gonzalez, and Wu (2006) present the new stress concentration factor (SCF) analysis methodology for rotary shouldered connections (RSCs) by using a finite element analysis as a primary method to calculate SCF. This represents the connecting performance. In fact, this paper has application in evaluating drill string connection design. However, it will not affect T&D calculations in terms of increasing T&D.

### **1.1.4 Buckling**

Wu and Juvkam-Wold (1993) discuss helical buckling and sinusoidal buckling of pipes in horizontal wells and drilling and completion technologies. It is a highly difficult technique when associated with transmitting compressive axial loads to the bit (or the packer) on the bottom due to frictional force between pipe and wellbore. This paper provides all of the buckling types in the horizontal wellbore that are used in this research.

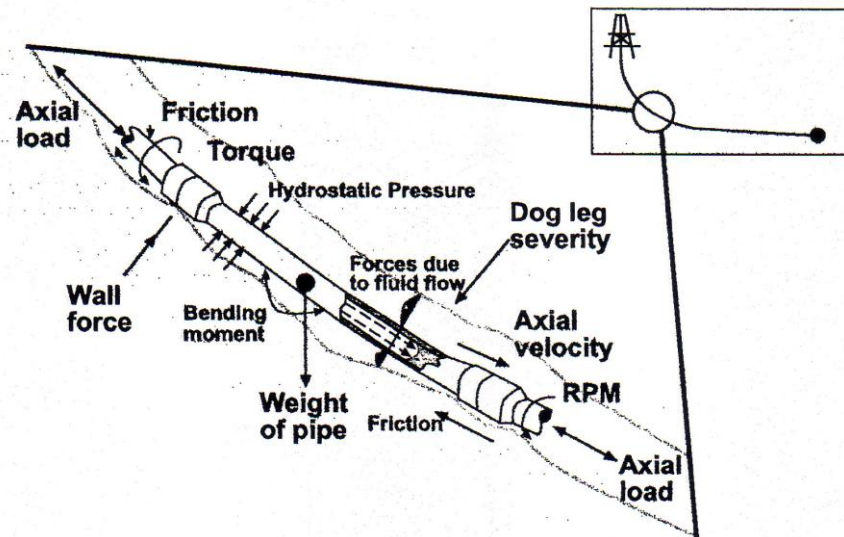


Fig. 1.1–Schematic of forces acting on downhole tubular assembly (Aston et al. 1998).

**Fig. 1.1** shows a schematic of the downhole forces acting on a tubular sliding and rotating in an inclined wellbore. This will help us to choose the torque and drag model for calculating torque and drag data. This picture shows all the forces that impact the drillstring while the drillstring is downhole. Also, this research will cover more than just T&D; the parameters that will be considered from the above figure will be axial load, wall force, friction, torque, weight of pipe, and dogleg severity.

## 1.2 Objectives and Organization

This research's objective will start by improving the equations that are normally used in T&D software calculations, reflecting on the state of current models and identifying future requirements. This research will provide more accurate T&D models that will help alleviate helical buckling problems; normally, helical buckling causes the potential for lock-up and impacts fatigue.

This research's second objective is to prevent T&D problems while drilling by trying to optimize well profiles before drilling begins. Moreover, this research will try to show the relation between well planning design and T&D calculation. This will make it easier to find out which type of well design is more suitable in each particular area. Additionally, this research will help tremendously in the design of long horizontal wellbores.

This research's third objective is to help field personnel prepare for any unexpected trend changes in a timely fashion during the drilling process. They will be able to anticipate these changes by just inputting wellbore data and T&D parameters.

Furthermore, the outcome of the data from the T&D calculation program will be more realistic because it will be based on a 3D model.

Chapter II will propose the new equations to be used in torque and drag analysis in three-dimensional wellbores. Chapter III will provide the equations that have been used in well planning; these are divided into four types of wellbore curves (build type, build & hold type, build & hold & drop type, and horizontal wellbore type). Chapter IV will explain the effect from tortuosity on torque and drag calculations. Chapter V discusses continuing processes on torque and drag analysis of each drillstring connecting joint. Chapter VI discusses buckling effects in T&D calculations. Chapter VII will emphasize numerical methods in torque and drag. Lastly, Chapter VIII will present conclusions as well as recommendations for future work.

## CHAPTER II

### TORQUE AND DRAG CALCULATIONS IN THREE-DIMENSIONAL WELLBORE METHODOLOGY

#### 2.1 Introduction

The mathematical model for torque and drag calculations in three-dimensional wellbore design is based on wellbore curve design. If we look at well planning just in a vertical depth plane, we could derive each type of assumed curve without tortuosity in vertical sections. We will divide the wellbore functions and hence the torque and drag calculations into three steps: rotation off the bottom, following through running in the hole, and pulling out of the hole (Wiggins, Choe, and Juvkam-Wold 1992). Dogleg severity ( $\delta$ ) will be considered. The wellbore will be divided into two planes for calculation: the vertical view and the horizontal view. We will start with T&D calculations for rotation off the bottom. For rotating on bottom, the calculation will be similar to rotation off bottom, however the difference for calculation is force at the bit ( $F_{bit}$ ). In addition, for sliding drilling, the calculation method is the same as running in the hole, however the difference will be  $F_{bit}$  (Juvkam-Wold and Wu 1992).

#### 2.2 Original Concept for Calculating Normal Contact Force

We start with a simple concept for normally contacting force calculations (N) (Aadnøy and Anderson 1998) by assuming that no friction (f) exists along the wellbore (rotating off bottom).



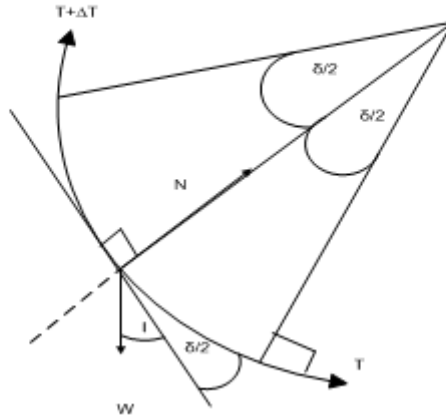


Fig. 2.1–Illustration of forces in build-up section (vertical view).

From **Fig. 2.1** neglecting friction (e.g., pipe rotation) will be expressed as follows

(Johancsik, Friesch, and Dawson 1984):

$$\Sigma F_{\text{along normal}}: W \sin I - (T + \Delta T) \sin \frac{\delta}{2} - T \sin \frac{\delta}{2} - N = 0 \quad (2.1)$$

$$W \sin I - 2T \sin \frac{\delta}{2} - \Delta T \sin \frac{\delta}{2} - N = 0 \quad (2.2)$$

$$N = W \sin I - 2T \sin \frac{\delta}{2} \quad (\text{assuming } \Delta T \sin \frac{\delta}{2} \rightarrow 0) \quad (2.3)$$

Note:  $f$  - Is the force of two surfaces in contact, or the force of a medium acting on a moving object, lbf

$W$  - In this research, refers to buoyed weight of the string element, lbf/ft

$I, \theta$  - A deviation or the degree of deviation from the vertical

$T$  - The tension force at the lower end of the string element, lbf

$\Delta$  - A normalized estimate of the overall curvature of an actual well path between two consecutive survey stations, degrees per 100 ft

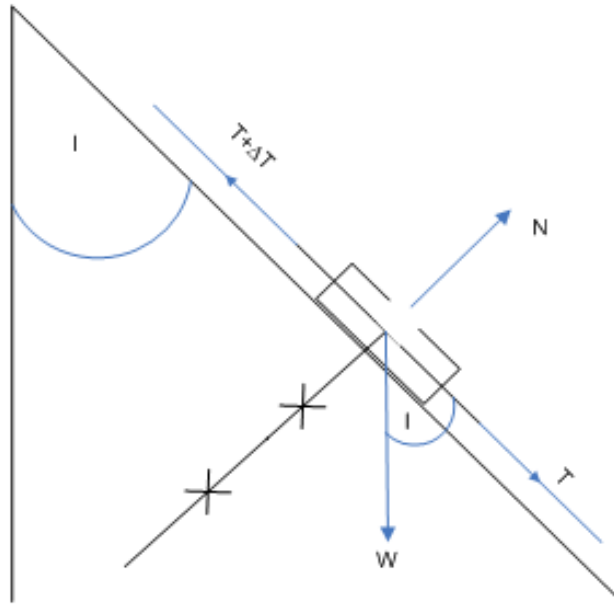


Fig. 2.2–Illustration of forces in inclined section (vertical view).

From **Fig. 2.2** neglecting friction (e.g., pipe rotation) will be illustrated as follows:

$$N = W \sin I \quad (2.4)$$

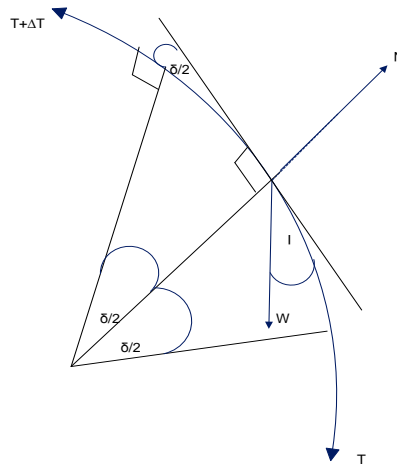


Fig. 2.3–Illustration of forces in drop section (vertical view).

From **Fig. 2.3** neglecting friction (e.g., pipe rotation) will be illustrated as follows:

$$\Sigma F_{\text{along normal}}: W \sin I + (T + \Delta T) \sin \frac{\delta}{2} + T \sin \frac{\delta}{2} - N = 0 \quad (2.5)$$

$$W \sin I + 2T \sin \frac{\delta}{2} + \Delta T \sin \frac{\delta}{2} - N = 0 \quad (2.6)$$

$$N = W \sin I + 2T \sin \frac{\delta}{2} \quad (\text{Assuming } \Delta T \sin \frac{\delta}{2} \rightarrow 0) \quad (2.7)$$

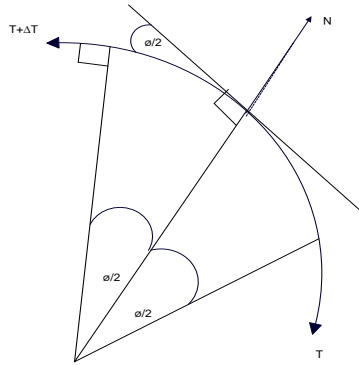


Fig. 2.4—Illustration of forces while the wellbore turns to the right (horizontal view).

From **Fig. 2.4** neglecting friction (e.g., pipe rotation) by using the same calculation as drop section; however,  $W$  and  $I$  will not be considered.

$$N_{\text{turn}} \approx (T + \Delta T) \sin \frac{\phi}{2} + T \sin \frac{\phi}{2} \quad (2.8)$$

$$N_{\text{turn}} = 2T \sin \frac{\phi}{2} \quad (\text{Assuming } \Delta T \sin \frac{\phi}{2} \rightarrow 0) \quad (2.9)$$

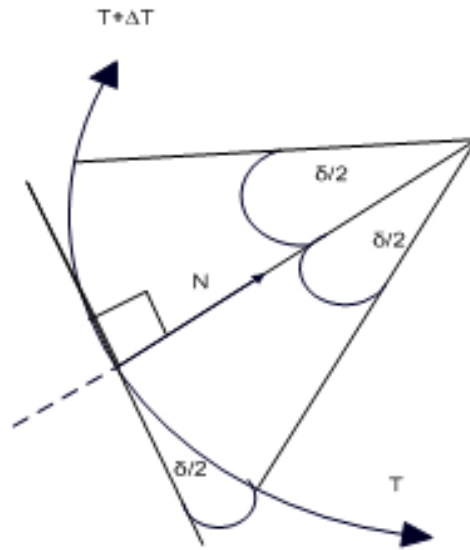


Fig. 2.5—Illustration of forces while the wellbore turns to the left (horizontal view).

From **Fig. 2.5** neglecting friction (e.g., pipe rotation) will be illustrated as follows:

$$N_{\text{turn}} \approx (T + \Delta T) \sin \frac{\phi}{2} + T \sin \frac{\phi}{2} \quad (2.10)$$

$$N_{\text{turn}} = 2T \sin \frac{\phi}{2} \quad (\text{Assuming } \Delta T \sin \frac{\phi}{2} \rightarrow 0) \quad (2.11)$$

### 2.3 Soft-string Model for Three-dimensional T&D Calculation

The original soft-string T&D programs are based on a model developed by Exxon Production Research (Mason and Chen 2007). The value of  $N$  (normal contact force) depends on how the wellbore contacts with the formation and the actual amount of normal contact force (Menand, Sellami, Tijani, Stab, Dupuis, and Simon 2006):

$$N \text{ total} = \sqrt{(T\Delta\phi \sin \theta)^2 + (T\Delta\phi + W \sin \theta)^2} \quad (2.12)$$

Note:  $T$  - The tension force at the lower end of the string element, lbf

$\Delta\theta$  - The change in azimuth angle over the string element, rad.

$I, \theta$  - A deviation or the degree of deviation from the vertical

$W$  - In this research, refers to buoyed weight of the string element, lbf/ft

If the wellbore turns neither left nor right,  $T\Delta\phi \sin \theta$  will equal 0; then using the normal contact force equation, the tension and torque change can be calculated from **Eq. 2.13** and **Eq. 2.14**.

$$\Delta T = W \cos \theta + / - \mu N \quad (2.13)$$

$$\Delta M = \mu NR \quad (2.14)$$

**Eq. 2.13** shows that whether it is plus (+) or minus (-) depends on which direction the friction will be, as illustrated in **Fig. 2.6**. The next section will discuss the case of lowering the pipe into the hole.

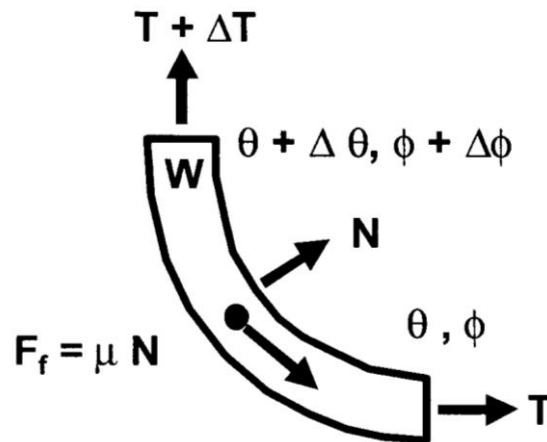


Fig. 2.6–Soft-string T&D model schematic (Mason and Chen 2007).

## 2.4 Lowering the Pipe into the Hole

This section will show the equations that will be used in three-dimensional wellbore designs while lowering the pipe into the hole (Maidla and Wojtanowicz 1987).

### 2.4.1 Lowering the pipe into the hole in the build section

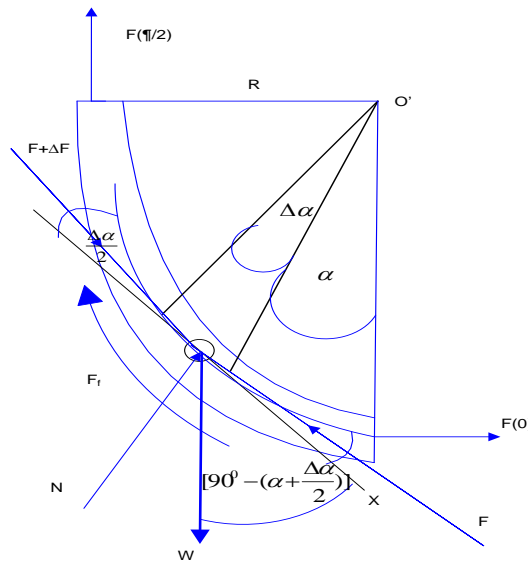


Fig. 2.7—Illustration of forces in build-up section (lowering the pipe into the hole, vertical view).

From **Fig. 2.7**  $\Sigma F$  along N axis will be illustrated as follows:

$$NR\Delta\alpha = (F + \Delta F)\sin\frac{\Delta\alpha}{2} + F\sin\frac{\Delta\alpha}{2} + WR\Delta\alpha\sin(90^\circ - (\alpha + \frac{\Delta\alpha}{2})) \quad (2.15)$$

From **Eq. 2.15** divide by  $R\Delta\alpha$ , thus

$$N = \frac{2F}{R\Delta\alpha}\sin\left(\frac{\Delta\alpha}{2}\right) + \frac{\Delta F}{R\Delta\alpha}\sin\left(\frac{\Delta\alpha}{2}\right) + W\cos\left(\alpha + \frac{\Delta\alpha}{2}\right) \quad (2.16)$$

When  $(\Delta\alpha \rightarrow 0)$ , then  $\sin\left(\frac{\Delta\alpha}{2}\right)$  will approach close to 0.

$$N = W\cos(\alpha) + \frac{F_c(\alpha)}{R} \quad (2.17)$$

From **Fig. 2.7**  $\Sigma F$  along X axis will be illustrated as follows:

Note: R - The radius of curvature of the string element while the wellbore is in the build section  
(vertical view), ft

A - The angle used to calculate the deviation of the wellbore, rad.

$$(F + \Delta F)\cos\left(\frac{\Delta\alpha}{2}\right) - F\cos\left(\frac{\Delta\alpha}{2}\right) - F_f R\Delta\alpha + WR\Delta\alpha\cos\left(90^\circ - \left(\alpha + \frac{\Delta\alpha}{2}\right)\right) = 0 \quad (2.18)$$

$$\Delta F\cos\left(\frac{\Delta\alpha}{2}\right) - F_f R\Delta\alpha + WR \Delta\alpha\sin\left(\alpha + \frac{\Delta\alpha}{2}\right) = 0 \quad (2.19)$$

**Eq. 2.19** divide by  $\Delta\alpha$

$$\frac{\Delta F}{\Delta\alpha} \cos\left(\frac{\Delta\alpha}{2}\right) = F_f R - WR\sin\left(\alpha + \frac{\Delta\alpha}{2}\right) \quad (2.20)$$

When  $\Delta\alpha \rightarrow 0$  
$$\frac{dF(\alpha)}{d(\alpha)} = F_f R - WR\sin(\alpha); F_f = \mu|N| \quad (2.21)$$

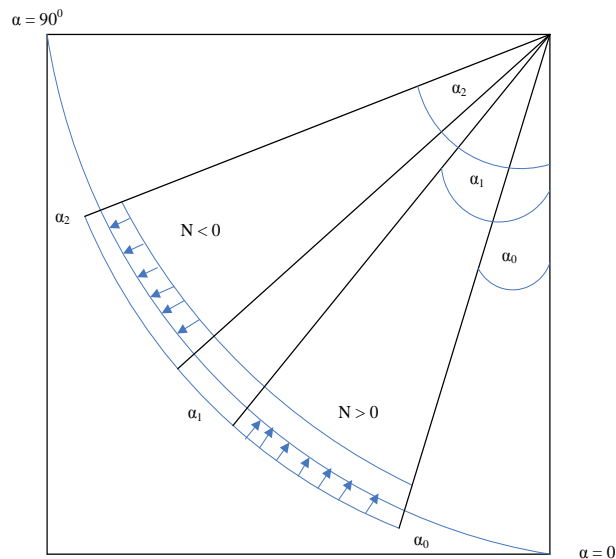


**Fig. 2.8**—Illustration of differences between positive and negative forces in build-up section (lowering the pipe into the hole, vertical view).

From **Fig. 2.8** for  $N > 0$

$$\frac{dF(\alpha)}{d(\alpha)} = \mu \left\{ \sqrt{\left[ w \cos(\alpha) + \frac{F_c(\alpha)}{R} \right]^2 + \left[ \frac{F_c(\alpha)}{R_{turn}} \right]^2} \right\} R - WR \sin(\alpha); (\alpha_1 \geq \alpha \geq \alpha_0) \quad (2.22)$$

\*The term  $\frac{F_c(\alpha)}{R_{turn}}$  comes from wellbore turning and will be shown in the next section of

this chapter. The value will be zero if there is no right or left turn of wellbore;  $F_c$  means

if compressive force  $F_c > 0$  and if tension force  $F_c < 0$  (Wu and Juvkam-Wold 1991).

From **Fig. 2.8** for  $N < 0$

$$\frac{dF(\alpha)}{d(\alpha)} = \mu \left\{ - \sqrt{\left[ w \cos(\alpha) + \frac{F_c(\alpha)}{R} \right]^2 + \left[ \frac{F_c(\alpha)}{R_{turn}} \right]^2} \right\} R - WR \sin(\alpha); (\alpha_2 \geq \alpha \geq \alpha_1) \quad (2.23)$$

\*The term  $\frac{F_c(\alpha)}{R_{turn}}$  comes from wellbore turning and will be shown in the next section of

this chapter. The value will be zero if there is no right or left turn of wellbore;  $F_c$  means

if compressive force  $F_c > 0$  and if tension force  $F_c < 0$ .

#### 2.4.2 Lowering the pipe into the hole in the hold section

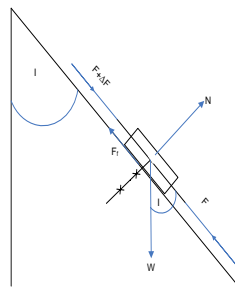


Fig. 2.9—Illustration of force in hold section (lowering the pipe into the hole, vertical view).



From **Fig. 2.9**  $\Sigma F$  along N axis will be illustrated as follows:

$\Sigma F$  along N axis:

$$N = W \sin I \quad (2.24)$$

The value of N depends on how the wellbore contacts with the formation and the actual amount of normal contact force:

$$N_{total} = \sqrt{N^2 + N_{turn}^2} \quad (2.25)$$

If the wellbore neither turns left nor right,  $N_{turn}$  will equal  $\rightarrow 0$ .

However, if the wellbore's deviation is towards a left or right turn,  $N_{turn}$  will be:  $\frac{Fc(\alpha)}{R}$

From **Fig. 2.9**  $\Sigma F$  along F axis will be illustrated as follows:

$$(F + \Delta F) + W \cos I = F_f + F \quad (2.26)$$

$$\Delta F = \mu N_{total} - W \cos I \quad (2.27)$$

### 2.4.3 Lowering the pipe into the hole in the drop section

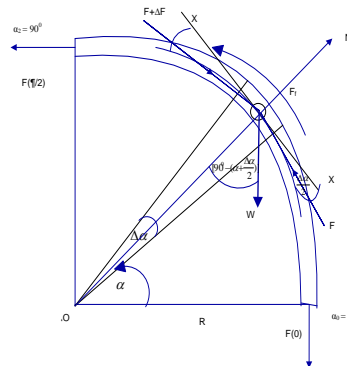


Fig. 2.10—Illustration of forces in drop section (lowering the pipe into the hole, vertical view).

From Fig. 2.10  $\Sigma F$  along N axis will be illustrated as follows:

$$\Sigma F \text{ along N axis: } NR\Delta\alpha + (F + \Delta F)\sin\frac{\Delta\alpha}{2} + F\sin\frac{\Delta\alpha}{2} = WR\Delta\alpha\sin(\alpha + \frac{\Delta\alpha}{2}) \quad (2.28)$$

$$N = - \left[ \frac{2F}{R\Delta\alpha} \sin\left(\frac{\Delta\alpha}{2}\right) + \frac{\Delta F}{R\Delta\alpha} \sin\left(\frac{\Delta\alpha}{2}\right) \right] + W\sin(\alpha + \frac{\Delta\alpha}{2}) \quad (2.29)$$

When  $(\Delta\alpha \rightarrow 0)$ ,  $\sin(\frac{\Delta\alpha}{2})$  will approach close to 0.

$$N = W\sin(\alpha) - \frac{Fc(\alpha)}{R} \quad (2.30)$$

From Fig. 2.10  $\Sigma F$  along X axis will be illustrated as follows:

$$(F + \Delta F)\cos\left(\frac{\Delta\alpha}{2}\right) - F\cos\left(\frac{\Delta\alpha}{2}\right) - F_f R\Delta\alpha + WR\Delta\alpha\sin(90^\circ - (\alpha + \frac{\Delta\alpha}{2})) = 0 \quad (2.31)$$

$$\Delta F\cos\left(\frac{\Delta\alpha}{2}\right) - F_f R\Delta\alpha + WR\Delta\alpha\cos(\alpha + \frac{\Delta\alpha}{2}) = 0 \quad (2.32)$$

**Eq. 2.32** Divide by  $\Delta\alpha$

$$\frac{\Delta F}{\Delta\alpha} \cos\left(\frac{\Delta\alpha}{2}\right) = F_f R - WR\cos(\alpha + \frac{\Delta\alpha}{2}) \quad (2.33)$$

When  $\Delta\alpha \rightarrow 0$

$$\frac{dF(\alpha)}{d(\alpha)} = F_f R - WR\cos(\alpha); F_f = \mu|N| \quad (2.34)$$

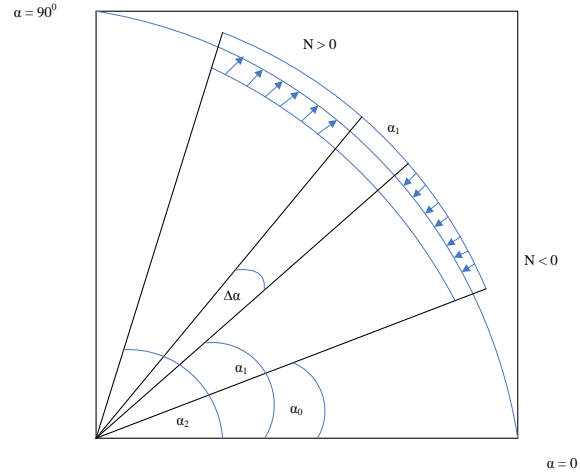


Fig. 2.11–Illustration of differences between positive and negative forces in drop section (lowering the pipe into the hole, vertical view).

From **Fig. 2.11** for  $N > 0$

$$\frac{dF(\alpha)}{d(\alpha)} = \mu \left\{ \sqrt{\left[ w \sin(\alpha) - \frac{F_c(\alpha)}{R} \right]^2 + \left[ \frac{F_c(\alpha)}{R_{turn}} \right]^2} \right\} R - WR \cos(\alpha); (\alpha_2 \geq \alpha \geq \alpha_1) \quad (2.35)$$

\*The term  $\frac{F_c(\alpha)}{R_{turn}}$  comes from the wellbore turning and will be shown in the next

section of this chapter. The value will be zero if there is no a right or a left turn;

$F_c$  means if compressive force  $F_c > 0$  and if tension force  $F_c < 0$ .

For  $N < 0$

$$\frac{dF(\alpha)}{d(\alpha)} = \mu \left\{ - \sqrt{\left[ w \sin(\alpha) + \frac{F_c(\alpha)}{R} \right]^2 + \left[ \frac{F_c(\alpha)}{R_{turn}} \right]^2} \right\} R - WR \cos(\alpha); (\alpha_1 \geq \alpha \geq \alpha_0) \quad (2.36)$$

\*The term  $\frac{F_c(\alpha)}{R_{turn}}$  comes from the wellbore turning and will be shown in the next

section of this chapter. The value will be zero if there is no right or left turn;  $F_c$  means if compressive force  $F_c > 0$  and if tension force  $F_c < 0$ .

#### 2.4.4 Lowering the pipe into the hole while the wellbore turns

This section will discuss drag calculation on the top view; the explanation will cover either the wellbore turning right or left in each section. It will be similar to those of the vertical calculations; however, the W term will not be shown in each equation, due to it is a horizontal view.

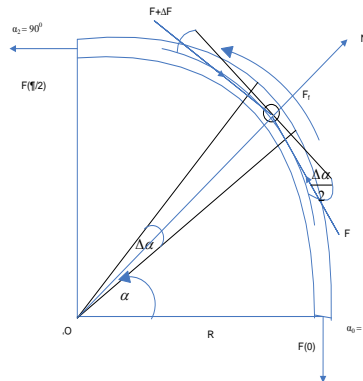


Fig. 2.12–Illustration of forces when the wellbore turns right (lowering the pipe into the hole, horizontal view).

From **Fig. 2.12**  $\Sigma F$  along N axis

$$N_{turn} R \Delta \alpha + (F + \Delta F) \sin \frac{\Delta \alpha}{2} + F \sin \frac{\Delta \alpha}{2} = 0 \quad (2.37)$$

$$N_{turn} = - \left[ \frac{2F}{R \Delta \alpha} \sin \left( \frac{\Delta \alpha}{2} \right) + \frac{\Delta F}{R \Delta \alpha} \sin \left( \frac{\Delta \alpha}{2} \right) \right] \quad (2.38)$$

When  $(\Delta\alpha \rightarrow 0)$ , then  $\sin\left(\frac{\Delta\alpha}{2}\right)$  will approach close to 0  $N_{turn} = -\frac{Fc(\alpha)}{R}$

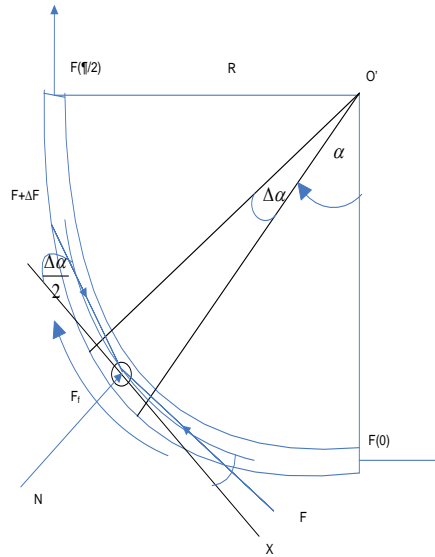


Fig. 2.13–Illustration of forces when the wellbore turns left (lowering the pipe into the hole, horizontal view).

From **Fig. 2.13**  $\Sigma F$  along N axis will be illustrated as follows:

$$N_{turn} R \Delta\alpha = (F + \Delta F) \sin \frac{\Delta\alpha}{2} + F \sin \frac{\Delta\alpha}{2} \quad (2.39)$$

**Eq. 2.39** divided by  $R\Delta\alpha$ , thus

$$N_{turn} = \frac{2F}{R\Delta\alpha} \sin\left(\frac{\Delta\alpha}{2}\right) + \frac{\Delta F}{R\Delta\alpha} \sin\left(\frac{\Delta\alpha}{2}\right) \quad (2.40)$$

When  $(\Delta\alpha \rightarrow 0)$ , then  $\sin\left(\frac{\Delta\alpha}{2}\right)$  will approach close to 0;  $N_{turn} = \frac{Fc(\alpha)}{R}$

## 2.5 Pulling the Pipe out of the Hole

This section will show the equations that will be used in three-dimensional wellbore designs while pulling the pipe out of the hole.

### 2.5.1 Pulling the pipe out of the hole in the build section

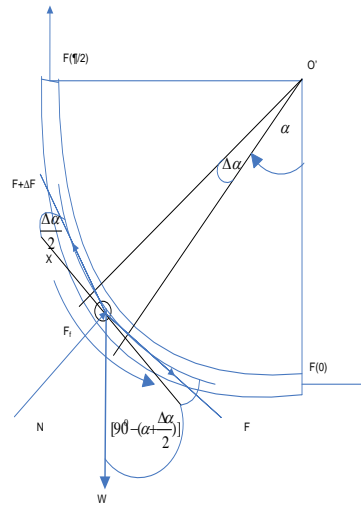


Fig. 2.14—Illustration of forces in build-up section (pulling the pipe out of the hole, vertical view).

From **Fig. 2.14**  $\Sigma F$  along N axis will be illustrated as follows:

$$(F + \Delta F)\sin \frac{\Delta\alpha}{2} + F\sin \frac{\Delta\alpha}{2} + NR\Delta\alpha - WR\Delta\alpha\sin(90^\circ - (\alpha + \frac{\Delta\alpha}{2})) = 0 \quad (2.41)$$

From **Eq. 2.41**

$$2F\sin(\frac{\Delta\alpha}{2}) + \Delta F\sin(\frac{\Delta\alpha}{2}) + NR\Delta\alpha - WR\Delta\alpha\cos(\alpha + \frac{\Delta\alpha}{2}) = 0 \quad (2.42)$$

$$NR\Delta\alpha = WR\Delta\alpha\cos(\alpha + \frac{\Delta\alpha}{2}) - \Delta F\sin(\frac{\Delta\alpha}{2}) - 2F\sin(\frac{\Delta\alpha}{2}) \quad (2.43)$$

$$N\Delta\alpha = W\Delta\alpha\cos(\alpha + \frac{\Delta\alpha}{2}) - \frac{\Delta F}{R} \sin(\frac{\Delta\alpha}{2}) - \frac{2F}{R} \sin(\frac{\Delta\alpha}{2}) \quad (2.44)$$

$$N = W\cos(\alpha + \frac{\Delta\alpha}{2}) - \frac{\Delta F}{\Delta\alpha R} \sin(\frac{\Delta\alpha}{2}) - \frac{2F}{\Delta\alpha R} \sin(\frac{\Delta\alpha}{2}) \quad (2.45)$$

If  $\Delta\alpha \rightarrow 0$ , then  $\sin(\frac{\Delta\alpha}{2})$  will approach close to 0

$$N(\alpha) = W\cos(\alpha) - \frac{F(\alpha)}{R} \quad (2.46)$$

From **Fig. 2.14**  $\Sigma F$  along X axis will be illustrated as follows:

$$\{(F + \Delta F)\cos(\frac{\Delta\alpha}{2}) - F\cos(\frac{\Delta\alpha}{2}) - F_f R\Delta\alpha - WR\Delta\alpha\cos(90^\circ - (\alpha + \frac{\Delta\alpha}{2}))\} = 0 \quad (2.47)$$

$$\Delta F\cos(\frac{\Delta\alpha}{2}) - F_f R\Delta\alpha - WR \Delta\alpha\sin(\alpha + \frac{\Delta\alpha}{2}) = 0 \quad (2.48)$$

**Eq. 2.48** Divide by  $\Delta\alpha$

$$\frac{\Delta F}{\Delta\alpha} \cos(\frac{\Delta\alpha}{2}) = F_f R + WR\sin(\alpha + \frac{\Delta\alpha}{2}) \quad (2.49)$$

$\Delta\alpha \rightarrow 0$

$$\frac{dF(\alpha)}{d(\alpha)} = F_f R + WR\sin(\alpha); F_f = \mu|N| \quad (2.50)$$

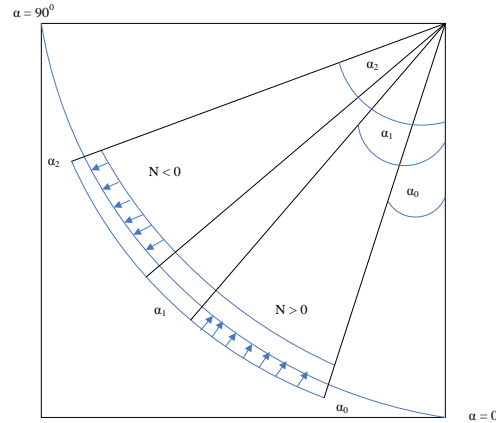


Fig. 2.15–Illustration of differences between positive and negative forces in build-up section (pulling the pipe out of the hole, vertical view).

From **Fig. 2.15** for  $N > 0$

$$\frac{dF(\alpha)}{d(\alpha)} = \mu \left\{ \sqrt{\left[ w \cos(\alpha) - \frac{F(\alpha)}{R} \right]^2 + \left[ \frac{F(\alpha)}{R_{turn}} \right]^2} \right\} R + WR \sin(\alpha); (\alpha_1 \geq \alpha \geq \alpha_0) \quad (2.51)$$

\*The term  $\frac{F(\alpha)}{R_{turn}}$  comes from the wellbore turning and will be explained in the next

section of this chapter; the value will be zero if there is no a right or a left turn;  $F$  means

if tension force  $F > 0$  and if compressive force  $F < 0$ .

For  $N < 0$

$$\frac{dF(\alpha)}{d(\alpha)} = \mu \left\{ -\sqrt{\left[ w \cos(\alpha) - \frac{F(\alpha)}{R} \right]^2 + \left[ \frac{F(\alpha)}{R_{turn}} \right]^2} \right\} R + WR \sin(\alpha); (\alpha_2 \geq \alpha \geq \alpha_1) \quad (2.52)$$

\*The term  $\frac{F(\alpha)}{R_{turn}}$  comes from the wellbore turning and will be explained in the next

section in this chapter. The value will be zero if there is no right or left turn;  $F$  means if

tension force  $F > 0$  and if compressive force  $F < 0$ .



### 2.5.2 Pulling the pipe out of the hole in the hold section

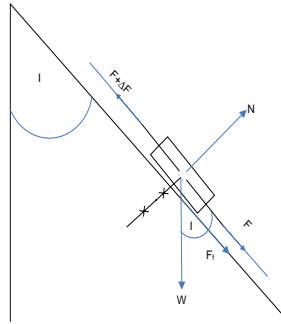


Fig. 2.16–Illustration of forces in the hold section (pulling the pipe out of the hole, vertical view).

From **Fig. 2.16**  $\Sigma F$  along N axis

$\Sigma F$  along N axis will be

$$N = W \sin I \quad (2.53)$$

The amount of N (normal contacts force) depends on how the wellbore contacts the formation, and the actual amount of normal contact force will be illustrated as follows:

$$N_{total} = \sqrt{N^2 + N_{turn}^2} \quad (2.54)$$

If neither a left turn nor a right turn is in the wellbore, the  $N_{turn}$  term will equal  $\rightarrow 0$ . The

next section will discuss lowering the pipe into the hole. However, if the wellbore

deviates toward a left turn or a right turn,  $N_{turn} = \frac{Fc(\alpha)}{R}$

From **Fig. 2.17**  $\Sigma F$  along F axis will be illustrated as follows:

$$(F+\Delta F) = F_f + F + W \cos I \quad (2.55)$$

$$\Delta F = \mu N_{\text{total}} + W \cos I \quad (2.56)$$

### 2.5.3 Pulling the pipe out of the hole in the drop section

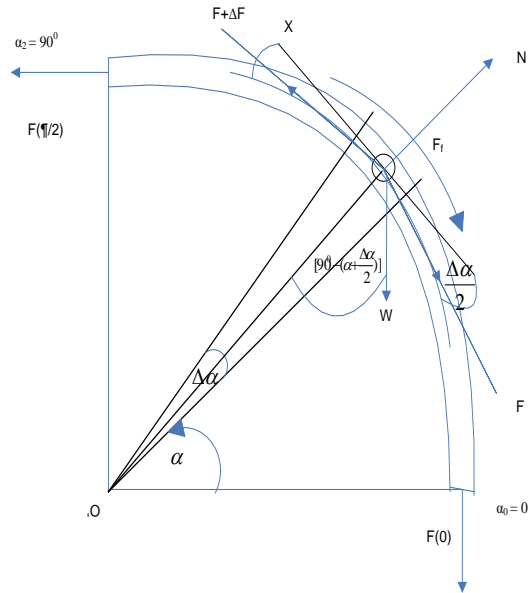


Fig. 2.17—Illustration of forces in the drop section (pulling the pipe out of the hole, vertical view).

From **Fig. 2.17**  $\Sigma F$  along N axis will be illustrated as follows:

$$NR\Delta\alpha = (F + \Delta F)\sin\frac{\Delta\alpha}{2} + F\sin\frac{\Delta\alpha}{2} + WR\Delta\alpha\sin(\alpha + \frac{\Delta\alpha}{2}) \quad (2.57)$$

$$N = \frac{2F}{R\Delta\alpha}\sin\left(\frac{\Delta\alpha}{2}\right) + \frac{\Delta F}{R\Delta\alpha}\sin\left(\frac{\Delta\alpha}{2}\right) + W\sin(\alpha + \frac{\Delta\alpha}{2}) \quad (2.58)$$

When  $\Delta\alpha \rightarrow 0$ , then  $\sin\left(\frac{\Delta\alpha}{2}\right)$  will approach close to 0.

$$N = W\sin(\alpha) + \frac{F(\alpha)}{R} \quad (2.59)$$

From **Fig. 2.17**  $\Sigma F$  along x axis will be illustrated as follows:

$$(F + \Delta F)\cos\left(\frac{\Delta\alpha}{2}\right) - F\cos\left(\frac{\Delta\alpha}{2}\right) - F_fR\Delta\alpha - WR\Delta\alpha\cos\left(\alpha + \frac{\Delta\alpha}{2}\right) = 0 \quad (2.60)$$

$$\Delta F\cos\left(\frac{\Delta\alpha}{2}\right) - F_fR\Delta\alpha - WR\Delta\alpha\cos\left(\alpha + \frac{\Delta\alpha}{2}\right) = 0 \quad (2.61)$$

**Eq. 2.61** divided by  $\Delta\alpha$

$$\frac{\Delta F}{\Delta\alpha}\cos\left(\frac{\Delta\alpha}{2}\right) = F_fR + WR\cos\left(\alpha + \frac{\Delta\alpha}{2}\right) \quad (2.62)$$

When  $\Delta\alpha \rightarrow 0$ ,  $\cos(0)$  will approach close to 1.

$$\frac{dF}{d\alpha} = F_fR + WR\cos(\alpha) \quad (2.63)$$

$$\text{From } F_f = \mu|N|; \quad (2.64)$$

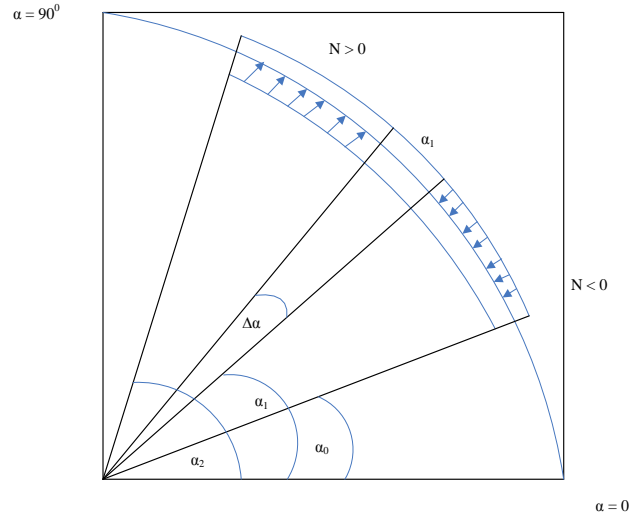


Fig. 2.18–Illustration of differences between positive and negative forces in the drop section (pulling the pipe out of the hole, vertical view).

For  $N > 0$  (**Fig. 2.18**) is separate in two cases of  $N$  value

$$\frac{dF}{d\alpha} = \mu \left\{ \sqrt{\left( W \sin(\alpha) + \frac{F(\alpha)}{R} \right)^2 + \left( \frac{F(\alpha)}{R_{turn}} \right)^2} \right\} R + WR \cos(\alpha); (\alpha_2 \geq \alpha \geq \alpha_1) \quad (2.65)$$

\*The term  $\frac{F(\alpha)}{R_{turn}}$  comes from the wellbore turning and will be explained in the next

section of this chapter. The value will be zero if there is no right or left turn;

$F$  means if tension force  $F > 0$  and if compressive force  $F < 0$ .

For  $N < 0$

$$\frac{dF}{d\alpha} = \mu \left\{ - \sqrt{\left( W \sin(\alpha) + \frac{F(\alpha)}{R} \right)^2 + \left( \frac{F(\alpha)}{R_{turn}} \right)^2} \right\} R + WR \cos(\alpha); (\alpha_1 \geq \alpha \geq \alpha_0) \quad (2.66)$$

\*The term  $\frac{F(\alpha)}{R_{turn}}$  comes from the wellbore turning and will be explained in the next section of this chapter. The value will be zero if there is no right or left turn;  $F$  means if tension force  $F > 0$  and if compressive force  $F < 0$ .

#### 2.5.4 Pulling the pipe out of the hole while the wellbore turns

This section will discuss mainly drag calculations from the top view while pulling out of the hole. The explanation will be covered largely on the wellbore turning either right or left in each section. This will be similar to those of the vertical calculations; however, the  $W$  term will not be considered in each equation, due to it is a horizontal view.

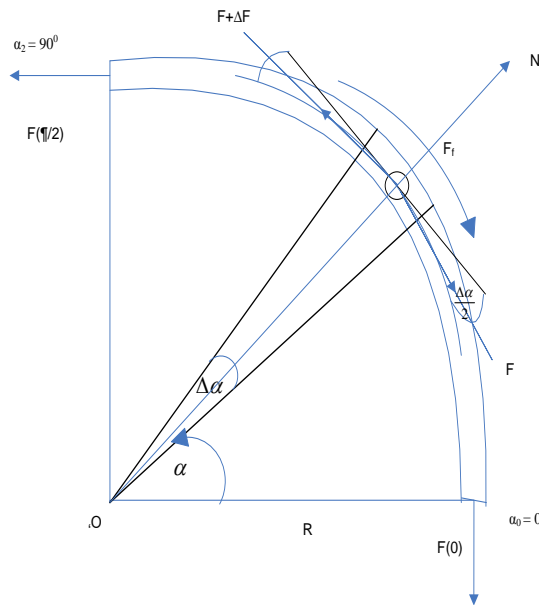


Fig. 2.19—Illustration of forces when the wellbore turns right (pulling the pipe out of the hole, horizontal view).

From **Fig. 2.19**  $\Sigma F$  along N axis

$$N_{turn} R \Delta \alpha = (F + \Delta F) \sin \frac{\Delta \alpha}{2} + F \sin \frac{\Delta \alpha}{2} \quad (2.67)$$

$$N_{turn} = \frac{2F}{R \Delta \alpha} \sin \left( \frac{\Delta \alpha}{2} \right) + \frac{\Delta F}{R \Delta \alpha} \sin \left( \frac{\Delta \alpha}{2} \right) \quad (2.68)$$

When  $(\Delta \alpha \rightarrow 0)$ , then  $\sin \left( \frac{\Delta \alpha}{2} \right)$  will approach close to 0;  $N_{turn} = \frac{F(\alpha)}{R}$

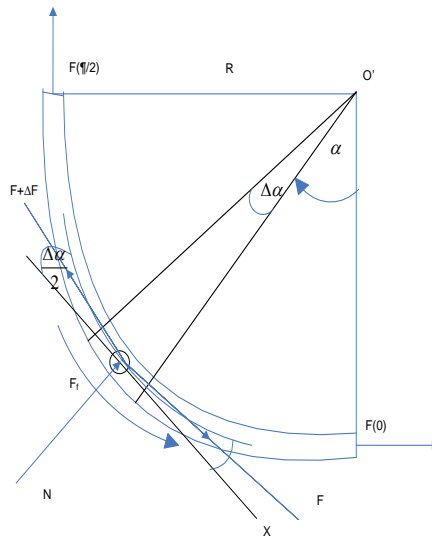


Fig. 2.20—Illustration of forces when the wellbore turns left (pulling the pipe out of the hole, horizontal view).

From **Fig. 20**  $\Sigma F$  along N axis will be illustrated as follows:

$$NR \Delta \alpha = -(F + \Delta F) \sin \frac{\Delta \alpha}{2} - F \sin \frac{\Delta \alpha}{2} \quad (2.69)$$

From the above equation, divided by  $R \Delta \alpha$ , thus

$$N = -\frac{2F}{R \Delta \alpha} \sin \left( \frac{\Delta \alpha}{2} \right) - \frac{\Delta F}{R \Delta \alpha} \sin \left( \frac{\Delta \alpha}{2} \right) \quad (2.70)$$

When  $(\Delta \alpha \rightarrow 0)$ , then  $\sin \left( \frac{\Delta \alpha}{2} \right)$  will approach close to 0;  $N_{turn} = \frac{F(\alpha)}{R}$

## 2.6 Conclusion

This section provides all necessary drag equations for three separate operations in the wellbore: rotating at bottom, lowering the pipe into the hole, and pulling the pipe out of the hole. This also provides the first order differential equation that will be used in the torque and drag calculations by the Visual Basic Application (VBA) program, which will provide the numerical solution from the torque and drag equations and the weight (W) that represents effective weight  $W_e$  as:

$$W_e = W_{air} * (1 - \frac{\rho_{mud}}{\rho_{steel}}) \quad (2.71)$$

The next chapter will discuss torque calculations by considering the tortuosity effect and giving recommendations on how to prevent this effect.

## CHAPTER III

### WELL PLANNING IN THREE-DIMENSIONAL WELLBORE

#### 3.1 Introduction

This particular program requires input from field data, starting from the tie-on survey to input parameters of MD TVD NC EC I AZ DLS and target directions of MD TVD NC EC. The wellbore path has started from the tie-on survey position to the target direction. The shape of the wellbore outcome will depend largely on which type of wellbore that the user has selected from the beginning. We input the required type of the wellbore data that should be used. As a result, we will have the final wellbore path in 3D from the tie-on survey to the target direction, however it depends on which type of wellbore that we chose. The overview project will be separated into 4 sections. Firstly, it will be well-planning calculations from tie-on surveys to target direction by using Visual Basic Application Software in an Excel Program to calculate the well plan. Secondly, it will be torque and drag calculations based on 3D equations by using Visual Basic Application. Thirdly it will display on wellbore planning in 3D program (by using MATLAB program to display wellbore path). Lastly, gathering all of the information in a software application program.

Note: *MD* - The actual distance traveled along the borehole, ft

*TVD* - The vertical distance between a specific location in a borehole and a horizontal plane passing through the surface, ft

*NC* - The distance traveled in the north-south direction in the horizontal plane (north is positive, south is negative), ft



- EC - The distance traveled in the east-west direction in the horizontal plane (east is positive, west is negative), ft
- $I, \theta$  - A deviation or the degree of deviation from the vertical
- $I_M$  - Moment of inertial of pipe, in (Gaynor et al. 2002)
- AZ - The direction or bearing toward which a sloping surface faces (e.g., a north-facing slope has an azimuth angle of  $360^\circ$ ; a northeast-facing slope, an azimuth angle of  $45^\circ$ ), degrees
- $D$  - A combination of aerodynamic or hydrodynamic forces which tends to reduce speed, lbf
- $D_{\text{drift}}$  - The average diameter that has been used in torque equations, in
- $D_{\text{ij}}$  - The diameter of tool joint, in

### 3.2 System Modeling

This section demonstrates equations of three-dimensional wellbore between the tie-on survey at the kick off point (KOP) and target direction, meanwhile demonstrating measured depth calculations of each wellbore planning design.

#### 3.2.1 Well-planning and math modeling between surveys

In this research I will show simple types of wellbore shapes (Build & Hold type in three-dimensional wellbore)

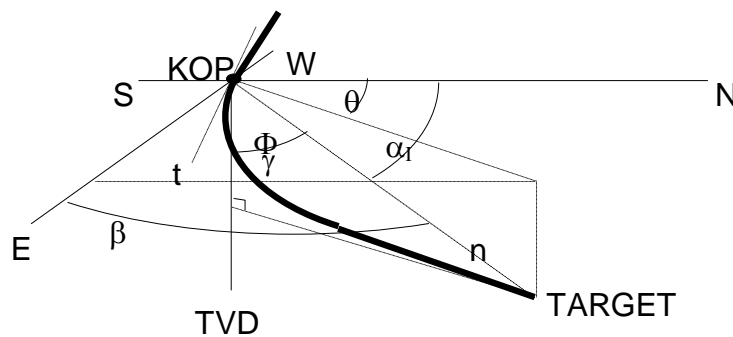


Fig. 3.1–Wellbore build & hold type in three-dimensional wellbore (Well Planning, 1975).

**Fig. 3.1** shows the three-dimensional wellbore design from the KOP to the target direction. It requires the user to put the tie-on survey data at the KOP and target direction. After that the software will calculate wellbore trajectory automatically, depending on which type of wellbore the user will select. **Fig. 3.1** demonstrates how it works, step-by-step as follows:

Calculate  $\Phi$

$$\Phi = \arctan(\text{abs}[EC_{\text{target}}]/\text{abs}[NC_{\text{target}}]) \quad (3.1)$$

### 3.2.1.1 Finding minimum curvature (DLS) to intersect target

Note:  $\Phi, \Delta\theta$  – The change in azimuth angle over the string element, rad.

#### Direction Cosines of the Tangent to the Turn Arc

$$\text{Cos } \alpha; t = \text{Sin}(I) * \text{Cos}(AZ) \quad (3.2)$$

$$\text{Cos } \beta; t = \text{Sin}(I) * \text{Sin}(AZ) \quad (3.3)$$

$$\text{Cos } \gamma; t = \text{Cos}(I) \quad (3.4)$$

#### Direction Cosines of the Line from the KOP to the Target

$$3\text{D Distance from the KOP to the Target} = [\Delta\text{TVD}^2 + \Delta\text{NC}^2 + \Delta\text{EC}^2]^{1/2} \quad (3.5)$$

$$\text{Cos } \alpha; \text{ target} = (\text{NC}_{\text{target}} - \text{NC}_{\text{tie on survey}}) / 3\text{D Distance from the KOP to Target} \quad (3.6)$$

$$\text{Cos } \beta; \text{ target} = (\text{EC}_{\text{target}} - \text{EC}_{\text{tie on survey}}) / 3\text{D Distance from the KOP to Target} \quad (3.7)$$

$$\text{Cos } \gamma; \text{ target} = (\text{TVD}_{\text{target}} - \text{TVD}_{\text{tie on survey}}) / 3\text{D Distance from the KOP to Target} \quad (3.8)$$

$$\alpha = \arccos(\text{Cos } \alpha; t * \text{Cos } \alpha; \text{ target} + \text{Cos } \beta; t * \text{Cos } \beta; \text{ target} + \text{Cos } \gamma; t * \text{Cos } \gamma; \text{ target}) \quad (3.9)$$

$$\text{Maximum radius of turn} = 3\text{D Distance from the KOP to the Target} / (2\alpha) \quad (3.10)$$

$$\text{Minimum DLS to minimum target} = 18,000 / (\pi * \text{Maximum radius of turn}) \quad (3.11)$$

$$\text{Selected Radius of Turn Arc; R (ft)} = 18000 / (\pi * \text{DLS}) \quad (3.12)$$

Note:  $t$  Tangent section

$\alpha_t$  The angle between the distance traveled in the north-south direction and 3D Distance from the KOP to Target, rad.

$\beta$  - The angle between the distance traveled in the east-west direction and 3D Distance from the KOP to Target, rad.

$\Gamma$  - The angle used to calculate the deviation of the wellbore in tangent section, rad.

$A$  - The angle used to calculate the deviation of the wellbore, rad.

DLS - A normalized estimate (e.g., degrees / 100 feet) of the overall curvature of an actual well path between two consecutive survey stations

#### Length of Selected ARC, S; ft

$$\text{Length e} = \text{Selected radius of turn} / \sin(\alpha) \quad (3.13)$$

$$\text{Length n} = 3\text{D distance from the KOP to target} \quad (3.14)$$

$$\text{Length f} = \text{Selected radius of turn} / \tan(\alpha) \quad (3.15)$$

$$\text{Length d} = ((\text{length n})^2 + (\text{Select radius of turn arch})^2 - 2 * (\text{length n}) * (\text{Select radius of turn arc}) * \sin(\alpha)) \quad (3.16)$$

$$\text{Length k} = \text{sqrt}((\text{length d})^2 - (\text{Select radius of turn arc})^2) \quad (3.17)$$

#### Finding Position in Three-dimensional Wellbores

$$\text{NC}_{\text{turn}} = \text{length e} * \text{Cos } \alpha; \text{ target} + \text{NC}_{\text{kop}} \quad (3.18)$$

$$\text{EC}_{\text{turn}} = \text{length e} * \text{Cos } \beta; \text{ target} + \text{EC}_{\text{kop}} \quad (3.19)$$

$$\text{TVD}_{\text{turn}} = \text{length e} * \text{Cos } \gamma; \text{ target} + \text{TVD}_{\text{kop}} \quad (3.20)$$

$$NC = \text{length } z * -\text{Cos } \alpha; t + NC_{\text{turn}} \quad (3.21)$$

$$EC = \text{length } z * -\text{Cos } \beta; t + EC_{\text{turn}} \quad (3.22)$$

$$TVD = \text{length } z * -\text{Cos } \gamma; t + TVD_{\text{turn}} \quad (3.22)$$

$$\lambda = \text{Acos}(\text{selected radius of turn arc; } R, \text{ ft} / \text{length } d) \quad (3.23)$$

$$B = \text{Acos}((\text{selected radius of turn arc}^2 + \text{length } d^2 - \text{length } n^2) / (2 * \text{selected radius of turn arc; } r, \text{ ft} * \text{length } d)) \quad (3.24)$$

$$\gamma = B - \gamma; (f > 0) \quad (3.25)$$

$$\gamma = 2 * \pi - B - \gamma; (f < 0) \quad (3.26)$$

$$\text{Cos } \alpha = (NC - NC_{\text{kop}}) / \text{Selected radius of turn arch} \quad (3.27)$$

$$\text{Cos } \beta = (EC - EC_{\text{kop}}) / \text{Selected radius of turn arch} \quad (3.28)$$

$$\text{Cos } \gamma = (TVD - TVD_{\text{kop}}) / \text{Selected radius of turn arch} \quad (3.29)$$

Note:  $e, n, z, d, k$  - Length parameters for mathematical algorithm in each wellbore trajectory calculations, ft

$\lambda, B$  - angle parameters for mathematical algorithm calculation, rad.

$$\text{Length } h; \text{ ft} = \text{Selected radius of turn arch} * \text{Cos } (\gamma) \quad (3.30)$$

$$\text{Length } m; \text{ ft} = \text{Selected radius of turn arch} * \text{Sin } (\gamma) \quad (3.31)$$

$$NC_{\text{final}} = N + \text{length } h * \text{Cos } \alpha; 2-4 + \text{length } m * \text{Cos } \alpha; t \quad (3.32)$$

$$EC_{\text{final}} = E + \text{length } h * \text{Cos } \beta; 2-4 + \text{length } m * \text{Cos } \beta; t \quad (3.33)$$

$$TVD_{\text{final}} = TVD + \text{length } h * \text{length } m + \text{length } m * \text{Cos } \gamma; t \quad (3.34)$$

$$\text{Cos } \alpha; k = (NC_{\text{target}} - NC_{\text{final}}) / \text{length } k \quad (3.35)$$

$$\text{Cos } \beta; k = (EC_{\text{target}} - EC_{\text{final}}) / \text{length } k \quad (3.36)$$

$$\text{Cos } \gamma; k = (TVD_{\text{target}} - TVD_{\text{final}}) / \text{length } k \quad (3.37)$$

$$\Delta \text{ North/South } k; \text{ ft} = NC_{\text{target}} - NC_{\text{final}} \quad (3.38)$$

$$\Delta \text{ East/West } k; \text{ ft} = EC_{\text{target}} - EC_{\text{final}} \quad (3.39)$$

$$\Phi = \text{Arctan}(\text{abs}(\Delta \text{ East/West}) / \text{abs}(\Delta \text{ North/South})) \quad (3.40)$$

### 3.2.1.2 Example tie-on surveys and target directions

**Table 3.1–Input field data for tie-on surveys and target directions**

**a) Target direction**

MD	TVD	NC	EC
6955	5000	-3000	2000

**b) Tie-on survey at KOP**

MD	TVD	NC	EC	I	AZ	DLS
90	90	-100	-70	57	300	5

Note:  $h, m$  – Length parameters for mathematical algorithm in each wellbore trajectory calculations, ft

From **Table 3.1**, we can calculate the above data and represent into 2D; one will be the surface plane, and the other will be the side view plane. After that we bring the data into the MATLAB program to represent 3D (**Figs. 3-2, 3-3 and 3-4**).

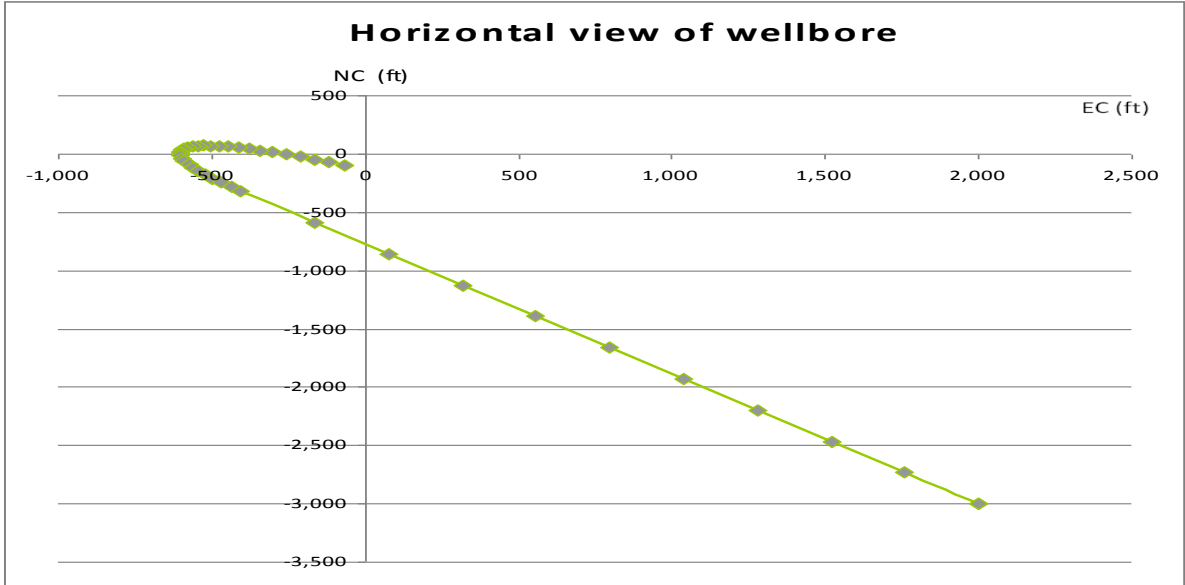


Fig. 3.2–Horizontal view of wellbore.

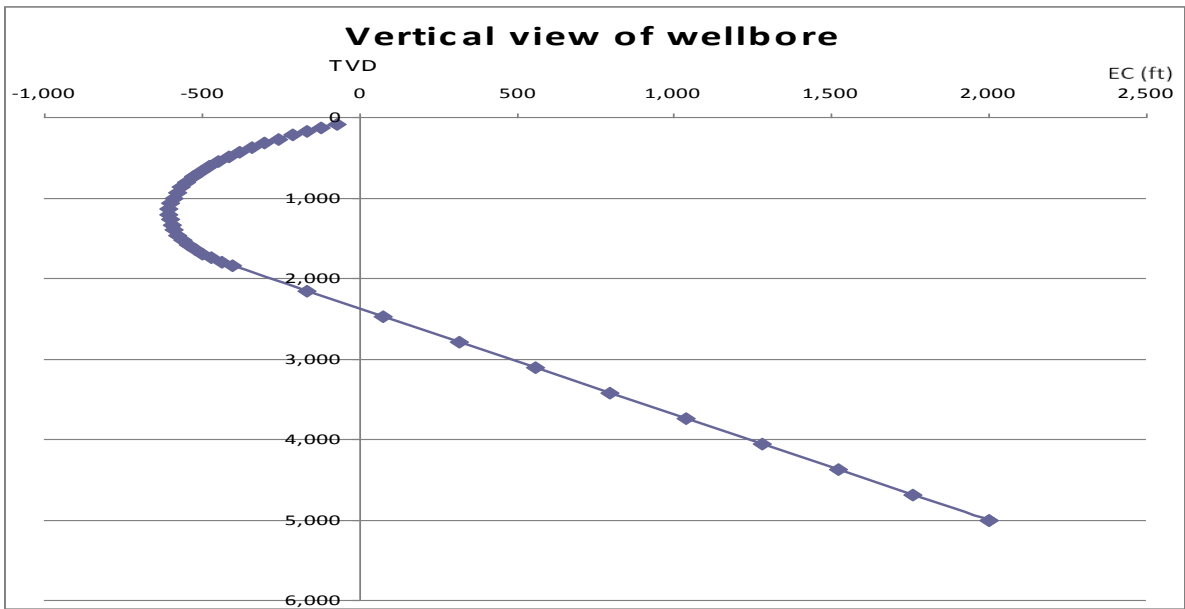


Fig. 3.3–Vertical view of wellbore.

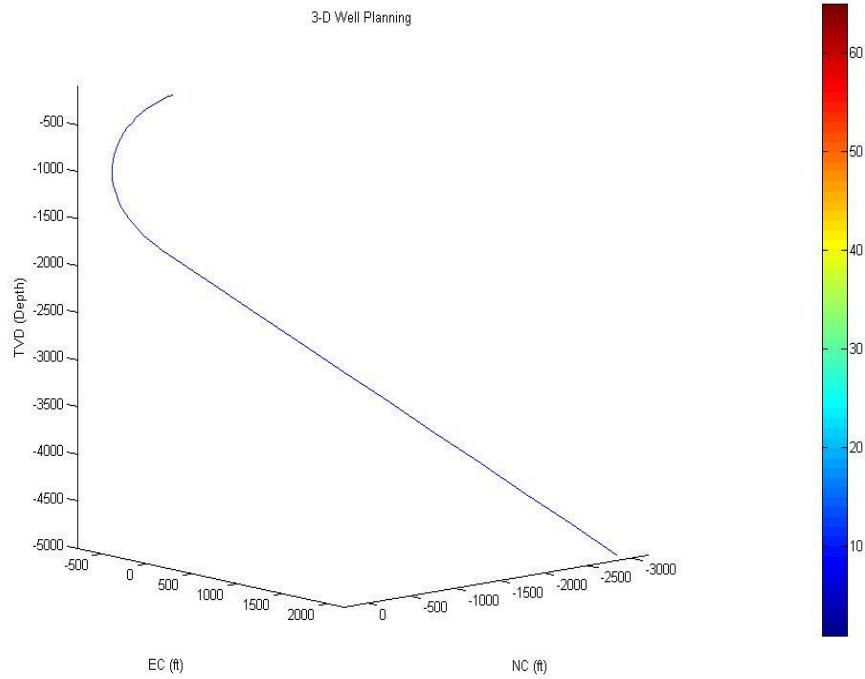


Fig. 3.4–3D wellbore path by MATLAB version 7.4.0.

### 3.2.2 Well-planning and math modeling for build type

This section illustrates wellbore in build type wellbore and also provides an equation to calculate measured depth (MD) (**Fig. 3.5**).

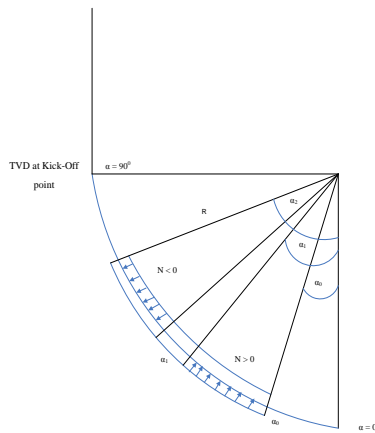


Fig. 3.5–Build type well design.

$$MD = T_{kop} + R * ((\Pi / 2) - \alpha_0) \quad (3.41)$$

### 3.2.3 Well-planning and math modeling for build and hold type

This section illustrates wellbore of build and hold type and also provides an equation to calculate measured depth (MD) (**Fig. 3.6**).

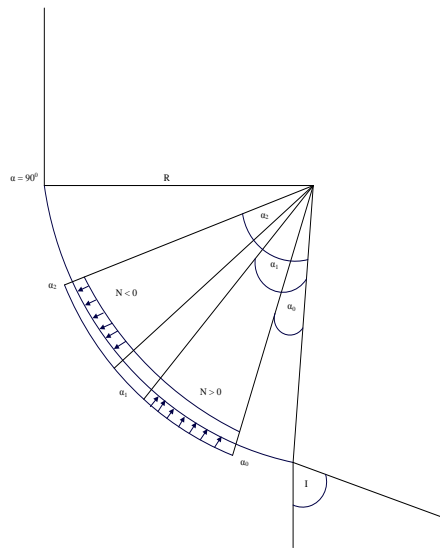


Fig. 3.6—Build and hold type well design.

$$MD = T_{kop} + R * ((\Pi / 2) - \alpha_0) + L_{tan} \quad (3.42)$$

### 3.2.4 Well-planning and math modeling for build hold and drop type

This section illustrates wellbore in build and hold type and also provides an equation to calculate measured depth (MD) (**Fig. 3.7**).



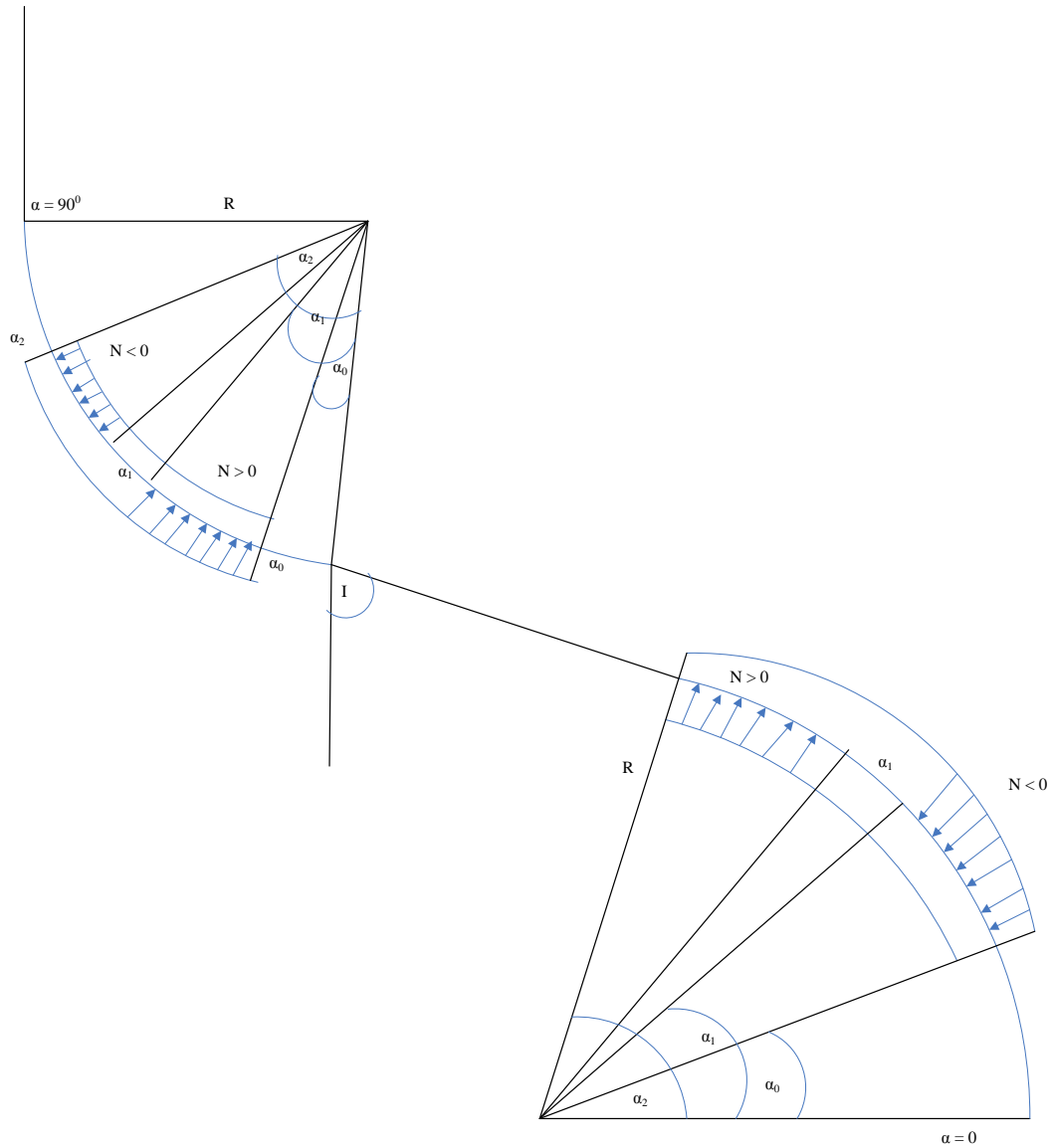


Fig. 3.7–Build hold and drop type well design.

$$MD = T_{kop} + R * ((\Pi / 2) - \alpha_0) + L_{tan} + R_{drop\ section} * (I - \alpha_{0,drop}) \quad (3.43)$$

### 3.2.5 Well-planning and math modeling for horizontal well design type

This section shows wellbore in horizontal well design type and also provides an equation to calculate measured depth (MD) (**Fig. 3.8**).

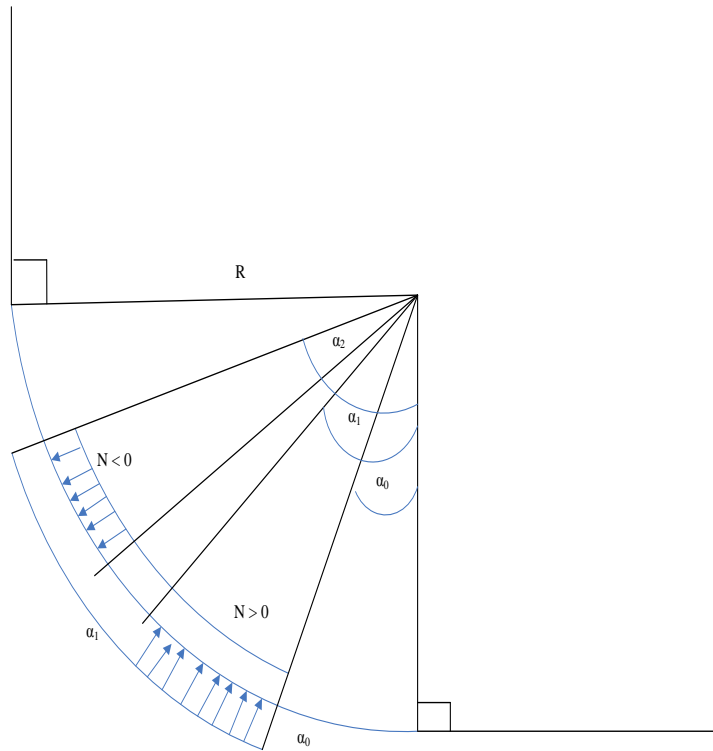


Fig. 3.8–Horizontal well design.

$$MD = T_{kop} + R * (\Pi / 2) + H_L \quad (3.44)$$

**Figs. 3.2** through **3.8** represented in horizontal view plane and  $R$  in this chapter is the radius of curvature in vertical view plane. However, for making 3D we need to have  $R_{turn}$  (radius of curvature in horizontal view plane which has already been mentioned in Chapter II) calculation.

## CHAPTER IV

### TORTUOSITY IN THREE-DIMENSIONAL WELLBORES AND THE EFFECT OF TORTUOSITIES ON TORQUE CALCULATION

#### 4.1 Introduction

Tortuosity occurs when a well has a deviation from a straight hole. The most commonly known tortuosity is a dogleg severity variation. However the tortuosity that we will emphasize pertains to the torque and drag calculation and includes micro-tortuosity in which the axial hole is spiraled instead of straight. This occurs when the bottom hole assembly uses the mud motor system and can be minimized by using a rotary steerable system instead. In this chapter we will consider the tortuosity effect and the effect of the equations that will be used in the torque and drag software. Since micro-tortuosity can cause poor hole quality, and spiraling is the primary cause of micro-tortuosity, eliminating these problems will improve hole quality tremendously.

#### 4.2 Oscillation in the Wellbore

Total tortuosity of an “as-drilled” well (T) can be calculated as the sum of the planned tortuosity ( $T_1$ ), the large-scale tortuosity ( $T_2$ ), and the micro tortuosity ( $T_3$ ):

$$T_{\text{total}} = T_1 + T_2 + T_3 \quad (4.1)$$

The following will explain the definition of each term.

$T_1$  is a planned tortuosity and will represent the summation of the total curvature including inclination and azimuth in the planned well trajectory divided by the well depth. For example, using degrees/100 feet for a well that builds from the vertical to 60 degrees inclination and, assuming no change in azimuth angle, will achieve a total curvature of 60 degrees. By having a total curvature of 60 degrees and the measured depth of the well of 10,000 feet, the planned tortuosity will be  $60/(10,000/100)$  or  $0.6^\circ/100$  ft.

Large Scale Tortuosity ( $T_2$ ) is the summation of the total curvature (inclination and azimuth changes) when a drilled well is measured by measurement while drilling (MWD) survey in dogleg severity and then subtracted by the planned tortuosity ( $T_1$ ). These dogleg results can vary from survey to survey and may take 30 to 90 feet, depending on which type of survey is being used in the drilling process. The result of changing rig activity from sliding to high dogleg rotation can lead to a section of high dogleg followed by a section of lower dogleg. Consequently, it will create a condition similar to the large scale tortuosity.

Micro-Tortuosity ( $T_3$ ) is defined as the tortuosity that occurs in the wellbore that is smaller in comparison to previous tortuosity. This phenomenon is from the spiral effect when drilling tools run into the wellbore with the rotary assembly, motor assembly and rotary assembly systems. The only ways to measure the micro-tortuosity are by the advanced wireline survey techniques, MWD acoustic caliper tools, and the application of back calculated friction factor.

### 4.3 Borehole Oscillations

The presence of borehole rippling, spiraling, and hour-glassing have been known for many years in the drilling industry. There have been publications in many papers concerning oscillation problems in the borehole due to the micro-tortuosity effect.

However, this research will largely consider equations that will be used in unpredictable situations and in difference shapes of hole spiral. They have to be tested for the borehole spiraling effects like bit speed, penetration rate, and rock strength. From these experimental situations, general guidelines can be derived on how to select the appropriate bit, BHA, and operating parameters, as well as rotary steerable tools.

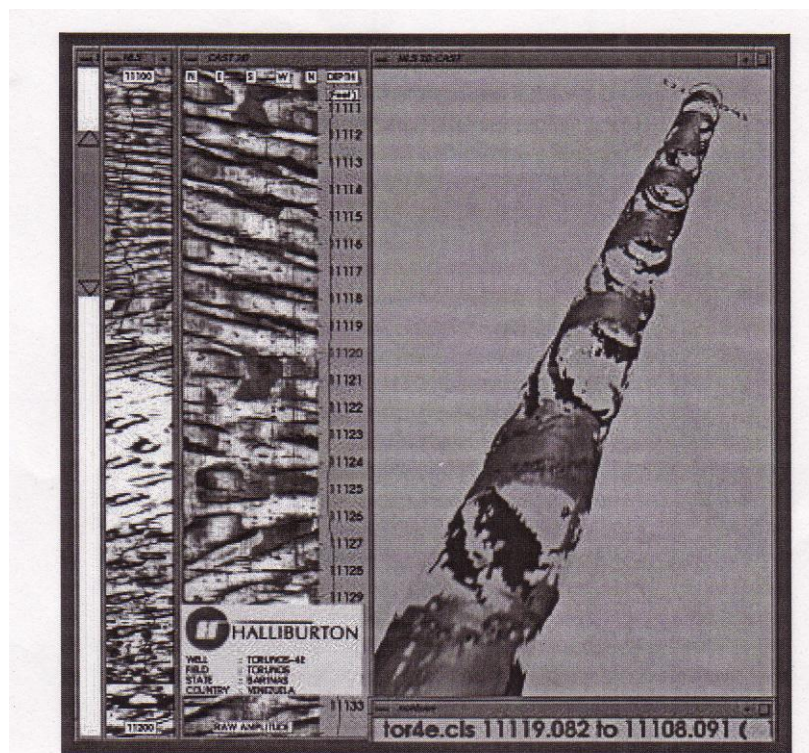


Fig. 4.1–Spiral borehole as shown in 2D (Tracks 1 and 2) and 3D images (Gaynor et al. 2002).

**Fig. 4.1** illustrates spiral borehole images taken from the wireline CAST (Circumferential Acoustic Scanning Tool) in a well in South America. The evidence of the spiraling hole is represented in the strong diagonal response of the CAST images running across the compressed and expanded 2D images as presented in tracks 1 and 2. The reverse 3D image is clearly presented in track 3 which indicates the wellbore spiraling while drilling. Note that the spiral seems to change its direction from time to time and has a pitch length of approximately 2 feet.

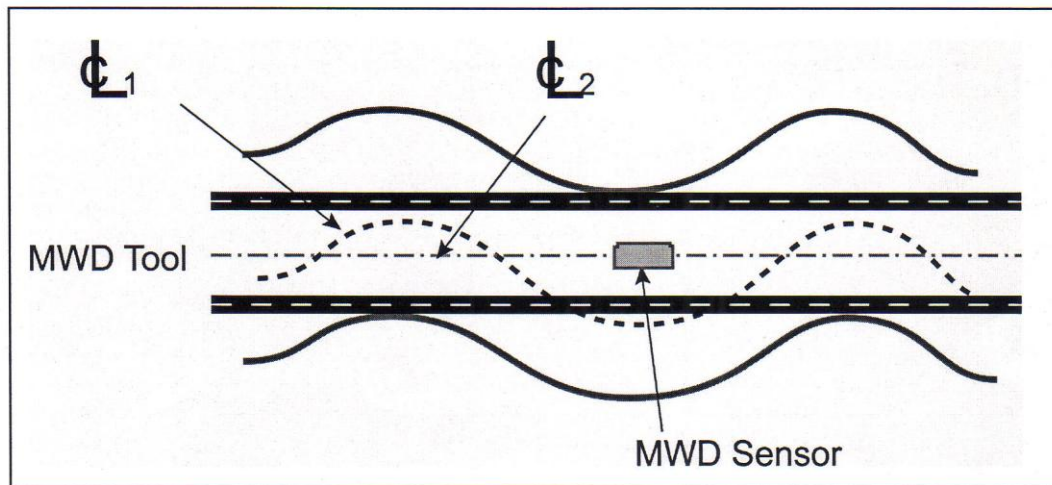


Fig. 4.2—An MWD survey tool cannot detect a tight spiral (Gaynor et al. 2002).

**Fig. 4.2** illustrates that short pitch tortuosity is cancelled over 30 feet (shown by centerline 1) because it measures the inclination and drift's direction (shown by centerline 2) instead of the wellbore itself. MWD cannot detect spiral hole because it measures the inclination and drift's direction instead of the wellbore itself.

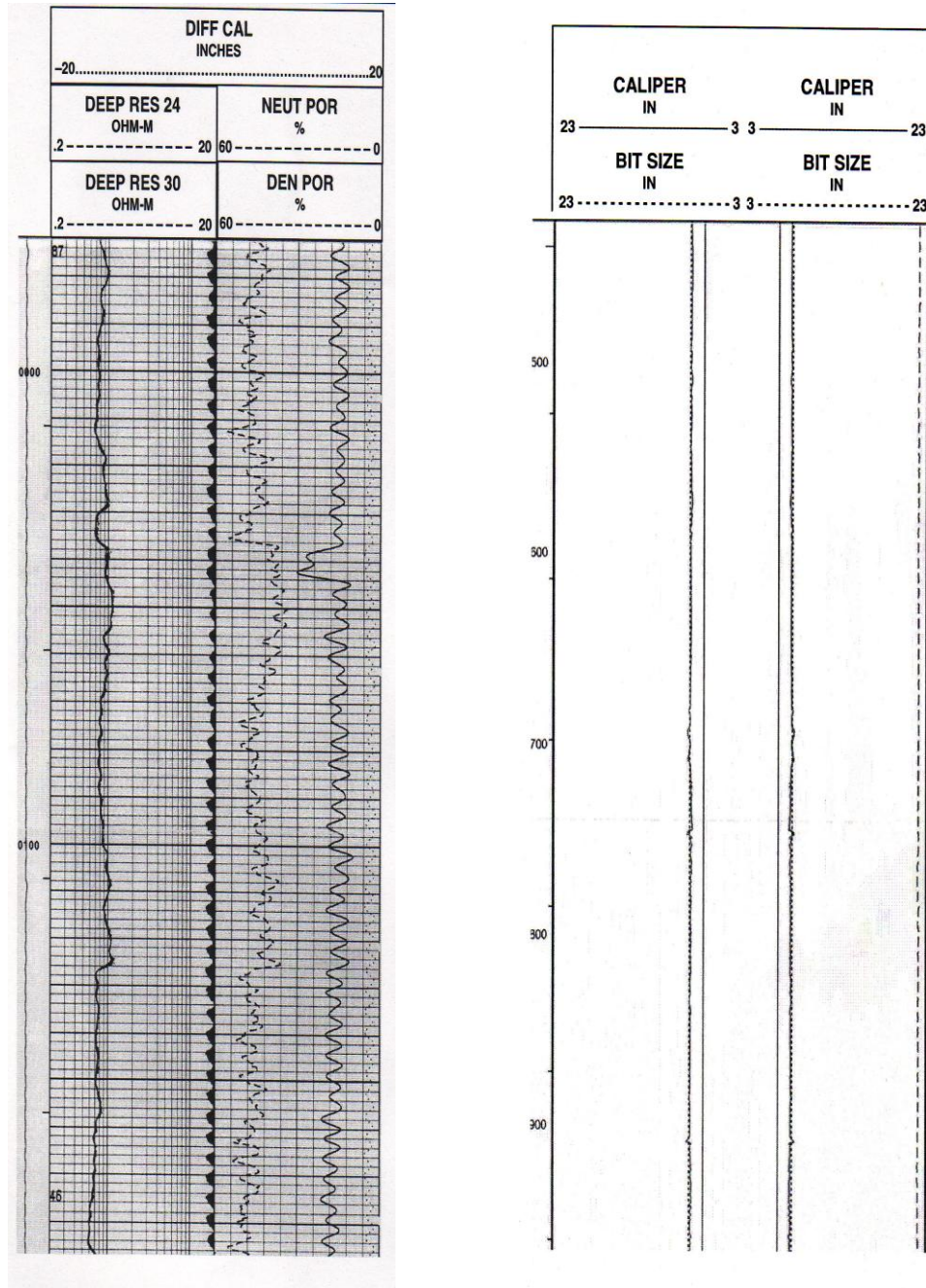


Fig. 4.3—Illustrates the evidence of profound spiraling (Gaynor et al. 2001).

**Fig. 4.3** illustrates a spiral hole as detected by a differential caliper tool on a wireline density measurement at a well in the Gulf of Mexico. The log indicates that the hole is under gauge approximately 1.5” for every 4 feet and rarely over gauge level. This

phenomenon is repeated over thousands of feet on this log. This drilling section had a 9-7/8" bit and 6-3/4" collars. Using the drift equation (new wellbore) calculation, there will be 8.31", a 1.56" (16%) reduction in wellbore OD which is exactly the same magnitude measured by the wireline tool. The reduction in the cross section area (drift vs. hole size) is calculated to equal 22.32 in<sup>2</sup> (29%). Compare this to the figure on the right, which illustrates a perfectly gauged hole drilled with a new steerable system (a matched long gauge bit and positive displacement mud motor) [The entire 12,000 ft interval drilling is only 2.7 days with no short trip.]

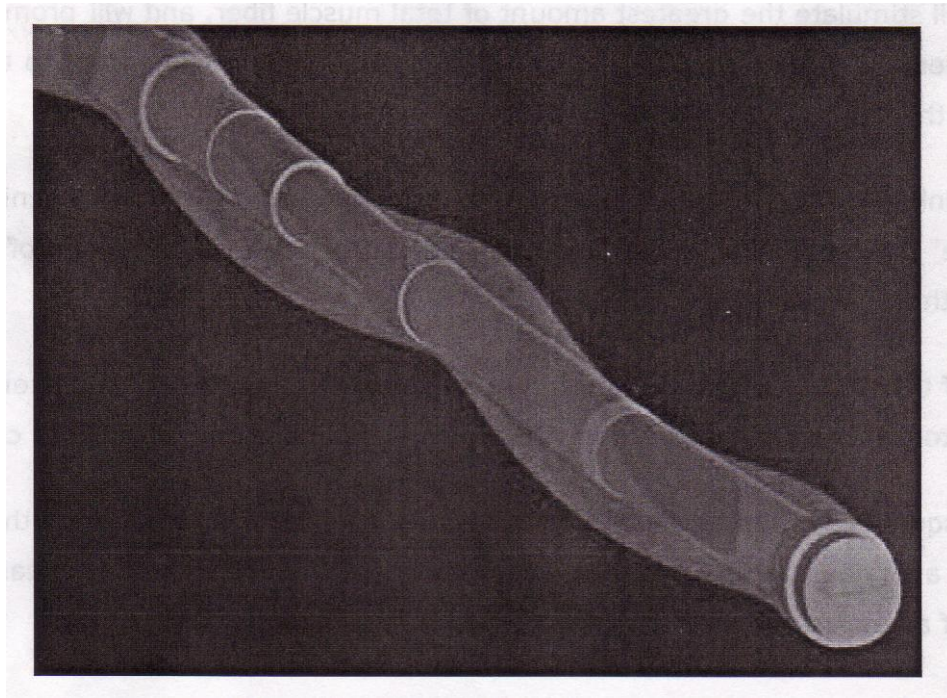


Fig. 4.4–3D CAD model of 12-1/4" borehole (Patusek, Brackin, and Christensen 2003).

Some of the bends in the BHA may be smoothed by drilling a spiraled hole. **Fig. 4.4** is a 3D CAD model of a 12-1/4" borehole from an offshore site in the Gulf of Mexico (GOM) with a model of the BHA that is placed as a spiral to minimize its contact points.



When this is animated for pipe rotation, it can be seen that spiraling hole is one way for the BHA to relax its preload.

There are at least three key issues to be analyzed and optimized when drilling directional wells with motors: tool face control, dogleg severity (DLS), and borehole quality. This thesis will focus on hole problems from the well path, not from sloughing, caving, erosion, etc. There are several types of oscillations that have been described in the past, often with different or conflicting names.

#### 4.4 Model of Borehole Oscillations

**Figs. 4.5 through 4.7** will show the different types of borehole tortuosities that occur in the wellbore.

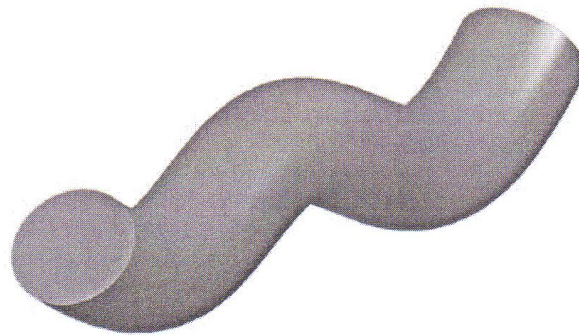


Fig. 4.5–Rippling 2D oscillation (Patusek et al. 2003).

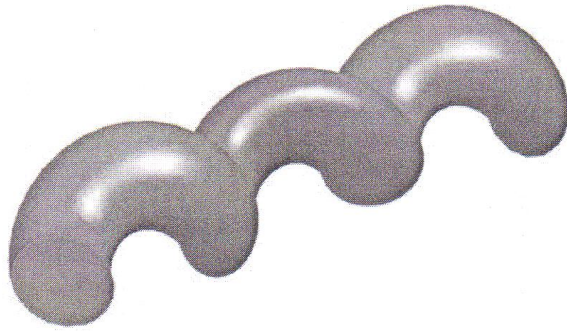


Fig. 4.6–Spiraling 3D corkscrew (Patusek et al. 2003).

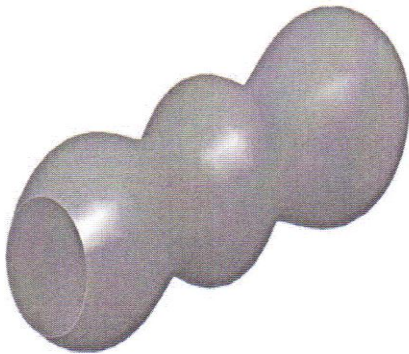


Fig. 4.7–Hour-glassing cyclic hole enlargement (Patusek et al. 2003).

The above three figures represent borehole rippling, spiraling, and hour-glassing, which have been known for many years in the drilling industry. Descriptions of these problems have become more precise with improved logging tools, yet the underlying mechanisms have not been presented in the past nor have there been any attempts to explain the steady state in response to the bottom hole assembly. Little has been published on the non-equilibriums or dynamics relating to the system.

There are at least three types of oscillations that have been described in the past. They are rippling/undulations, helical spiraling/corkscrew, and hour-glassing. The above figures represent the exterior of the three most common forms of borehole oscillation.

The oscillation can be solved by the drift equation. This will affect torque equations mentioned earlier, which will become more accurate and affect all of the torque equations.

#### 4.5 Mathematical Model for Torque Calculations

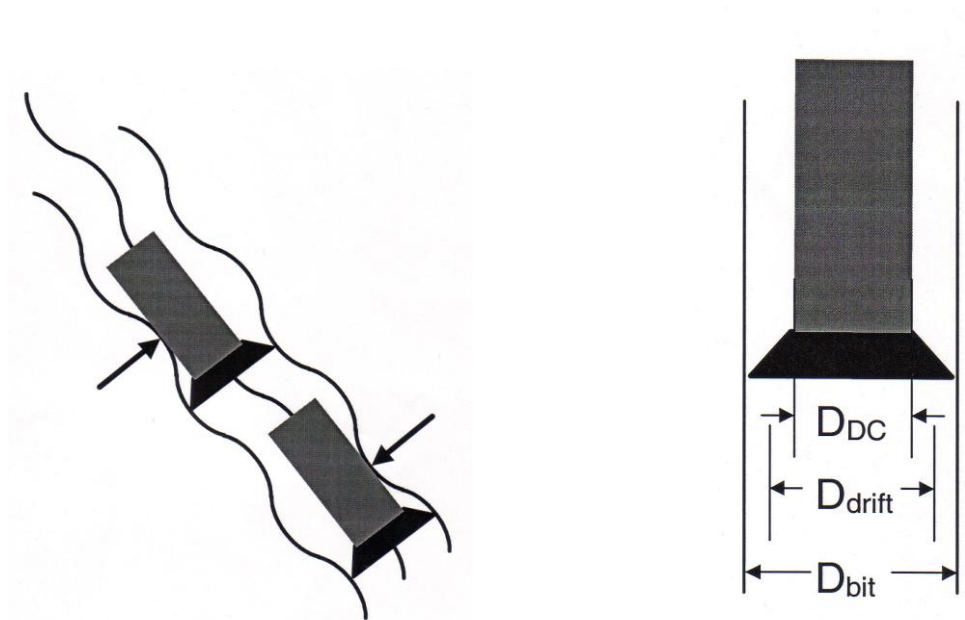


Fig. 4.8—Showing the two-dimensional schematic of the drift equation (Gaynor et al. 2001).

The collars will act directly to limit the amount of lateral movement of the bit off the center line of the hole (**Fig. 4.8**). Thus the spiral amplitude will be determined by the relative size of the bit and collars. This is exactly what was described by determining the

maximum wellbore “drift.” Using Lubinski’s calculation for maximum drift creates a crooked hole as (Rezmer-Cooper, Chau, Hendricks, Woodfine, Stacey, and Downton 1999):

$$D_{\text{drift}} = (\text{Bit Diameter} + \text{Collar Diameter})/2 \quad (4.2)$$

Torque calculations in build and drop sections from Chapter II will use the adapted equation by (Maidla and Haci 2004):

$$T(\alpha_2) = \int_{\alpha_0}^{\alpha_2} \mu |N(\alpha)| \frac{D_{\text{drift}}}{24} R d\alpha \quad (4.3)$$

However, the next step of this equation will be separated by the integral theory, thus

$$T(\alpha_2) = \int_{\alpha_0}^{\alpha_1} \mu |N(\alpha)| \frac{D_{\text{drift}}}{24} R d\alpha + \int_{\alpha_1}^{\alpha_2} \mu |N(\alpha)| \frac{D_{\text{drift}}}{24} R d\alpha \quad (4.4)$$

And it will depend on how the drillstring contacts the wellbore. From **Eq. 4.4** and  $N(\alpha)$  from Chapter II, using visual basic application software will give us a numerical method to solve torque and drag in the wellbore.

## CHAPTER V

### STRESS CONCENTRATION WITHIN TOOL JOINT

#### 5.1 Introduction

In this section we will mainly consider the stress between drillpipe connections.

Although this will not affect the torque and drag in the wellbore, this will help the user to be aware of the drillpipe failure while working in the borehole. If the torque between connections exceeds the recommended torque, it will affect the pulling out of the hole phase since the drillstring connection cannot be broken. This might cause the drillpipe to buckle while the drillstring is in the wellbore. This chapter will use the back calculation to prevent the above-mentioned problem with the tripping process. This will help to confirm and warn the rig personnel of any upcoming situation.

#### 5.2 Stress Concentration

This section will address a new Stress Concentration Factor (SCF) analysis methodology for Rotary Shouldered Connections (RSCs) by using Finite Element Analysis (FEA) as a primary tool to explore the maximum peak trends in RSCs and calculating SCF to represent the connection performance (Ring, Deltombe, York, and Baker 2007). Also in this chapter we will cover the SCF analysis methodology and its application in the evaluation of drillstring connection designs, advanced rotary shouldered connection designs incorporating multiple shoulders, and metal-to-metal seals as well as further

adding to the complexity of the stress distribution throughout the connection (Plessis, You, and Prideco 2005).

The Stress Concentration Factor (SCF) is an important and useful parameter to evaluate the maximum peak stress within the connection in response to an operational pipe's load.

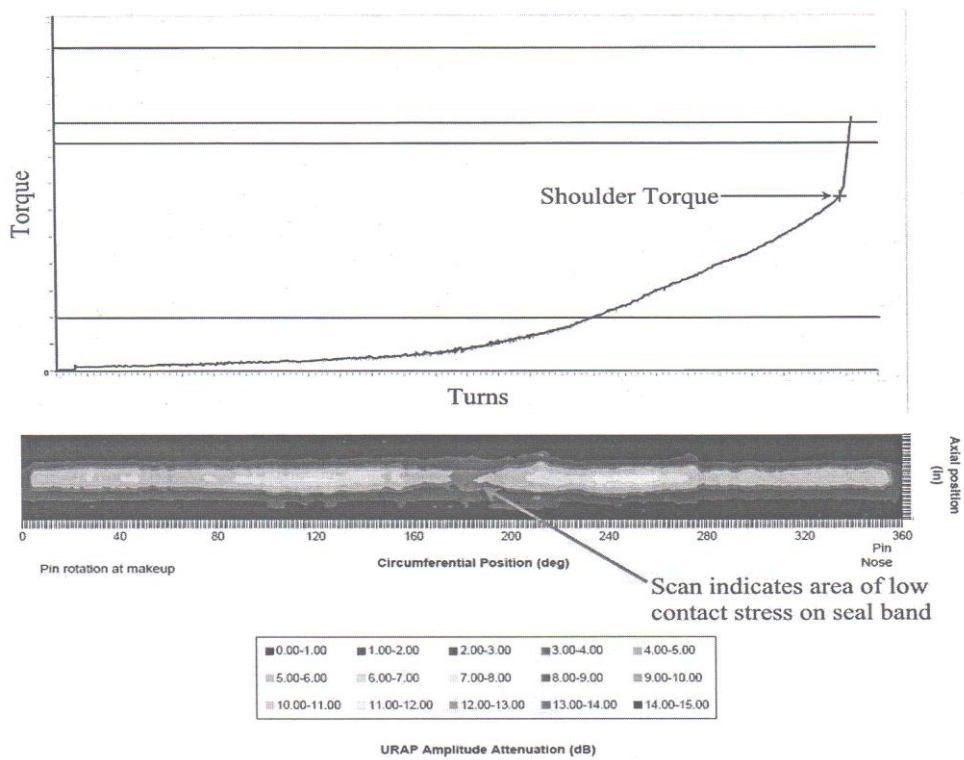
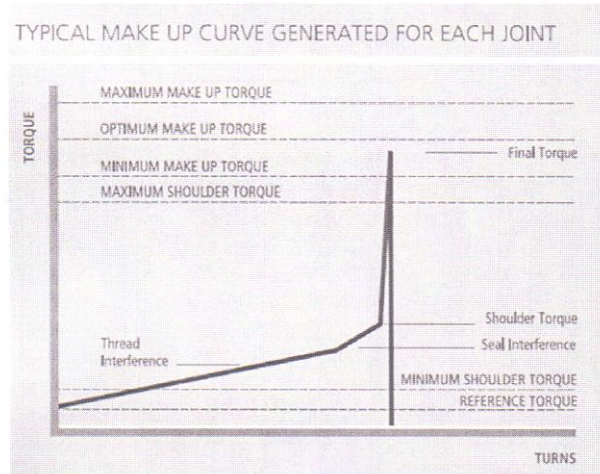


Fig. 5.1–Torque-turn curve (Hamilton, Wagg, and Roth 2007).

Torque-turn curve of a premium connection that has passed the vendor make-up acceptance criteria and the ultrasonic representation of contact stress along the connection's metal-to-metal seal.



Courtesy of Tenaris Connections

Fig. 5.2—Representative torque-turn curve with torque ranges shown (Hamilton et al. 2007).

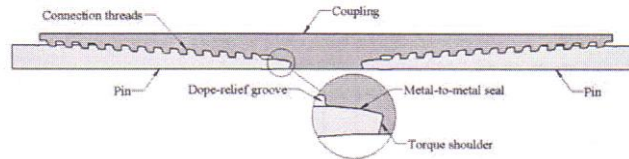


Fig. 5.3—Cross-sectional view of a typical premium connection shown (Hamilton et al. 2007).

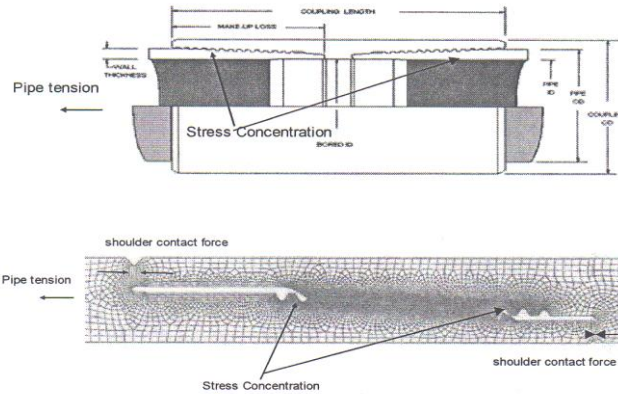


Fig. 5.4—A comparison of a premium casing connection and a proprietary rotary shouldered connection (Tang et al. 2006).

Figures 5.1 through 5.4 show that the connection stress forces as well as torque are more than normal along the drillpipe. Because of the increasingly aggressive drilling conditions and newer applications requiring multiple shoulders and metal-to-metal seals in rotary shouldered connections, the need for SCF analysis ensues. This research's results on a number of evaluations suggest further explorations on various aspects of SCF analysis to find a logical and conservative approach to evaluate the maximum peak stress trend in rotary shouldered connections in response to applied pipe loads. This will help to understand RSC fatigue characteristics in newer applications.

### 5.3 Mathematical Model for the Stress Concentration Factor

The stress Concentration Factor (SCF) is a concept for well-defined various mechanical systems. It is also defined as a ratio of the peak stress ( $\Sigma$ ) versus normal stress ( $\sigma$ ). Peak stress is the highest principal stress at a geometric discontinuity location.

$$\text{SCF} = \Sigma/\sigma_{\text{app}} \text{ or } \Sigma = \text{SCF} * \sigma_{\text{app}} \quad (5.1)$$

It is quite simple and straightforward if the mechanical system is at a zero preload condition, such as welded offshore structures. In this matter the maximum peak stress can be proportionally calculated through the SCF value based on a known applied normal stress  $\sigma_{\text{app}}$ . But if the mechanical system has a large amount of preload during an assembly process like the makeup process in RSCs, the definition of the Stress Concentration Factor has to be revised to the following:

$$\text{SCF} = (\Sigma - \Sigma_{\text{mean}}) \quad (5.2)$$



Another similar parameter is the Stress Amplification Factor,

$$SAF = (\Sigma - \Sigma_{preload}) / (\sigma_{app} - \sigma_{preload}) \quad (5.3)$$

As a result, the only difference between these two equations is the reference stress; the SCF equation references any of the operational mean stresses: The SAF equation references a specified preload stress, which is referred to as makeup stress. The SCF or SAF is associated with a pre-defined reference stress point, either “preload stress” or “mean stress.” It involves two components,  $\Sigma_{mean}$  or  $\Sigma_{preload}$  and  $\sigma_{mean}$  or  $\sigma_{preload}$ . The peak stress change ( $\Sigma - \Sigma_{mean}$ ) is actually a result of change in the pipe stress ( $\sigma - \sigma_{mean}$ ). Then, if one needs to know the absolute peak stress level, especially at a geometric discontinuity location proportional to an applied load or stress in the pipe body, the formula can be used as follows:

$$\Sigma = \Sigma_{mean} + SCF * \Delta \text{pipe-stress} \quad (5.4)$$

$$\text{Where } \Delta \text{pipe-stress} = \sigma_{app} - \sigma_{mean} \quad (5.5)$$

A similar approach for SAF will be:

$$\Sigma = \Sigma_{pre-load} + SAF * \Delta \text{pipe stress} \quad (5.6)$$

$$\text{Where } \Delta \text{pipe stress} = \sigma_{app} - \sigma_{pre-load} \quad (5.7)$$

In this research, a practical analysis approach is recommended to address these three concerns with SCF for RSCs being defined as follows:

$$\Sigma_{max} = \Sigma_{max \text{ mean}} + SCF * \Delta \text{pipe stress} \quad (5.8)$$

$$\text{Where } \Delta \text{pipe stress} = \sigma_{app} - \sigma_{mean} = (f_{app} - f_{mean}) / A \quad (5.9)$$

$$SCF = (\Sigma_{\max} - \Sigma_{\max \text{ mean}})/(\sigma_{\text{app}} - \sigma_{\text{mean}}) \quad (5.10)$$

$$SCF = A*(\Sigma_{\max} - \Sigma_{\max \text{ mean}})/(f_{\text{app}} - f_{\text{mean}}) \quad (5.11)$$

**Table 5.1–Maximum SCF values and locations in shouldered connections  
(Tang et al. 2006)**

Rotary Shouldered Connection	Max. SCF up to Pipe Tension Capacity	Max. SCF up to TJ Tension Capacity	Makeup Torque (ft-lb)	Critical Location
API NC 38 (4-7/8-in. OD X 2-9/16-in. ID)	1.18	2.77	12,000	Pin Thread #2
1 <sup>st</sup> GEN-38 (4-7/8-in. OD X 2-9/16-in. ID)	1.11	1.13	17,665	Pin Thread #2
2 <sup>nd</sup> GEN-39 (4-7/8-in. OD X 2-9/16-in. ID)	0.91	0.91	22,190	Box Thread #1
API 5-12 FH (7-1/4-in. OD X 3-12-in. ID)	0.66	0.92	43,342	Pin Thread #2
1 <sup>st</sup> GEN-55 (7-in. OD X 4-in. ID)	1.00	1.03	46,347	Pin Thread #3
2 <sup>nd</sup> GEN-57 (7-in. OD X 4-1/4-in. ID)	0.68	0.74	56,600	Box Thread #3

Maximum SCF with specified 4-in or 5-1/2-in pipe configuration is shown in **Table 5.1**;

if the pipe force between connections ( $f_{\text{mean}}$ ) is more than the calculated data that we

have from torque and drag software, we will use

$$SCF = (\Sigma_{\max} - \Sigma_{\max \text{ mean}})/(\sigma_{\text{app}} - \sigma_{\text{mean}}) \quad (5.12)$$

$$SCF = A*(\Sigma_{\max} - \Sigma_{\max \text{ mean}})/(f_{\text{app}} - f_{\text{mean}}) \quad (5.13)$$

Then, finding  $f_{\text{app}}$  and using  $f_{\text{app}}$  for the force between the connections will be called back

calculation. As a result, if the pipe force between connections is ( $f_{\text{mean}}$ ) more than the

calculated data from torque and drag software, we have to use  $f_{\text{mean}}$  for torque and drag calculation.

## CHAPTER VI

### BUCKLING

#### 6.1 Introduction

Buckling is a very important issue in T&D calculation. The buckling can cause an increase in contact force between the string and the wellbore. This means that after the drillstring is released from the derrick, the entire drillstring will be supported by wellbore friction instead of the bit force. This phenomenon, called “lock-up,” occurs when the drillstring weight exceeds the drill string limitation. A lock-up situation can occur when working on coiled tubing operations; if this situation happens, it will cost a lot of money due to increasing the rig time activities.

Buckling, as presented in this chapter, refers to sinusoidal buckling and helical buckling. If the axial compression continues to increase in the string, the buckling will begin when there is the string snake phenomenon along the wellbore (sinusoidal buckling as in **Fig. 6.1**). As the axial compression continues to increase, the buckling will change into a helix drillstring (also known as helical buckling as shown in **Fig. 6.2**).

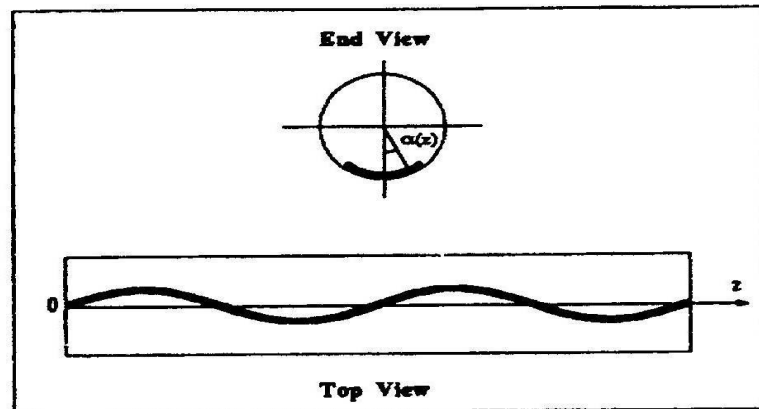


Fig. 6.1–Sinusoidal buckling of the pipe in a horizontal wellbore (Wu and Juvkam-Wold 1993).

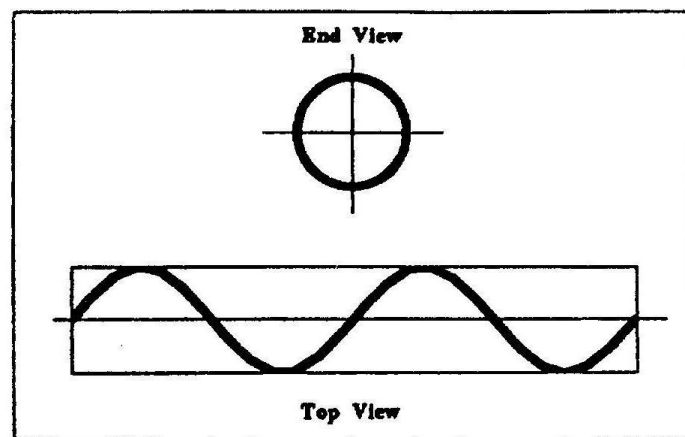


Fig. 6.2–Helical buckling of the pipe in a horizontal wellbore (Wu and Juvkam-Wold 1993).

## 6.2 System Modeling for a Deviation Wellbore

A long pipe in a wellbore will be buckled into a sinusoid along the lower side of the hole at an axial compressive force of Wu and Juvkam-Wold's model (1991)

$$F_s = 2\sqrt{\frac{EIw}{r}} \sin \theta \quad (6.1)$$

A helical buckling mode will not occur until the axial force is (Wu, Chen and Cheatham model)

$$F_H = \sqrt{2} F_s \quad (6.2)$$

Buckling may then be assessed by calculating the friction force and using case selection below to define

$$F < F_s \quad \text{no buckling} \quad (6.3)$$

$$F_s < F < \sqrt{2} F_s \quad \text{sinusoidal buckling initiated} \quad (6.4)$$

$$\sqrt{2} F_s < F < (2\sqrt{2} - 1)F_s \quad \text{helical buckling initiated} \quad (6.5)$$

$$(2\sqrt{2} - 1)F_s < F \quad \text{helical buckling from Wu and Juvkam-Wold's (1991) equation} \quad (6.6)$$

In the case of sinusoidal buckling, there is no significant increase in wall force; however, in the case of helical buckling, wall force increases, and the drilling engineer will pick up the best well design and attempt to avoid the buckling problem. In general for sinusoidal buckling, case may be acceptable, but for helical buckling case has to be avoided. But if the helical buckling is unavoidable, then T&D models need to be improved more; thus, it has to be solved by equations from this research. However in the vertical section, buckling calculations will be used differently.

### 6.3 Buckling in a Vertical Well

In 1950, researchers derived the following buckling load equation for the initial buckling of tubular assembly in vertical wellbores (Rezmer-Cooper et al. 1999):

$$F_s = 1.94 * (EI_M W_e^2)^{1/3} \quad (6.7)$$

A helical buckling load for weighty tubular assembly in vertical wellbores was derived through an energy analysis to predict the occurrence of helical buckling:

$$F_{hel,b} = 5.55 * (EI_M W_e^2)^{1/3} \quad (6.8)$$

The top helical buckling load  $F_{hel,t}$  is calculated by simply subtracting the tubular weight of the initial one-pitch of the helically buckled pipe from the helical buckling load  $F_{hel,b}$ .

$$F_{hel,t} = 0.14 * (EI_M W_e^2)^{1/3} \quad (6.9)$$

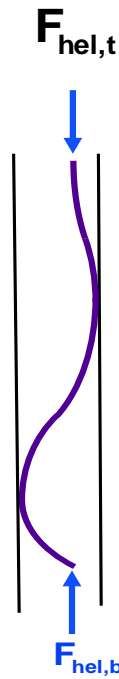


Fig. 6.3–Helical buckling in vertical wellbores.

**Fig. 6.3** shows helical buckling in vertical wellbores when the drilling pipe has compressive force. All of the above equations that illustrate this research are to provide the information towards users and avoid being buckled while working on well planning and drilling processes. The information has already been in T&D software.

## CHAPTER VII

### NUMERICAL METHOD SOLVING T&D CALCULATION

#### 7.1 Introduction

Applying the numerical method solves torque and drag calculations in three-dimensional wellbores. This will benefit future work by others to solve T&D calculations. This chapter will illustrate the numerical method that can be used to solve the torque and drag calculations by using a visual basic application program to solve the equations.

#### 7.2 Euler's Theory

From the first order in differential equations in Chapter II, using Euler's Method in Numerical Analysis serves to illustrate the concepts involved in the advanced methods (Kaw 2006). It has a limitation in use because there are a lot of errors that accumulate during the procedure. However, it is worth studying since the error analysis can be understood easily.

##### 7.2.1 Euler's method

Let  $[a,b]$  be the interval over which we want to find the solution of the well-posed Initial Value Problem (I.V.P.)  $y' = f(t,y)$  with  $y(a) = y_0$ . In actuality, we will not find a differentiable function that satisfies the I.V.P. Instead, a set of points  $(t_k, y_k)$  is generated, and the points are used for an approximation (i.e.,  $y(t_k) \approx y_k$ ). Then how can we proceed to construct a "set of points" that will "satisfy a differential equation



approximately”? First, we choose the abscissas for the points, then for being convenient we subdivide the interval  $[a,b]$  into  $M$  equals subintervals and select the mesh points as follows:

$$T_k = a + kh \text{ for } k=0,1, \dots, M \text{ where } h = \frac{b-a}{M} \quad (7.1)$$

The value  $h$  is called the step size. Now we can proceed to solve the equation approximately.

$$Y' = f(t,y) \text{ over } [t_0,t_M] \text{ with } y(t_0) = y_0 \quad (7.2)$$

Assuming that  $y(t)$ ,  $y'(t)$ , and  $y''(t)$  are constantly continuous, then we use Taylor's theorem to expand  $y(t)$  roughly  $t=t_0$ . For each  $t$  value there exists a value  $c_1$  that lies between  $t_0$  and  $t$ , so that

$$Y(t) = y(t_0) + y'(t_0)(t - t_0) + \frac{y''(c_1)(t - t_0)^2}{2} \quad (7.3)$$

When  $y'(t_0) = f(t_0, y(t_0))$  and  $h = t_1 - t_0$  are substituted in the **Eq. 7.3**, the result is shown below:

$$Y(t_1) = y(t_0) + hf(t_0, y(t_0)) + y''(c_1) \frac{h^2}{2} \quad (7.4)$$

If the chosen step size  $h$  is small enough, we can neglect the second-order term (involving  $h^2$ ) and have

$$Y_1 = y_0 + hf(t_0, y_0) \quad (7.5)$$

This is Euler's approximation; the process is repeated and generates a sequence of points that approximates the solution curve  $y = y(t)$ . The general step for Euler's method is

$$T_{k+1} = t_{k+h}, y_{k+1} = y_k + hf(t_k, y_k) \text{ for } k=0, 1, \dots, M-1 \quad (7.6)$$

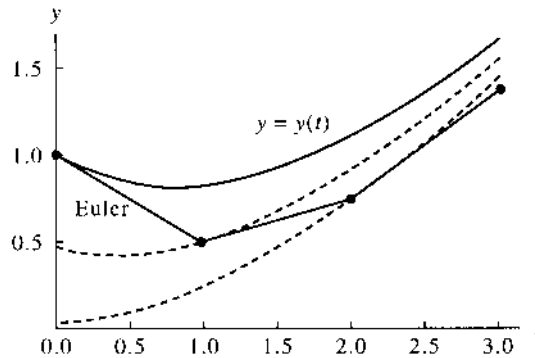


Fig. 7.1–Euler's approximations  $y_{k-1} = y_k + h f(t_k, y_k)$  (John and Fink 2004).

### 7.2.2 Geometric description

As can be seen in **Fig. 7.1**, if you start at the point  $t_0, y_0$  and compute the value of the slope  $m_0 = f(t_0, y_0)$  and move the value of  $h$  horizontally and vertically  $hf(t_0, y_0)$ , then you move along the tangent line to  $y(t)$  and will end up at the point  $(t_1, y_1)$ . Notice that  $(t_1, y_1)$  is not on the desired solution curve. But this is the approximation that we are generating. Hence we must use  $(t_1, y_1)$  as though it were correct and proceed by computing the slope  $m_1 = f(t_1, y_1)$  and use it to obtain the next vertical displacement  $hf(t_1, y_1)$  to locate  $(t_2, y_2)$  and so on.

### 7.2.3 Step size versus error

From above, the methods that we introduce for approximating the solution of an initial value problem are called *difference methods* or *discrete variable methods*. The solution is approximated at a set of discrete points called a grid (or mesh) of points. A basic single-step method has the formula  $y_{k+1} = y_k + h\phi(t_k, y_k)$  for some functions  $\phi$  will be called *increment functions*.

In using any discrete variable method to solve an initial value problem approximately, there will be two sources of errors: discretization and rounding off. Assuming that  $\{(t_k, y_k)\}_{k=0}^M$  is the set of discrete approximations, then  $y = y(t)$  is the unique solution to the initial value problem. The **global discretization error** is defined by

$$e_k = y(t_k) - y_k \text{ for } k=0,1,\dots,M \quad (7.7)$$

There is a difference between the unique solution and the solution obtained by the discrete variable method. The local discretization error  $e_{k+1}$  is defined by

$$e_{k+1} = y(t_{k+1}) - y_k - h\phi(t_k, y_k) \text{ for } k=0,1,\dots,M-1 \quad (7.8)$$

It is the error committed in the single step from  $t_k$  to  $t_{k+1}$ . When we obtained **Eq. 7.4** for Euler's method, the neglected term for each step was  $y''(c_k)(h^2/2)$ . Then if this was the only error at each step, at the end of the interval  $[a,b]$  (after  $M$  steps have been made) the accumulated error would be

$$\sum_{k=1}^M y^{(2)}(C_k) \frac{h^2}{2} \approx M y^{(2)}(c) \frac{h^2}{2} = \frac{hM}{2} y^{(2)}(c) h = \frac{(b-a)y^{(2)}(c)}{2} h = O(h^1) \quad (7.9)$$

There could be some more errors, but this estimate predominates. A detailed discussion on this topic can be found in advanced texts on numerical methods for differential equations. Theorem (Precision of Euler's Method), assumes that  $y(t)$  is the solution to the I.V.P. given. If  $y(t)$  in  $C^2[t_0, b]$  and  $\{(t_k, y_k)\}_{k=0}^M$  is the sequence of approximation generated by Euler's method, then

$$|e_k| = |y(t_k) - y_k| = O(h) \quad (7.10)$$

$$|e_{k+1}| = |y(t_{k+1}) - y_{k+1}| = O(h^2) \quad (7.11)$$

The error at the end of the interval is called the **final global error (F.G.E.)**:

$$E(y(b), h) = |y(b) - y_M| = O(h) \quad (7.12)$$

The final global error  $E\{y(b), h\}$  has been used to study the behavior of the error for various step sizes. It can be used to give us an idea of how much computing effort must be done in order to obtain an accurate approximation.

#### 7.2.4 Example of the step size effect in Euler's method

For example, the step size effect uses Euler's method to solve I.V.P.

$$Y' = \frac{t-y}{2} \text{ on } [0, 3] \text{ with } y(0) = 1 \quad (7.13)$$

Compare solutions for  $h = 1, \frac{1}{2}, \frac{1}{4}, \text{ and } \frac{1}{8}$ .

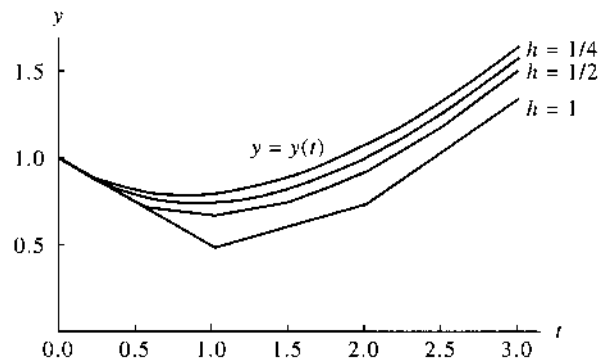


Fig. 7.2–Comparison of Euler solutions with different step sizes (John and Fink 2004).

**Fig. 7.2** shows a comparison of Euler solutions with different step sizes for  $y' = (t-y)/2$  over  $[0,3]$  with the initial condition  $y(0) = 1$ , presenting four Euler solutions and the exact solution curve

$$y(t) = 3e^{-t/2} - 2 + t \quad (7.13)$$

Using Euler's method will definitely solve a numerical solution that has been mentioned in Chapter II. Note that this method only presents a numerical solution, not an analytical solution.

### 7.2.5 Euler's method calculated in a three-dimensional wellbore

A wellbore for a build section (lowering the pipe into the hole) starting from  $\alpha_0 = 0^\circ$  to  $\alpha_1 = 90^\circ$ , assuming no  $r_{\text{turn}}$  and having all of the parameters is shown below in **Table 7.1**.

**Table 7.1–Showing parameters for build section**

Parameters	Values	Unit
Tkop	1,509	Ft
Teoc	3,308	Ft
$\mu$	0.1	
We	19.5	lb/ft
R	1,146	Ft
$\alpha_0$	0	Degree
$\alpha_1$	90	degree
Feoc	10,000(compressive)	lb

Wu and Juvkam-Wold's (1991) equations will be

$$F_c(\alpha) = [F_c(\alpha_0) - A\sin(\alpha_0) + B\cos(\alpha_0)]e^{\mu(\alpha-\alpha_0)} + A\sin\alpha - B\cos\alpha \quad (7.14)$$

Where

$$A = \frac{2\mu}{1+\mu^2} W_e R \quad (7.15)$$

$$B = -\frac{1-\mu^2}{1+\mu^2} W_e R \quad (7.16)$$

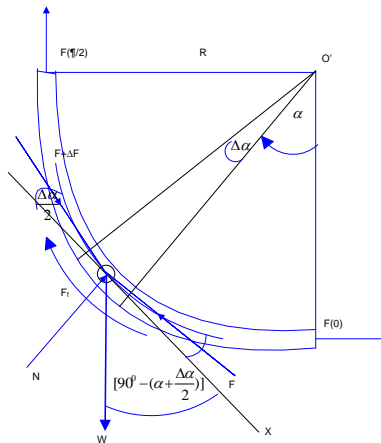


Fig. 7.3–Illustrates force in the build-up section (lowering the pipe into the hole, vertical view).

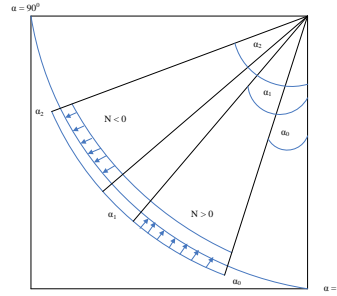


Fig. 7.4—Illustrates the differences between positive and negative forces in the build-up section (lowering the pipe into the hole).

From **Figs. 7.3 and 7.4** for  $N > 0$ ,

$$\frac{dF(\alpha)}{d(\alpha)} = \mu \left\{ \sqrt{\left[ w \cos(\alpha) + \frac{F_c(\alpha)}{R} \right]^2 + \left[ \frac{F_c(\alpha)}{R} \right]^2} \right\} R - WR \sin(\alpha); (\alpha_1 \geq \alpha \geq \alpha_0) \quad (6.17)$$

\*The term  $\frac{F_c(\alpha)}{R}$  comes from the wellbore turning and will be 0 because there is no

left or right turn;  $F_c$  means compressive force  $F_c > 0$  and tensile force  $F_c < 0$ .

**Fig. 7.5** shows that for a very small step size (1.25 degree), the result from the numerical solution is close to the analytical solution; moreover, this will show force value in every 1.25 degrees. This means the procedure of the numerical method that has been used to solve the first order differential equation is used by a small step size (such as 1.25 degree). Consequently, the results in this research are close to Wu and Juvkam-Wold's (1991) analytical equation and are realistic. From the equations in this research, in first derivative order that uses Euler's method can solve problems in a three-dimensional wellbore.

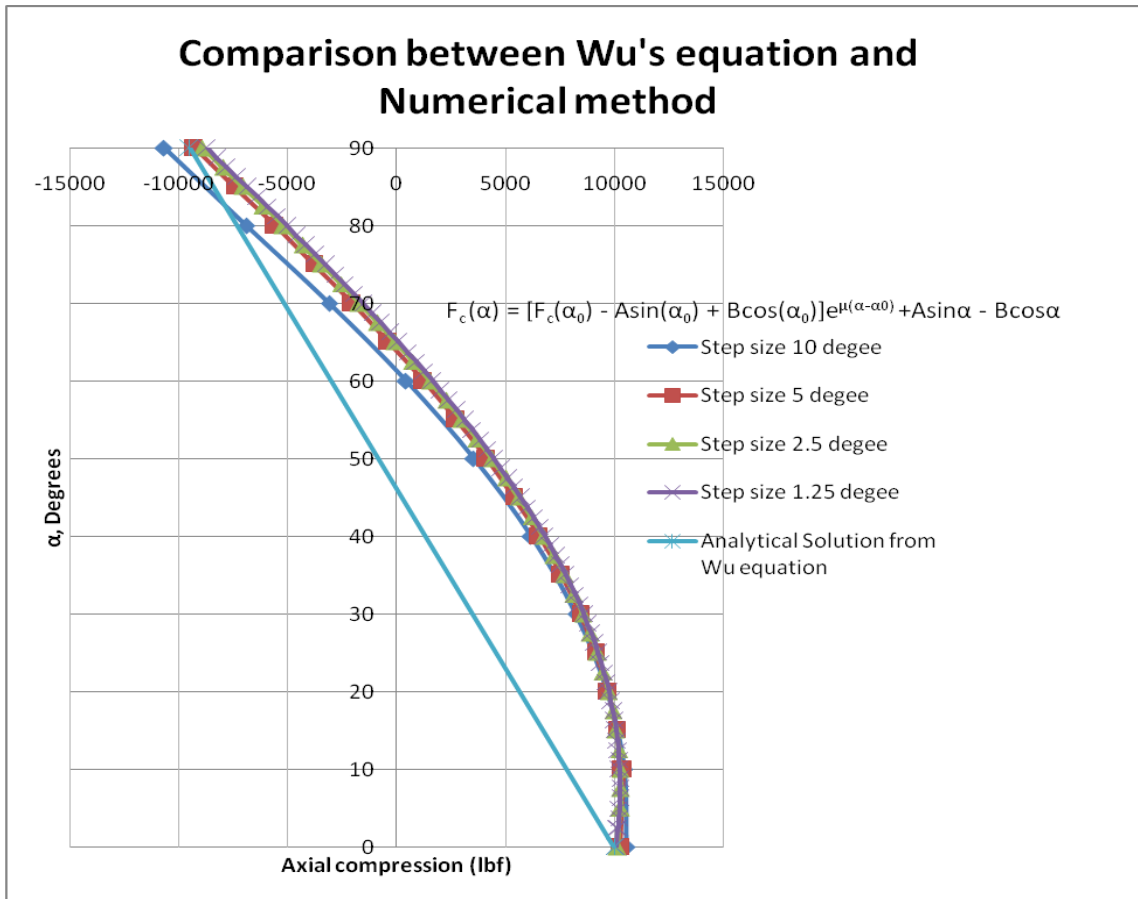


Fig. 7.5—Comparison between Wu and Juvkam-Wold's (1991) equations and numerical methods.



## CHAPTER VIII

### DISCUSSION OF RESULTS

#### 8.1 Introduction

This research developed torque and drag equations to be used in three-dimensional wellbore designs based on Wu and Juvkam-Wold's (1991) equations by using numerical methods as well as considering the stress concentration factor (SCF), tortuosity effects, and buckling. After going through literature reviews, we have equations for torque and drag calculation, in Chapter II shown below, as well as providing some examples.

#### 8.2 Mathematical Models for Three-dimensional Wellbores

This section shows the equations that are being used in three-dimensional wellbores.

##### 8.2.1 Lowering the pipe into the hole

###### 8.2.1.1 Build section

For  $N > 0$

$$\frac{dF(\alpha)}{d(\alpha)} = \mu \left\{ \sqrt{\left[ W \cos(\alpha) + \frac{F_c(\alpha)}{R} \right]^2 + \left[ \frac{F_c(\alpha)}{R_{turn}} \right]^2} \right\} R - WR \sin(\alpha); (\alpha_1 \geq \alpha \geq \alpha_0) \quad (8.1)$$

\*  $\frac{F(\alpha)}{R_{turn}}$  is from the wellbore turning (which will be explained in the next section of this

chapter), and the value will be 0 if there is no turning right or turning left of the

wellbore, and if there is tension force, then  $F$  will be  $F > 0$ , and if there is compressive force, then  $F$  will be  $F < 0$ .

For  $N < 0$

$$\frac{dF(\alpha)}{d(\alpha)} = \mu \left\{ - \sqrt{\left[ w \cos(\alpha) + \frac{F_c(\alpha)}{R} \right]^2 + \left[ \frac{F_c(\alpha)}{R_{turn}} \right]^2} \right\} R - WR \sin(\alpha); (\alpha_2 \geq \alpha \geq \alpha_1) \quad (8.2)$$

\*  $\frac{F(\alpha)}{R_{turn}}$  is from the wellbore turning (which will be explained in the next section of this chapter), and the value will be 0 if there is no right or left turn of the wellbore, and if there is tension force;  $F$  will be  $F > 0$ , and if there is compressive force, then  $F$  will be  $F < 0$ .

### 8.2.1.2 Drop section

For  $N > 0$

$$\frac{dF(\alpha)}{d(\alpha)} = \mu \left\{ \sqrt{\left[ w \sin(\alpha) - \frac{F_c(\alpha)}{R} \right]^2 + \left[ \frac{F_c(\alpha)}{R_{turn}} \right]^2} \right\} R - WR \cos(\alpha); (\alpha_2 \geq \alpha \geq \alpha_1) \quad (8.3)$$

\*  $\frac{F(\alpha)}{R_{turn}}$  is from the wellbore turning (which will be explained in the next section of this chapter), and the value will be 0 if there is no right or left turn of the wellbore, and if there is tension force;  $F$  will be  $F > 0$ , and if there is compressive force, then  $F$  will be  $F < 0$ .

For  $N < 0$

$$\frac{dF(\alpha)}{d(\alpha)} = \mu \left\{ - \sqrt{\left[ w \sin(\alpha) + \frac{F_c(\alpha)}{R} \right]^2 + \left[ \frac{F_c(\alpha)}{R_{turn}} \right]^2} \right\} R - WR \cos(\alpha); (\alpha_1 \geq \alpha \geq \alpha_0) \quad (8.4)$$

\*  $\frac{F_c(\alpha)}{R_{turn}}$  is from the wellbore turning (which will be explained in the next section of this

chapter), and the value will be 0 if there is no right or left turn of the wellbore, and if there is tension force;  $F$  will be  $F > 0$ , and if there is compressive force, then  $F$  will be  $F < 0$ .

## 8.2.2 Pulling the pipe out of the hole

### 8.2.2.1 Build section

For  $N > 0$

$$\frac{dF(\alpha)}{d(\alpha)} = \mu \left\{ \sqrt{\left[ w \cos(\alpha) - \frac{F(\alpha)}{R} \right]^2 + \left[ \frac{F(\alpha)}{R_{turn}} \right]^2} \right\} R + WR \sin(\alpha); (\alpha_1 \geq \alpha \geq \alpha_0) \quad (8.5)$$

\*  $\frac{F(\alpha)}{R_{turn}}$  is from the wellbore turning (which will be explained in the next section of this

chapter), and the value will be 0 if there is no right or left turn of the wellbore, and if there is tension force;  $F$  will be  $F > 0$ , and if there is compressive force, then  $F$  will be  $F < 0$ .

For  $N < 0$

$$\frac{dF(\alpha)}{d(\alpha)} = \mu \left\{ -\sqrt{\left[ W \cos(\alpha) - \frac{F(\alpha)}{R} \right]^2 + \left[ \frac{F(\alpha)}{R_{turn}} \right]^2} \right\} R + WR \sin(\alpha); (\alpha_2 \geq \alpha \geq \alpha_1) \quad (8.6)$$

\*  $\frac{F(\alpha)}{R_{turn}}$  is from the wellbore turning (which will be explained in the next section of this chapter), and the value will be 0 if there is no right turn or left turn of the wellbore, and if there is tension force;  $F$  will be  $F > 0$ , and if there is compressive force, then  $F$  will be  $F < 0$ .

### 8.2.2.2 Drop section

For  $N > 0$

$$\frac{dF}{d\alpha} = \mu \left\{ \sqrt{\left( W \sin(\alpha) + \frac{F(\alpha)}{R} \right)^2 + \left( \frac{F(\alpha)}{R_{turn}} \right)^2} \right\} R + WR \cos(\alpha); (\alpha_2 \geq \alpha \geq \alpha_1) \quad (8.7)$$

\*  $\frac{F(\alpha)}{R_{turn}}$  is from the wellbore turning (which will be explained in the next section of this chapter), and the value will be 0 if there is no right or left turn of the wellbore, and if there is tension force;  $F$  will be  $F > 0$ , and if there is compressive force;  $F$  will be  $F < 0$ .

For  $N < 0$

$$\frac{dF}{d\alpha} = \mu \left\{ -\sqrt{\left( W \sin(\alpha) + \frac{F(\alpha)}{R} \right)^2 + \left( \frac{F(\alpha)}{R_{turn}} \right)^2} \right\} R + WR \cos(\alpha); (\alpha_1 \geq \alpha \geq \alpha_0) \quad (8.8)$$

\*  $\frac{F(\alpha)}{R_{turn}}$  is from the wellbore turning (which will be explained in the next section of this chapter), and the value will be 0 if there is no right or left turn of the wellbore, and if there is tension force;  $F$  will be  $F > 0$ , and if there is compressive force;  $F$  will be  $F < 0$ .

In addition, a hold section that has a deviation in either a left or right turn will consider

$N_{turn}$  term with  $\frac{F(\alpha)}{R_{turn}}$ .

All of the above equations cannot be solved by analytical methods; however, they can be solved by numerical methods by using an Euler method to solve this first degree differential equation. The next section will provide an example that will be used to compare Wu and Juvkam-Wold's (1991) analytical equation with the research method using Euler's numerical methods.

### 8.3 Soft-string Model for Three-dimensional T&D Calculations

The original soft-string T&D programs were based on a model developed by Exxon Production research (Mason and Chen 2007). The value of  $N$  (normal contact force) depends on how the pipe contacts the formation and the actual amount of normal contact force:

$$N \text{ total} = \sqrt{(T\Delta\phi \sin \theta)^2 + (T\Delta\phi + W \sin \theta)^2} \quad (8.9)$$

If the wellbore turns neither left nor right,  $T\Delta\phi\sin\theta$  will equal  $\rightarrow 0$ ; meanwhile, using the normal contact force equation to evaluate the tension and torque changes details in **Eq. 2.13** and **Eq. 2.14**:

$$\Delta T = W \cos \theta + / - \mu N \quad (8.10)$$

$$\Delta M = \mu NR \quad (8.11)$$

#### 8.4 Example and Comparison in Force Calculations

The wellbore for the build section (lowering the pipe into the hole) starting from  $\alpha_0 = 0^\circ$  to  $\alpha_1 = 90^\circ$ , assuming no  $R_{\text{turn}}$ , and having all the parameter shown below in **Fig. 8.1** and **Table 8.1**, respectively.

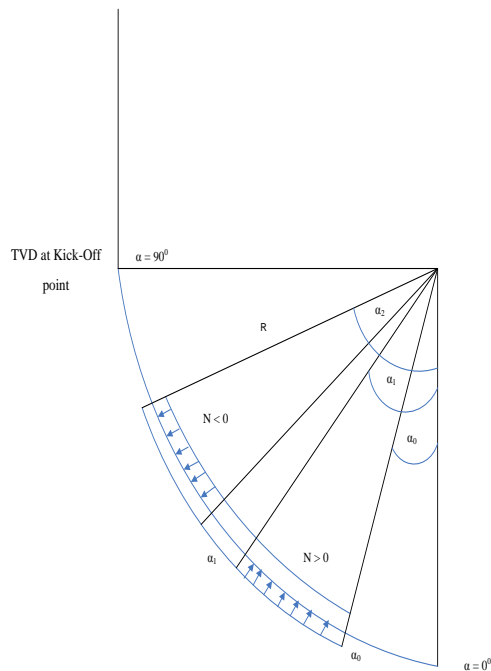


Fig. 8.1—Wellbore geometry for this example.

**Table 8.1–Showing parameters**

Parameters	Values	Unit
Tkop	1,509	ft
Teoc	3,308	ft
$\mu$	0.1	
We	19.5	lb/ft
R	1146	ft
$\alpha_0$	0	degree
$\alpha_1$	90	degree
Feoc	10,000	lb
Ftop	-9,504	lb

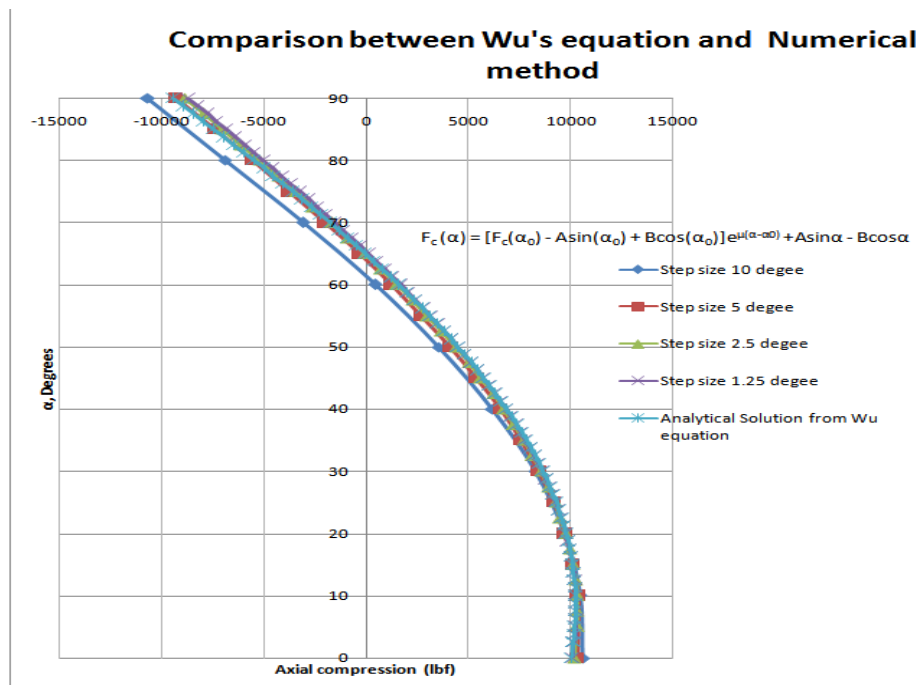


Fig. 8.2–Comparison between Wu and Juvkam-Wold's (1991) equations and numerical methods.

**Fig. 8.2** Illustrates a very small step size (1.25 degree) as the result from a numerical solution, which is close to an analytical solution. Moreover, this will show a force value every 1.25 degrees. This means that the procedure for numerical methods used to solve the first degree differential equation is to use a small step size (such as 1.25 degree) and,

as revealed in this research, is close to Wu and Juvkam-Wold's (1991) analytical equation and is realistic. Equations from this research in the first derivative degree using Euler's method can solve problems in three-dimensional wellbores.

### 8.5 Example and Comparison in Torque Calculations

Torque calculations in the build and drop sections (while rotating off the bottom) from Chapter III also consider tortuosity effects and will use the adapted equation by

$$T(\alpha_2) = \int_{\alpha_0}^{\alpha_2} \mu |N(\alpha)| \frac{D_{drift}}{24} R d\alpha \quad (8.12)$$

However, the next step of this equation will be separated by the integral theory, thus

$$T(\alpha_2) = \int_{\alpha_0}^{\alpha_1} \mu |N(\alpha)| \frac{D_{drift}}{24} R d\alpha + \int_{\alpha_1}^{\alpha_2} \mu |N(\alpha)| \frac{D_{drift}}{24} R d\alpha \quad (8.13)$$

It will depend on how the drillstring contacts the wellbore. From the above equation and  $N(\alpha)$  for three-dimensional wellbores from Chapter II, using visual basic application software will give us a numerical method to solve torque and drag.

#### 8.5.1 Example while rotating off the bottom

An example of torque calculations when comparing Wu and Juvkam-Wold's (1991) equation with the numerical solutions is shown below:

Rotary Drilling with  $F_{eoc} = 40,000$  lbf (tension) shows the well profile as an Extended reach well with final  $I = 65$  deg.  $BUR = 5.08$  deg./100 ft  $\mu = 0.333$ ,  $I_{kop} = 0$ ,  $T_{kop} = 1,509$  ft Mud wt = 9.6 ppg Pipe wt = 16.6 lb/ft in air and Density of steel = 65.5 ppg



$$N_{EOC} = 14.17 \cos 25 - 40,000/1,128 = - 22.63 \text{ lb/ft (upside contact)} \quad (8.14)$$

Axial drag = 0, but

$$F(\alpha_2) = F(\alpha_0) + F_d - W_e R (\cos \alpha_2 - \cos \alpha_0) \quad (8.15)$$

$$F_{KOP} = 40,000 + 0 - 15,979 (\cos 90^\circ - \cos 25^\circ) \quad (8.16)$$

$$F_{KOP} = 54,480 \text{ lb}_f \quad (8.17)$$

From Wu and Juvkam-Wold's (1991) equation

$$T(\alpha_2) = \int_{\alpha_0}^{\alpha_2} \mu \left| 2W_e \cos \alpha - W_e \cos \alpha_0 - \frac{F(\alpha_0)}{R} \right| \frac{D_{ij}}{24} R d\alpha \quad (8.18)$$

From Wu and Juvkam-Wold's (1991) equation

$$N(\alpha) = 2W_e \cos \alpha - W_e \cos \alpha_0 - \frac{F(\alpha_0)}{R} \quad (8.19)$$

Using integrate properties with Wu and Juvkam-Wold's (1991) equation

$$T(\alpha_2) = \int_{\alpha_0}^{\alpha_2} \mu |N| \frac{D_{ij}}{24} R d\alpha = \int_{\alpha_0}^{\alpha_1} \mu N(\alpha) \frac{D_{ij}}{24} R d\alpha + \int_{\alpha_1}^{\alpha_2} -\mu N(\alpha) \frac{D_{ij}}{24} R d\alpha \quad (8.20)$$

$$T\left(\frac{\pi}{2}\right) = \int_{\frac{25\pi}{180}}^{\frac{\pi}{2}} -\mu (2W_e \cos \alpha - W_e \cos \alpha_0 - \frac{F(\alpha_0)}{R}) \frac{D_{ij}}{24} R d\alpha \quad (8.21)$$

$$\text{Thus, } T_{kop} = 3,760 \text{ ft-lb}_f \quad (8.22)$$

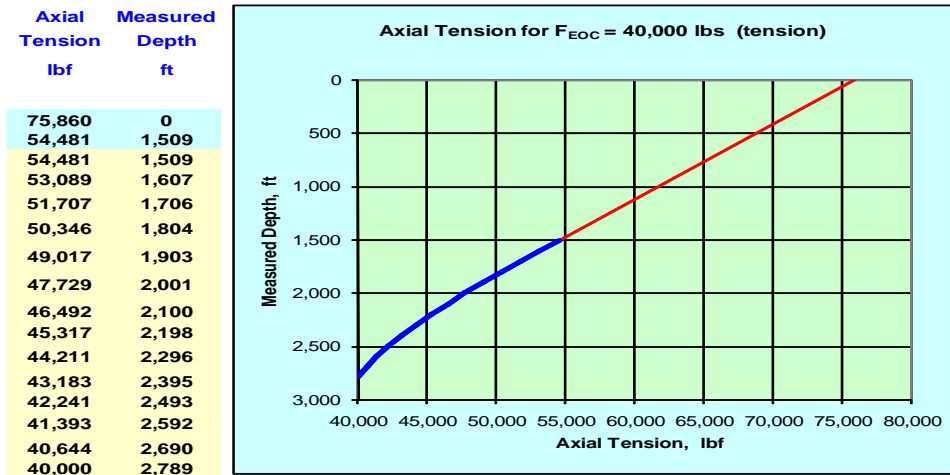


Fig. 8.3–Axial tension plot for this example using Wu and Juvkam-Wold’s (1991) method (Juvkam-Wold 2007).

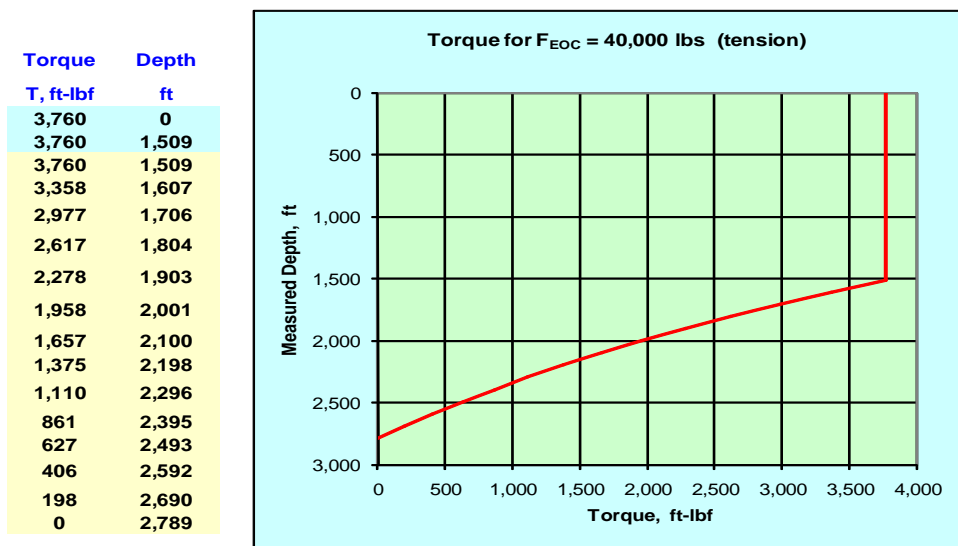


Fig. 8.4–Torque plot for this example using Wu and Juvkam-Wold’s (1991) method (Juvkam-Wold 2007).

**Figs. 8.3** and **8.4** demonstrate the result from Wu and Juvkam-Wold’s (1991) calculated method. The next step will compare the results from the software using the torque equations, from this research:

For  $N > 0$

$$N = \sqrt{[w \cos(\alpha) - \cos(\alpha_0)]^2 + \left[\frac{F_c(\alpha)}{R_{turn}}\right]^2}; (\alpha_1 \geq \alpha \geq \alpha_0) \quad (8.23)$$

For  $N < 0$

$$N = -\sqrt{[w \cos(\alpha) - \cos(\alpha_0)]^2 + \left[\frac{F_c(\alpha)}{R_{turn}}\right]^2}; (\alpha_2 \geq \alpha \geq \alpha_1) \quad (8.24)$$

\*  $\frac{F(\alpha)}{R}$  is from the wellbore turning (which will be explained in the next section of this chapter), and the value will be 0 if there is no right or left turn of the wellbore, and if there is tension force;  $F$  will be  $F > 0$ , and if there is compressive force;  $F$  will be  $F < 0$ .

For this example,  $\left(\frac{F_c(\alpha)}{R_{turn}}\right)$  will be 0 since the two-dimensional wellbore does not have any turning.

$$\frac{dF(\alpha)}{d(\alpha)} = \text{WOB} - \sqrt{[w (\cos(\alpha) - \cos(\alpha_0))]^2 + \left[\frac{F(\alpha)}{R_{turn}}\right]^2} * R; (\alpha_1 \geq \alpha \geq \alpha_0) \quad (8.25)$$

Using Euler's method to solve this equation will be shown below.

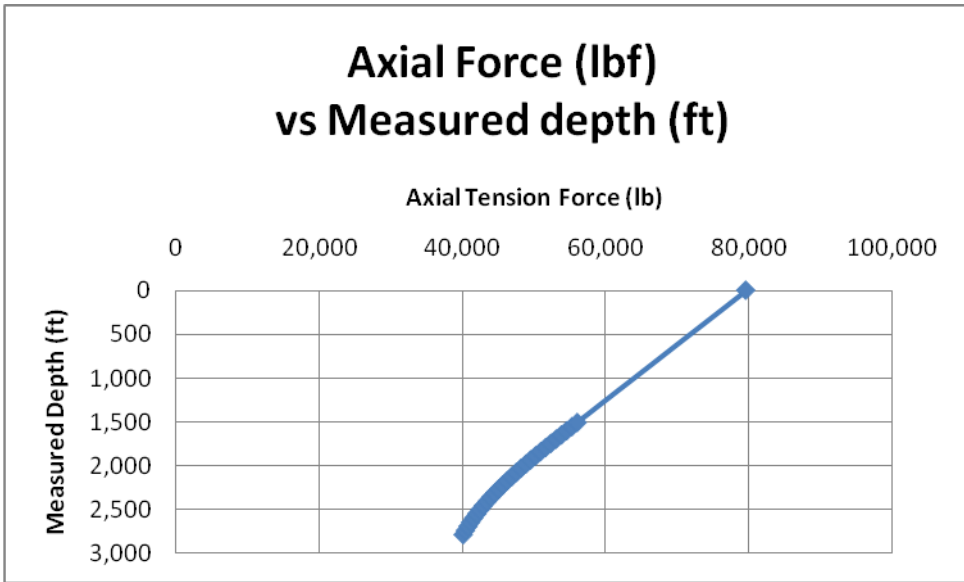


Fig. 8.5–Axial tension plot for this example using numerical method.

Fig. 8.5 shows the axial tension plot for this example. Using torque calculations in the build and drop sections from Chapter II will use the adaptive equation

$$T(\alpha_2) = \int_{\alpha_0}^{\alpha_2} \mu |N(\alpha)| \frac{D_{drift}}{24} R d\alpha ; (\alpha_2 = 90^0 \text{ and } \alpha_0 = 25^0) \tag{8.26}$$

By Eq. 8.26 and  $N(\alpha)$  from Eq. 8.24, using visual basic application software to help us will give us a numerical method answer of torque and drag.

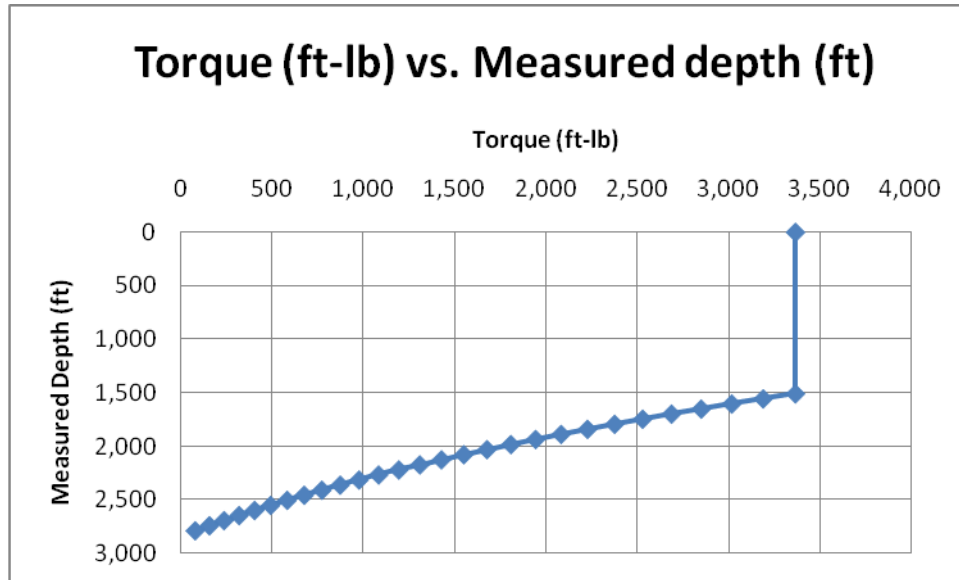


Fig. 8.6–Torque plot for this example using numerical method.

**Fig. 8.6** shows that there will be a very small difference in T&D calculations from Wu and Juvkam-Wold's (1991) equation and T&D from numerical methods. This will prove that numerical methods can be used to solve two-dimensional problems; also Wu and Juvkam-Wold's (1991) equation cannot solve problems in three-dimensional wellbores.

Moreover, this thesis can calculate well planning between the tie-on survey at the KOP to the target direction by using Visual Basic Application program and MATLAB together; the example below will show the results.

### 8.5.2 Example for survey calculations

For example, if we have a tie-on survey and a target direction (**Table 8.2**), we can also use numerical method to solve this example.

**Table 8.2–Input field data for tie-on surveys and target directions for 3D wellbore paths**

**a) Target direction**

MD	TVD	NC	EC
6955.28	5000	-3000	2000

**b) Tie-on survey at KOP**

MD	TVD	NC	EC	I	AZ	DLS
90	90	-100	-70	57	300	5

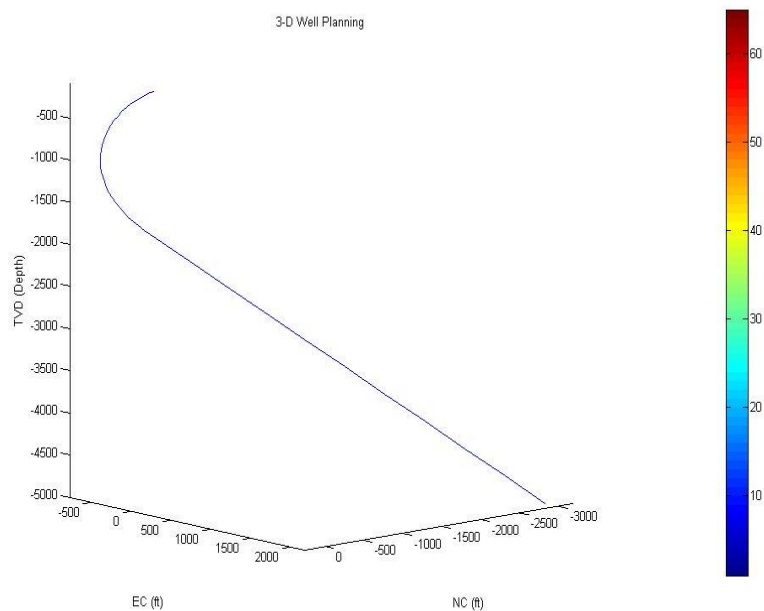


**Fig. 8.7–3D wellbore path by MATLAB version 7.4.0.**

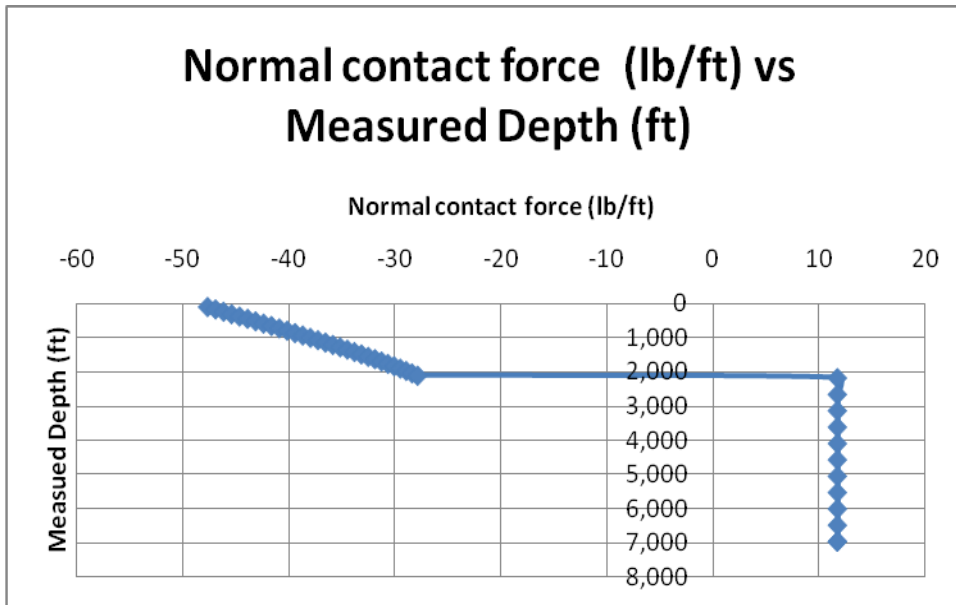


Fig. 8.8—Normal contact force (lb/ft) versus measured depth (ft).

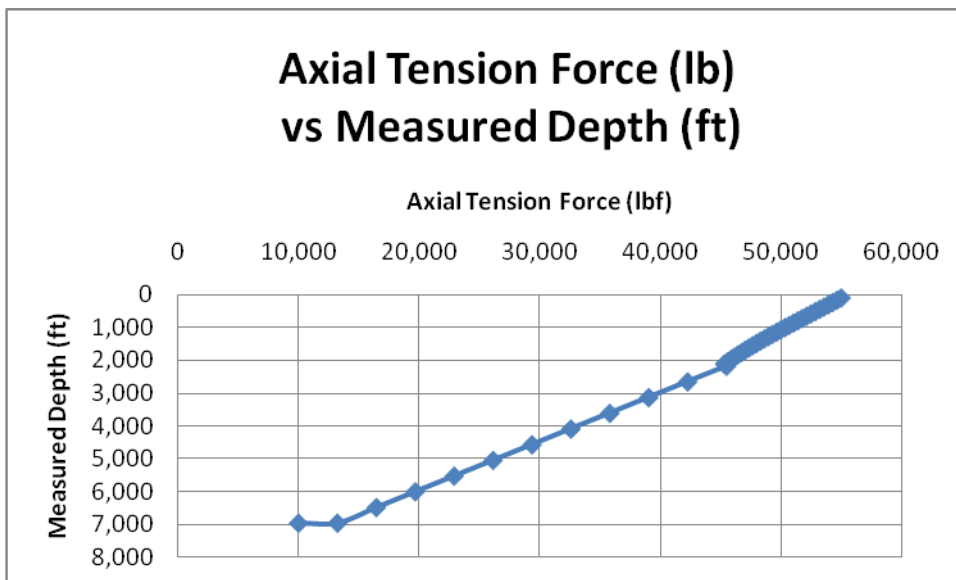


Fig. 8.9—Axial force (lb) versus measured depth (ft).

More examples and comparison will be provided in the appendices.

Note: **Figs. 8.7, 8.8** and **8.9** are based on **Fig. 8.6** geometry.

## CHAPTER IX

### CONCLUSIONS AND RECOMMENDATIONS

#### 9.1 Conclusions

This research began by improving the equations that are normally used in T&D software calculations, reflecting the state of current models and identifying future requirements.

This provides more accurate T&D models because this research's calculations are based on 3D calculations that will help alleviate helical bucking problems since normally helical bucking causes lock-up and fatigue potential.

This research's software prevents T&D problems while drilling by trying to optimize well profiles before drilling begins. Moreover, this research shows the relationship between well planning design and T&D calculations in 3D. This makes it easier to find out which type of well design is more suitable in each particular area. Besides, this will help in designing of long horizontal wellbores tremendously. From all the above, this research helps the user to find how to optimize the wellbore trajectory in each particular area based on 3D calculations (in Chapter VIII has already compared between 2D calculations and 3D calculations with various examples in the appendices).

This software helps field personnel to prepare for unexpected trend changes in a timely fashion during the drilling process. A user is able to anticipate T&D values by only



inputting wellbore data and T&D parameters. Consequently, the outcome of the data from the T&D calculation program is more realistic because it is based on a 3D model. Also a user can adjust the input data if there is more information during the drilling process, this will provide even more accurate output.

## **9.2 Recommendations**

Future work should be to improve the Soft-string assumption for calculating T&D models. This means that the T&D software should consider bending stresses. These include maximum stress calculations, fatigue limits, and fixed end or free end assumptions. If the above-mentioned were included in new T&D programs, this would provide more accurate T&D calculations.

## NOMENCLATURE

$A$ -	Pipe cross sectional area
$AZ$ -	The direction or bearing toward which a sloping surface faces (e.g., a north-facing slope has an azimuth angle of $360^\circ$ ; a northeast-facing slope, an azimuth angle of $45^\circ$ ), degrees
$B$ -	Angle parameter for mathematical algorithm calculation, rad.
$d$ -	Length parameters for mathematical algorithm in wellbore trajectory calculation, ft
$D$ -	A combination of aerodynamic or hydrodynamic forces which tends to reduce speed, lbf
$D_{drift}$ -	The average diameter that has been used in torque equations, in
$D_{ij}$ -	The diameter of tool joint, in
$DLS$ -	A normalized estimate (e.g., degrees / 100 feet) of the overall curvature of an actual well path between two consecutive survey stations.
$e$ -	Length parameters for mathematical algorithm in wellbore trajectory calculation, ft
$E$ -	Young's modulus, psi
$EC$ -	The distance traveled in the east-west direction in the horizontal plane (east is positive, west is negative), ft
$f$ -	Is the <a href="#">force</a> of two <a href="#">surfaces</a> in contact, or the force of a medium acting on a moving object, lbf
$F(\alpha)$ -	Tensile force, lbf
$F_c(\alpha)$ -	Compressive force, lbf
$F_{hel}$ -	New helical buckling load, lbf
$F_s$ -	Axial compressive load to initiate sinusoidal buckling of pipe, lbf
$FEA$ -	Finite Element Analysis

$h$ -	Length parameters for mathematical algorithm in wellbore trajectory calculation, ft
$H_L$ -	Length of wellbore in horizontal section, ft
$I, \theta$ -	A deviation or the degree of deviation from the vertical
$I_M$ -	Moment of inertial of pipe, in (Gaynor et al. 2002)
$k$ -	Length parameters for mathematical algorithm in wellbore trajectory calculation, ft
$m$ -	Length parameters for mathematical algorithm in wellbore trajectory calculation, ft
$\Delta M$ -	The increment in torque across the string element, ft-lbf
$MD$ -	The actual distance traveled along the borehole, ft
$n$ -	Length parameters for mathematical algorithm in wellbore trajectory calculation, ft
$N$ -	The component perpendicular to the surface of contact of the contact force, lbf/ft
$N_{turn}$ -	The normal contact force while the wellbore is turning, lbf/ft
$NC$ -	The distance traveled in the north-south direction in the horizontal plane (north is positive, south is negative), ft
$R$ -	The radius of curvature of the string element while the wellbore is in the build or the drop section (vertical view), ft
$R_{turn}$ -	The radius of curvature of the string element while the wellbore is turning (horizontal view), ft
$RSCs$ -	Rotary Shouldered Connections
$SCF$ -	Stress Concentration Factor
$t$ -	Tangent section
$T$ -	The tension force at the lower end of the string element, lbf

$T_1$ -	The planned tortuosity represent the summation of the total curvature including inclination and azimuth in the planned well trajectory divided by the well depth
$T_2$ -	The large-scale tortuosity represent the summation of the total curvature (inclination and azimuth changes) when a drilled well is measured by measurement while drilling (MWD)
$T_3$ -	The micro tortuosity defined as the tortuosity that occurs in the wellbore that is smaller in comparison to previous tortuosity
$\Delta T$ -	The increment in tension across the string element, lbf
$T(\alpha)$ -	(or often called a <i>moment</i> ) can informally be thought of as "rotational force" or "angular force" which causes a change in rotational motion. This force is defined by linear force multiplied by a radius, ft-lbf
$T_{kop}$ -	Depth in vertical section (ft)
$TD$ -	The assumed trajectory of the wellbore, ft
$TVD$ -	The vertical distance between a specific location in a borehole and a horizontal plane passing through the surface, ft
$W, W_e$ -	In this research, refers to buoyed weight of the string element (provided by Eq. 2.71), lbf/ft
$z$ -	Length parameters for mathematical algorithm in wellbore trajectory calculation, ft
$\alpha_I$ -	The angle between the distance traveled in the north-south direction and 3D distance from the KOP to Target, rad.
$\alpha$ -	The angle used to calculate the deviation of the wellbore, rad.
$\beta$ -	The angle between the distance traveled in the east-west direction and 3D distance from the KOP to Target, rad.
$\gamma$ -	The angle used to calculate the deviation of the wellbore in tangent section, rad.
$\sigma_{app}$ -	Applied normal stress in pipe body
$\sigma_{mean}$ -	Average normal stress in pipe body

$\Sigma$ -	Local peak stress within connection
$\Sigma_{\max}$ -	Maximum peak stress within connection
$\Sigma_{\max \text{ mean}}$ -	Average maximum peak stress within connection
$\Phi, \Delta\theta$ -	The change in azimuth angle over the string element, rad.
$\delta$ -	A normalized estimate of the overall curvature of an actual well path between two consecutive survey stations, degrees per 100 ft
$\mu$ -	The coefficient of friction between the string and the wellbore
$\lambda$ -	Angle parameter for mathematical algorithm calculation, rad.
$\rho_{\text{mud}}$ -	Density of drilling fluid (lb/gallon)
$\rho_{\text{steel}}$ -	Density of drill pipe (lb/gallon)

## REFERENCES

- Aadnøy, B.S., and Anderson, K. 1998. Friction Analysis for Long-Reach Wells. Paper SPE/IADC 39391 presented at the SPE/IADC Drilling Conference, Dallas, Texas, 3-6 March.
- Adewuya, O.A., and Pham, S.V. 1998. A Robust Torque and Drag Analysis Approach for Well Planning and Drillstring Design. Paper SPE/IADC 39321 presented at the SPE/IADC Drilling Conference, Dallas, Texas, 3-6 March.
- Aston, M.S., Hearn, P.J., and McGhee, G. 1998. Techniques for Solving Torque and Drag Problems in Today's Drilling Environment. Paper SPE 48939 presented at the SPE Annual Technical Conference and Exhibition, New Orleans, Louisiana, 27-30 September.
- Gaynor, T., Chen, D.C., Stuart D., and Comeaux, B. 2001. Tortuosity Versus Micro-Tortuosity – Why Little Things Mean a Lot. Paper SPE/IADC 67818 presented at the SPE/IADC Drilling Conference, Amsterdam, The Netherlands, 27 February-1 March.
- Gaynor, T., Halmer, D., Chen, D.C., and Stuart, D. 2002. Quantifying Tortuosities by Friction Factors in Torque and Drag Model. Paper SPE 77617 presented at the SPE Annual Technical Conference and Exhibition, San Antonio, Texas, 29 September-2 October.
- Haduch, G.A., Procter, R.L., and Samuels, D.D. 1994. Solution of Common Stuck Pipe Problems through the Adaptation of Torque/Drag Calculations. Paper SPE 27490 presented at the SPE/IADC Drilling Conference, Dallas, Texas, 15-18 February.
- Hamilton, K., Wagg, B., and Roth, T. 2007. Using Ultrasonic Techniques to Accurately Examine Seal Surface Contact Stress in Premium Connections. Paper SPE 110675 presented at the SPE Annual Technical Conference and Exhibition, Anaheim, California, 11-14 November.
- Johancsik, C.A., Friesch, D.B., and Dawson, R. 1984. Torque and Drag in Directional Wells-Prediction and Measurement. *Journal of Petroleum Technology* **36**: 987-992.
- John, H. M., and Fink, K.K. 2004. *Numerical Methods Using MATLAB*, fourth edition. Upper Saddle River, New Jersey: Pearson.
- Juvkam-Wold, H.C. 2007, Spring. *PETE 432*, Class Lecture, Texas A&M University, College Station, Texas.

- Juvkam-Wold, H.C., and Wu, J. 1992. Casing Deflection and Centralizer Spacing Calculations. *SPE Drilling Engineering* 7 (4): 268-274.
- Kaw, K.K. 2006. *An Interactive E-book for Illustrating Euler's Method of Solving Ordinary Differential Equations*. Tampa, Florida: Holistic Numerical Methods Institute, College of Engineering, University of South Florida.
- Logging While Drilling. 2008. Houston: Weatherford International, Inc., 10-25.
- Maidla, E., and Haci, M. 2004. Understanding Torque: The Key to Slide-Drilling Directional Wells. Paper SPE 87162 presented at the SPE/IADC Drilling Conference, Dallas, Texas, 2-4 March.
- Maidla, E., Haci, M., Cluchey, M., Alexander, M., and Warren, T. 2005. Field Proof of the New Sliding Technology for Directional Drilling. Paper SPE/IADC 92558 presented at the SPE/IADC Drilling Conference, Amsterdam, The Netherlands, 23-25 February.
- Maidla, E.E., and Wojtanowicz, A.K. 1987. Field Comparison of 2-D and 3-D Methods for the Borehole Friction Evaluation in Directional Wells. Paper SPE 16663 presented at the SPE Annual Technical Conference and Exhibition, Dallas, Texas, 27-30 September.
- Mason, C.J., and Chen, D.C. 2007. Step Changes Needed To Modernize T&D Software. Paper SPE/IADC 104609 presented at the SPE/IADC Drilling Conference, Amsterdam, The Netherlands, 20-22 February.
- Menand, S., Sellami, H., Tijani, M., Stab, O., Dupuis, D., and Simon, C. 2006. Advancement in 3D Drillstring Mechanic: From the Bit to the Topdrive. Paper SPE/IADC 98965 presented at the SPE Drilling Conference, Miami, Florida, 21-23 February.
- Patusek, P., Brackin, V., and Christensen, H. 2003. A Model for Borehole Oscillations. Paper SPE 84448 presented at the SPE Annual Technical Conference and Exhibition, Denver, Colorado, 5-8 October.
- Plessis, G.J., You, J.B., and Prideco, G. 2005. The Challenge of Selecting Appropriate Drill String Enhancing Features for Drilling in the Middle East Harsh Environment. Paper SPE/IADC 97368 presented at the Middle East SPE Drilling Technology Conference and Exhibition, Dubai, U.A.E., 12-14 September.
- Rezmer-Cooper, I., Chau, M., Hendricks, A., Woodfine, M., Stacey, B., and Downton, N. 1999. Field Data Supports the Use of Stiffness and Tortuosity in Solving Complex Well Design Problems. Paper SPE/IADC 52819 presented at the SPE/IADC Drilling Conference, Amsterdam, The Netherlands, 9-11 March.

- Ring, L., Deltombe, P., York, P., and Baker, R.V. 2007. New Level of Expandable Connector Qualification Helps Minimize Operational Risk in Solid Expandable Liners. Paper SPE 110920 presented at the SPE Annual Technical Conference and Exhibition, Anaheim, California, 11-14 November.
- Tang, W., Muradov, A., Chandler, R.B., Jellison, M.J., Prideco, G., Gonzalez M.E., and Wu, J. 2006. A Novel Approach for Determining, Evaluating, and Applying Stress Concentration Factors for Rotary-Shouldered Connections. Paper SPE 103052 presented at the SPE Annual Technical Conference and Exhibition, San Antonio, Texas, 24-27 September.
- Well Planning. 1975. The Woodlands, Texas: Mitchell Energy and Development Corp., 35.
- Wiggins, M.L., Choe, J., and Juvkam-Wold, H.D. 1992. Single Equation Simplifies Horizontal, Directional Drilling Plans. *Oil & Gas J.* **90**: 74-79.
- Wu, J., and Juvkam-Wold, H.C., 1991. Drag and Torque Calculation for Horizontal Wells Simplified for Field Use. *Oil & Gas J.* **89**: unpagged.
- Wu, J., and Juvkam-Wold, H.C. 1993. Study of Helical Buckling of Pipes in Horizontal Wells. Paper SPE 25503 presented at the Production Operations Symposium, Oklahoma City, Oklahoma, 21-23 March.



## **APPENDIX A**

### **INTRODUCTION TO THREE-DIMENSIONAL CALCULATION SOFTWARE PROGRAM USING NUMERICAL METHOD ANALYSIS**

This section will guide users in how to use T&D software that has been mentioned in this research. This software will be used to calculate three-dimensional wellbore designs by using numerical method analysis; this T&D software program also consists of seven sections that explain procedures step by step. The first section in this program requires users to follow Terms & Agreements, then users have to press this button prior to continuing the process. After users click this button, they can choose any type of wellbore design to calculate torque and drag data.

The screenshot shows the 'UserForm4' window with the following sections:

- Frame1 (Input Section):**
  - Frame31 (Left):** MD: 90 ft, TVD: 90 ft, NC: -100 ft, EC: -70 ft, I: 57 Degree, AZ: 300 Degree, DLS: 5 Degree.
  - Frame31 (Right):** MD: 6955.28 ft, TVD: 5000 ft, NC: -3000 ft, EC: 2000 ft.
  - Method of Calculation:**
    - Rotating off bottom
    - Pulling out of the hole (WOB > 0 for tension, WOB < 0 for compression)
    - Running into the hole (WOB < 0 for tension, WOB > 0 for compression)
  - Frame32 (Bottom Left):** Weight on Bit: 10000 lbf, DC Diameter: 6 Inch, Bit Diameter: 5 Inch, Unit Weight of Drillpipe (in Air): 19.5 lb/ft, Density of Drilling Fluid: 13 lb/gal, Density of Steel: 65.5 lb/gal, Coefficient: 0.1.
- Frame2 (Result Section):**
  - Frame5:** Ftop: 55453.8 lb, Torque too: [ ] lb-ft, [ CALCULATE ]
  - Frame6:** Four sub-panels showing wellbore diagrams and graphs.
- Frame4 (Diagram):** Wellbore geometry diagram with KOP, W, S, N, E, and TARGET labels. Includes options for 'Left turn' and 'Right turn' with corresponding diagrams.

Fig. A.1–T&D calculations for 3D well planning user form.

**Fig. A.1** is a user form of this T&D (torque and drag) software program for T&D Calculations for 3D Well Planning Designs. This program consists of input data frames and result data frames. The input data frame consists of the tie-on survey of the kick off point (KOP), the target direction for well planning with the method of calculation (rotating off bottom, pulling out of the hole, and running into the hole), and the drilling parameters. The right-hand end frame shows the planning picture of input data (user can see large picture by clicking on any pictures in 3D software as **Fig. A.2**).

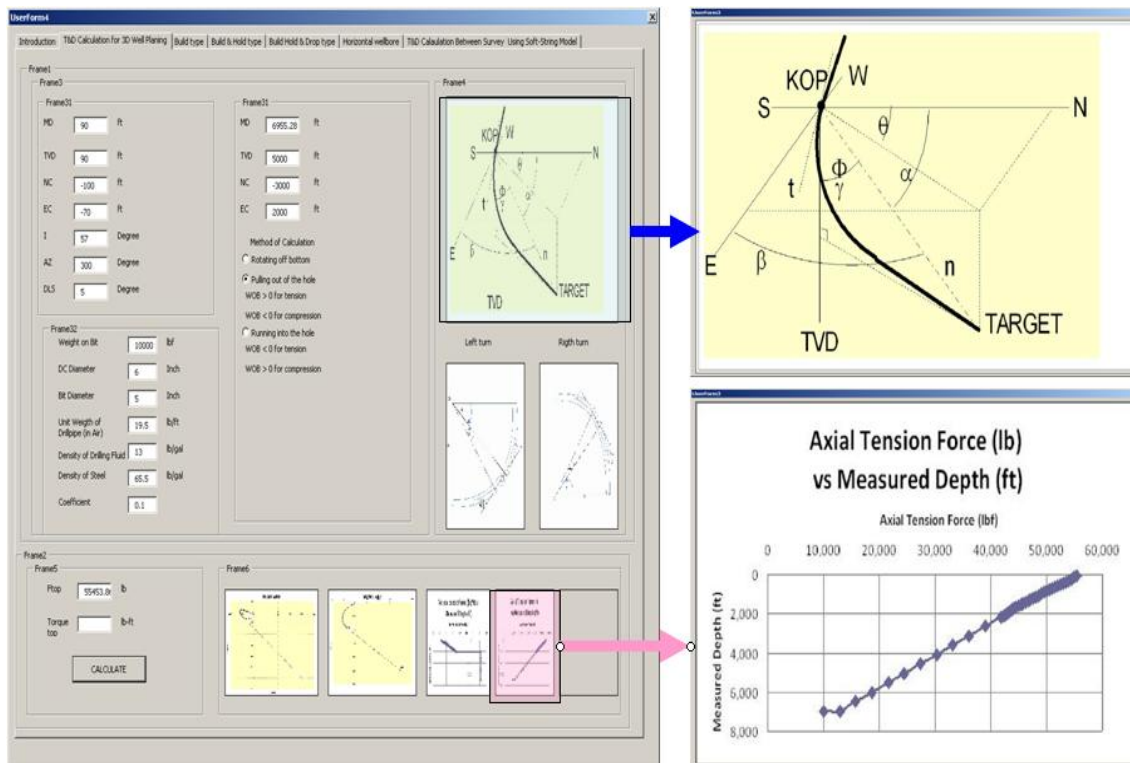


Fig. A.2—Showing enlarge picture application in 3D software.

The result frame provides all torque and drag output calculations. It shows the graph from the horizontal view of wellbore trajectory, vertical view of wellbore trajectory, normal contact force (lbf/ft) versus measured depth, axial tension/compression force

(lbf) versus measured depth, and torque (ft-lbf) versus measured depth. The result will depend on which method the user has chosen for method of calculation. Again the user can see a large picture of the graph by clicking on the result's picture.

The screenshot shows a software window titled "UserForm4" with a menu bar containing: Introduction | T&D Calculation for 3D Well Planning | Build type | Build & Hold type | Build Hold & Drop type | Horizontal wellbore | T&D Calculation Between Survey Using Soft-String Model.

**Frame 1:** Introduction

**Frame 3:** Input data

**Frame 31:** Kick off Point: 1509 ft; Build rate: 5.08 Deg/100 ft; Left, Right turn: 0 Deg/100 ft; Alpha zero: 25 Deg.

**Frame 32:** Weight on Bit: 10000 lbf; Wellbore Diameter: 6 Inch; Bit Diameter: 5 Inch; Unit Weight of Drillpipe (in Air): 19.5 lb/ft; Density of Drilling Fluid: 13 lb/gal; Density of Steel: 65.5 lb/gal; Coefficient: 0.333.

**Frame 4:** Well planning for input data. Includes diagrams for "Left turn" and "Right turn" showing wellbore curvature.

**Frame 2:** Method of Calculation. Options:
 

- Rotating off bottom
- Pulling out of the hole (WOB > 0 for tension, WOB < 0 for compression)
- Running into the hole (WOB < 0 for tension, WOB > 0 for compression)

**Frame 5:** Ftop: [ ] lb; Torque too: [ ] lb-ft; [ CALCULATE ]

**Frame 6:** Normal contact force (lb/ft) vs. measure depth (MD); Axial Force (lb) vs. measure depth (MD); Torque (lb-ft) vs. measure depth (MD). Each has an empty plot area.

Fig. A.3—Build type user form.

**Fig. A.3** is a user form in this T&D software program for T&D calculations in Build type well planning designs. This consists of input data frames and result data frames. The input data frame consists of the method of calculation (rotating off bottom, pulling out of the hole, and running into the hole) and the drilling parameters. The right-hand

end frame shows the planning picture for input data (user can see large picture by clicking on the picture).

The result frame provides all torque and drag output calculations. It shows the graph from normal contact force (lbf/ft) versus measured depth, axial tension/compression force (lbf) versus measured depth, and torque (ft-lbf) versus measured depth. The result will depend on which methods user has chosen the method of calculation. Again for the user can see a large picture of the graph by clicking on the result's picture.

The screenshot shows the 'UserForm4' application window with the following components:

- Navigation Bar:** Introduction | T&D Calculation for 3D Well Planning | Build type | Build & Hold type | Build Hold & Drop type | Horizontal wellbore | T&D Calculation Between Survey
- Frame 1:**
  - Frame 31:** Kick off Point (3000 ft), Hold section (0 ft), Build rate (5 Deg/100 ft), I (90 Deg), Left, Right turn in build section (0 Deg/100 ft), Left, Right turn in hold section (0 Deg/100 ft).
  - Frame 32:** Weight on Bit (10000 lbf), DC Diameter (6 Inch), Bit Diameter (5 Inch), Unit Weight of Drillpipe (in Air) (19.5 lb/ft), Density of Drilling Fluid (13 lb/gal), Density of Steel (65.5 lb/gal), Coefficient (0.1).
  - Frame 45:** Method of Calculation:
    - Rotating off bottom
    - Pulling out of the hole (WOB > 0 for tension, WOB < 0 for compression)
    - Running into the hole (WOB < 0 for tension, WOB > 0 for compression)
- Frame 4:** Well planning for input data. Contains a large well path diagram and two smaller diagrams labeled 'Left turn' and 'Right turn'.
- Frame 2:**
  - Frame 5:** Ftop (input field, lb), Torque too (input field, lb-ft), CommandButton1.
  - Frame 6:** Three empty graph areas:
    - Normal contact force (lb/ft) vs. measure depth(MD)
    - Force(lb) vs. measure depth (MD)
    - Torque(lb-ft) vs. measure depth (MD)

Fig. A.4–Build & hold type user form.

**Fig. A.4** is a user form in this T&D software program for T&D calculations in Build & Hold type well planning designs, which consists of input data frames and result data frames. The input data frame consists of the method of calculation (rotating off bottom, pulling out of the hole, and running into the hole) and the drilling parameters. The right-hand end frame shows the planning picture for input data (user can see large picture by clicking on the picture).

The result frame provides all torque and drag output calculations. It shows the graph from normal contact force (lbf/ft) versus measured depth, axial tension/compression force (lbf) versus measured depth, and torque (ft-lbf) versus measured depth. The result will depend on which methods the user has chosen for method of calculation. Again the user can see a large picture of the graph by clicking on the result's picture.

Fig. A.5–Build hold & drop type user form.

**Fig. A.5** is a user form in this T&D software program for T&D calculations in Build Hold & Drop type well planning designs, which consists of input data frames and result data frames. The input data frame consists of method of calculation (rotating off bottom, pulling out of the hole, and running into the hole) and the drilling parameters. The right-hand end frame shows the planning picture for input data (user can see large picture by clicking on the picture).

The result frame provides all torque and drag output calculations, which shows the graph from normal contact force (lbf/ft) versus measured depth, axial tension/compression

force (lbf) versus measured depth, and torque (ft-lbf) versus measured depth. The result depends on which method user has chosen the method of calculation. Again for the user can see a large picture of the graph by clicking on the result's picture.

The screenshot shows a software interface titled "UserForm4" with a menu bar containing "Introduction", "T&D Calculation for 3D Well Planning", "Build type", "Build & Hold type", "Build Hold & Drop type", "Horizontal wellbore", and "T&D Calculation Between Survey Using Soft-String Model".

The interface is organized into several frames:

- Frame 1:** Contains input fields for "Kick off Point" (1509 ft), "Left, Right turn in horizontal section" (0 Deg/100), "Build rate" (5.08 Dec/), "Left, Right turn in build section" (0 Deg/100 ft), and "Horizontal Section" (0 ft).
- Frame 31:** Contains input fields for "Left, Right turn in horizontal section" (0 Deg/100) and "Horizontal Section" (0 ft).
- Frame 32:** Contains input fields for "Weight on Bit" (10000 lbf), "Wellbore Diameter" (6 Inch), "Bit Diameter" (5 Inch), "Unit Weight of Drillpipe (in Air)" (19.5 lb/ft), "Density of Drilling Fluid" (13.5 lb/gal), "Density of Steel" (65.5 lb/gal), and "Coefficient" (0.333).
- Frame 4:** Titled "Well planning for input data", it displays a diagram of a well path with "Left turn" and "Right turn" views below it.
- Frame 2:** Contains input fields for "Ftop" (lb) and "Torque too" (lb-ft), and a "CALCULATE" button.
- Frame 5:** Contains three empty result frames labeled "Normal contact force (lb/ft) vs. measure depth(MD)", "Axial force(lb) vs. measure depth (MD)", and "Torque(lb-ft) vs. measure depth (MD)".

Fig. A.6–Horizontal wellbore user form.

**Fig. A.6** is a user form in this T&D software program for T&D calculations in horizontal wellbore type well planning designs, which consists of input data frames and result data frame. The input data frame consists of the method of calculation (rotating off bottom, pulling out of the hole, and running into the hole) and the drilling parameters. The right-hand end frame shows the planning picture for input data (user can see large picture by clicking on the picture).



The result frame provides all torque and drag output calculations; this shows the graph from normal contact force (lbf/ft) versus measured depth, axial tension/compression force (lbf) versus measured depth, and torque (ft-lbf) versus measured depth. The result will depend on which method the user has chosen for method of calculation. Again the user can see a large picture of the graph by clicking on the result's picture.

The screenshot shows the 'UserForm4' window with the following components:

- Frame50:** A table of input parameters for wellbore geometry.
 

MD (ft)	TVD (ft)	NC +/-	EC +/-	I (Degree)	AZ (Degree)	Deg/100 ft
90	90	-100	-70	57	300	5 DLS
159.33	129.44	-71.94	-119.62	53.64	298.97	5 DLS
228.66	172.15	-45.98	-167.65	50.29	297.83	5 DLS
- Frame32:** Material and weight input fields.
 

Weight on Bit	10000 lbf	Density of Drilling Fluid	13.5 lb/gal
Wellbore Diameter	6 Inch	Density of Steel	65.5 lb/gal
Bit Diameter	5 Inch	Coefficient	0.333
Unit Weight of Drillpipe (in Air)	19.5 lb/ft		
- Frame51:** A diagram of a wellbore showing the KOP (Kick-off Point), W (Wellbore), S (Surface), N (North), E (East), and a TARGET. It also labels TVD (True Vertical Depth) and various angles like  $\phi$ ,  $\alpha$ , and  $\beta$ .
- Frame52:** Contains a 'CALCULATE' button and three placeholder frames for results:
  - Normal contact force (lb/ft) vs. measure depth(MD) - Frame53
  - Axial force(lb) vs. measure depth (MD) - Frame54
  - Torque(lb-ft) vs. measure depth (MD) - Frame55

Fig. A.7–T&D calculation between survey user form.

**Fig. A.7** is a user form in this T&D software program for T&D calculations during the survey. This section of calculation includes buckling effects and the stress concentration factor (SCF), which consists of input data frames and result data frame. The input data

frame consists of the method of calculation (rotating off bottom, pulling out of the hole, and running into the hole), the drilling parameters, and the survey data in each position. The right-hand end frame shows the planning picture for input data (user can see large picture by clicking on the picture).

The result frame provides all of the information on torque and drag output calculations. It shows the graph from normal contact force (lbf/ft) versus measured depth, axial tension/compression force (lbf) versus measured depth, and torque (ft-lbf) versus measured depth. The result will depend on which method the user has chosen for method of calculation. Again the user can see a large picture of the graph by clicking on the result's picture.

If the user installs 3D software with MATLAB Program Version 7.4.0, he/she can use Excel link icon to show 3D wellbore trajectory.

**For example** (from T&D Calculation for 3D Well Planning User Form),

*Input field data*

**a) Target direction**

MD	TVD	NC	EC
6955.28	5000	-3000	2000

**b) Tie-on survey at KOP**

MD	TVD	NC	EC	I	AZ	DLS
90	90	-100	-70	57	300	5

Note: NC is negative, means the wellbore trajectory moves to south direction  
EC is negative, means the wellbore trajectory moves to west direction

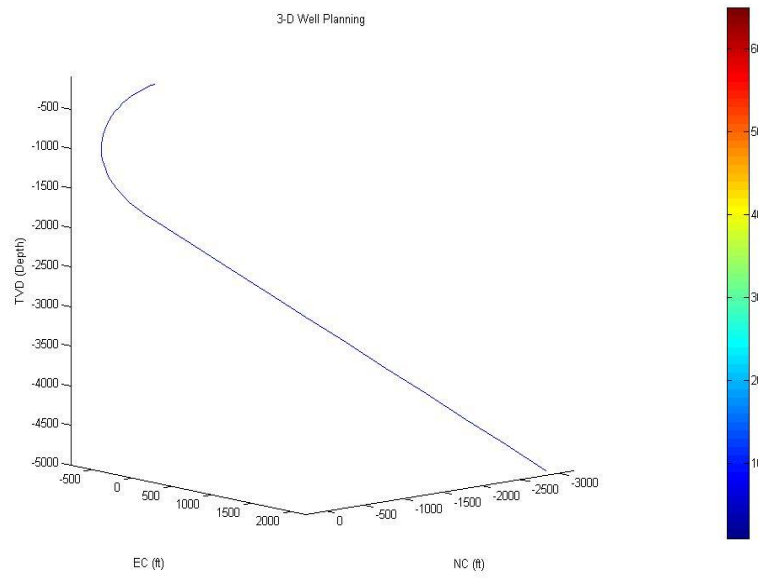


Fig. A.8–3D wellbore path by MATLAB version 7.4.0.

## **APPENDIX B**

### **COMPARISON BETWEEN WU AND JUVKAM-WOLD'S EQUATION AND NUMERICAL METHOD WHILE PULLING OUT OF THE HOLE**

In this appendix will show a comparison between Wu and Juvkam-Wold's (1991) equation and Numerical method while pulling out of the hole with  $F_{\text{eoc}} = 100,000$  lbf (tension); Extended reach well with final  $I = 65$  deg, BUR = 5.08 deg./100 ft,  $\mu = 0.333$ ,  $I_{\text{KOP}} = 0$ ,  $T_{\text{KOP}} = 1,509$  ft; Mud wt = 9.6 ppg, Pipe wt = 16.6 lb/ft in air and Density of steel = 65.5 ppg.

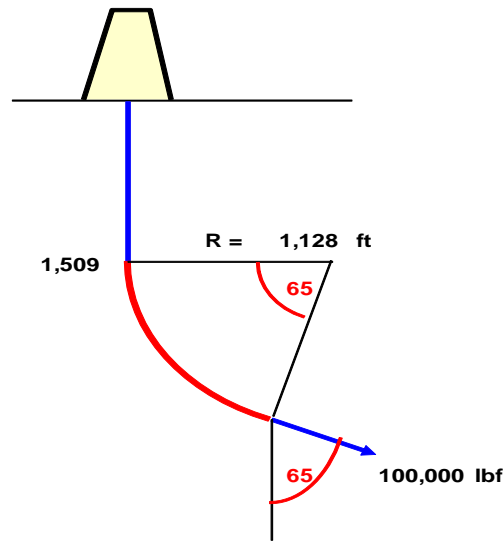


Fig. B.1–Wellbore schematic for example in Appendix B (Juvkam-Wold, 2007).

$$\alpha_0 = 25^\circ, \quad \alpha_2 = 90^\circ, \quad W_e = 16.6 (1 - 9.6/65.5) = 14.18 \text{ lb/ft}, \quad R = 18,000 / (5.08) = 1,128 \text{ ft}$$

$$\text{From Eq. 2.46, } N_{\text{EOC}} = W_e \cos \alpha_0 - F(a_0)/R$$

$$N_{\text{EOC}} = 14.18 \cos 25^\circ - 100,000/1,128$$

$$= -75.8 \text{ lbf/ft (upside contact)}$$

$$W_e R = 14.18 \text{ lb/ft} * 1,128 \text{ ft} = 15,979 \text{ lbf}$$

From **Eq. 7.15**,  $A = 9,579$  lbf

From **Eq. 7.16**,  $B = -12,789$  lbf

From **Eq. 7.14**

$$F_{KOP} = [100,000 + 9,579 \sin 25^\circ + 12,789 \cos 25^\circ] \exp[0.333 (\frac{\pi}{2} - 25^\circ \frac{\pi}{180})] - 9,579 \sin 90^\circ - 12,789 \cos 90^\circ$$

$$F_{KOP} = 159,140 \text{ lbf}$$

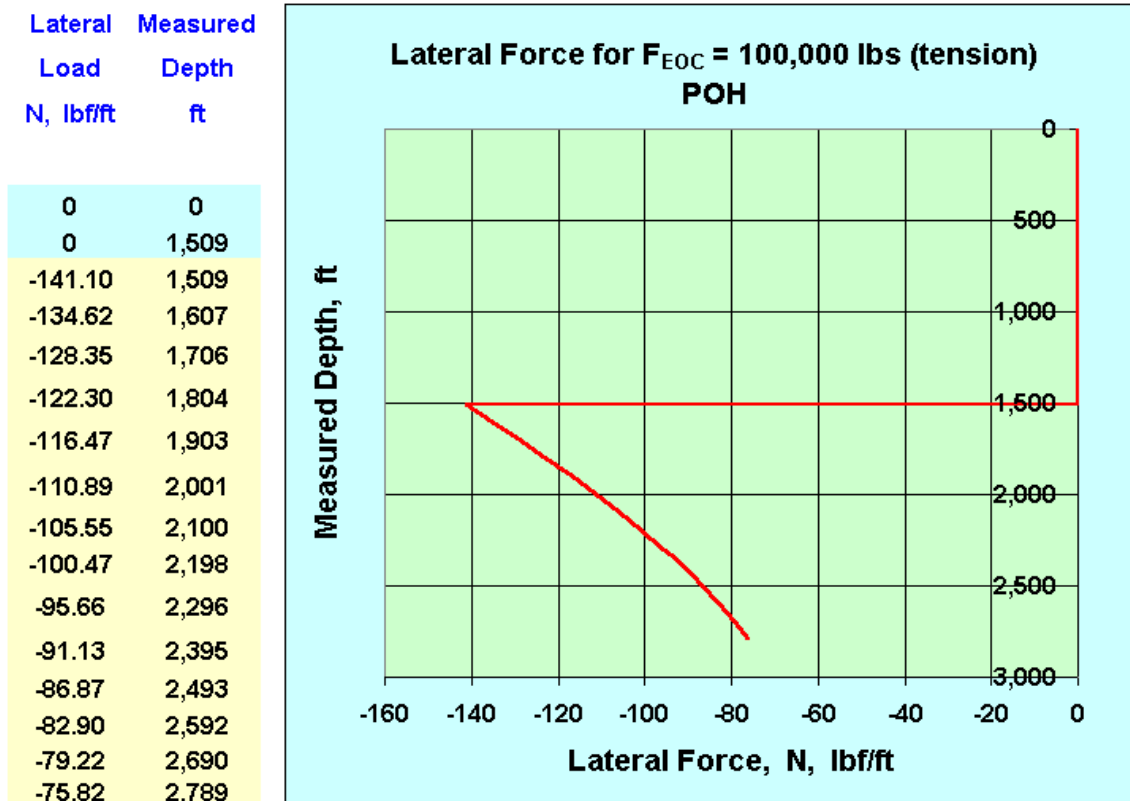


Fig. B.2—Normal contact force (lb/ft) versus measured depth (ft) for this example using Wu and Juvkam-Wold's (1991) method (Juvkam-Wold, 2007).

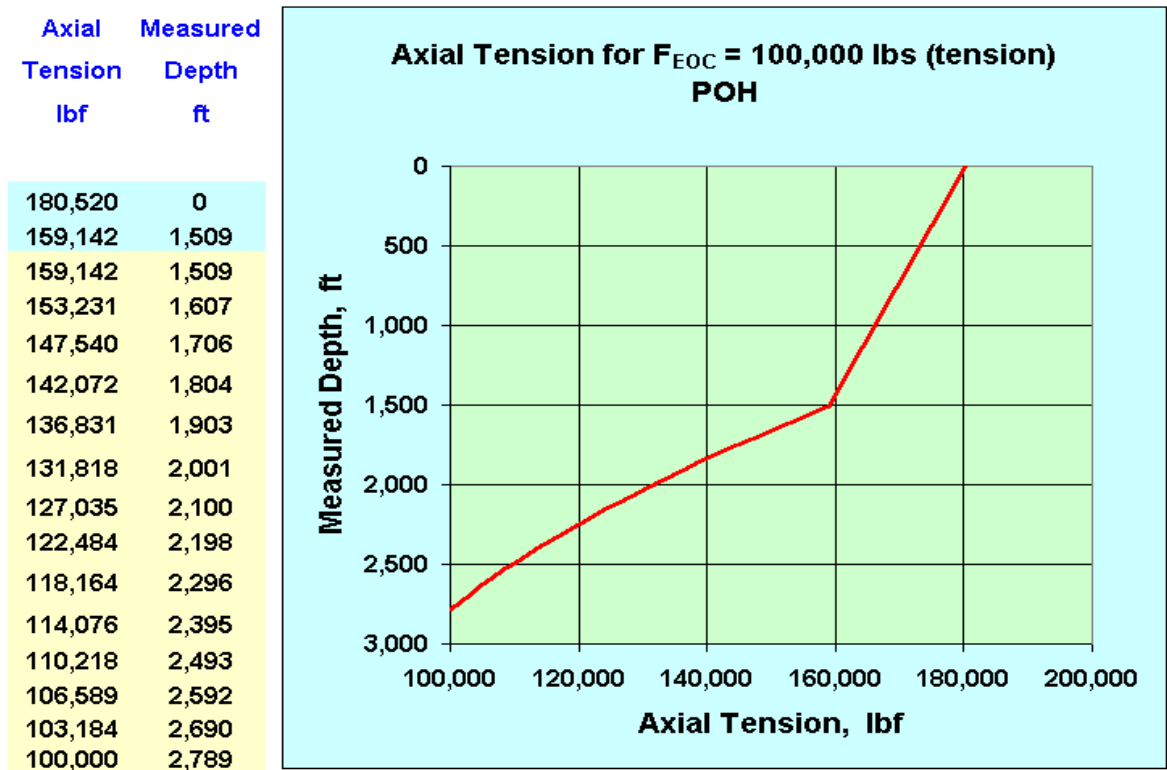


Fig. B.3—Axial tension plot for this example using Wu and Juvkam-Wold's (1991) method (Juvkam-Wold, 2007).

In this section will be numerical analysis method.

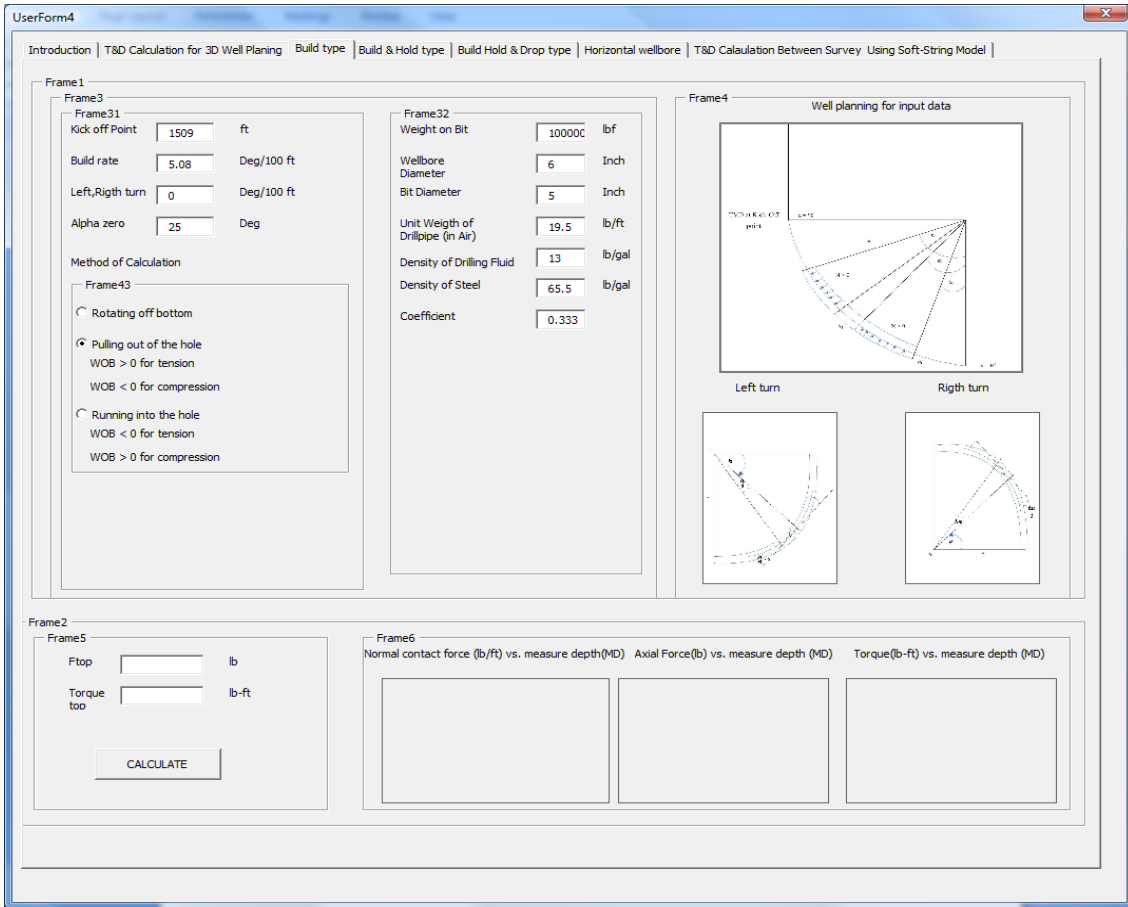


Fig. B.4—User dorm of Appendix B example.



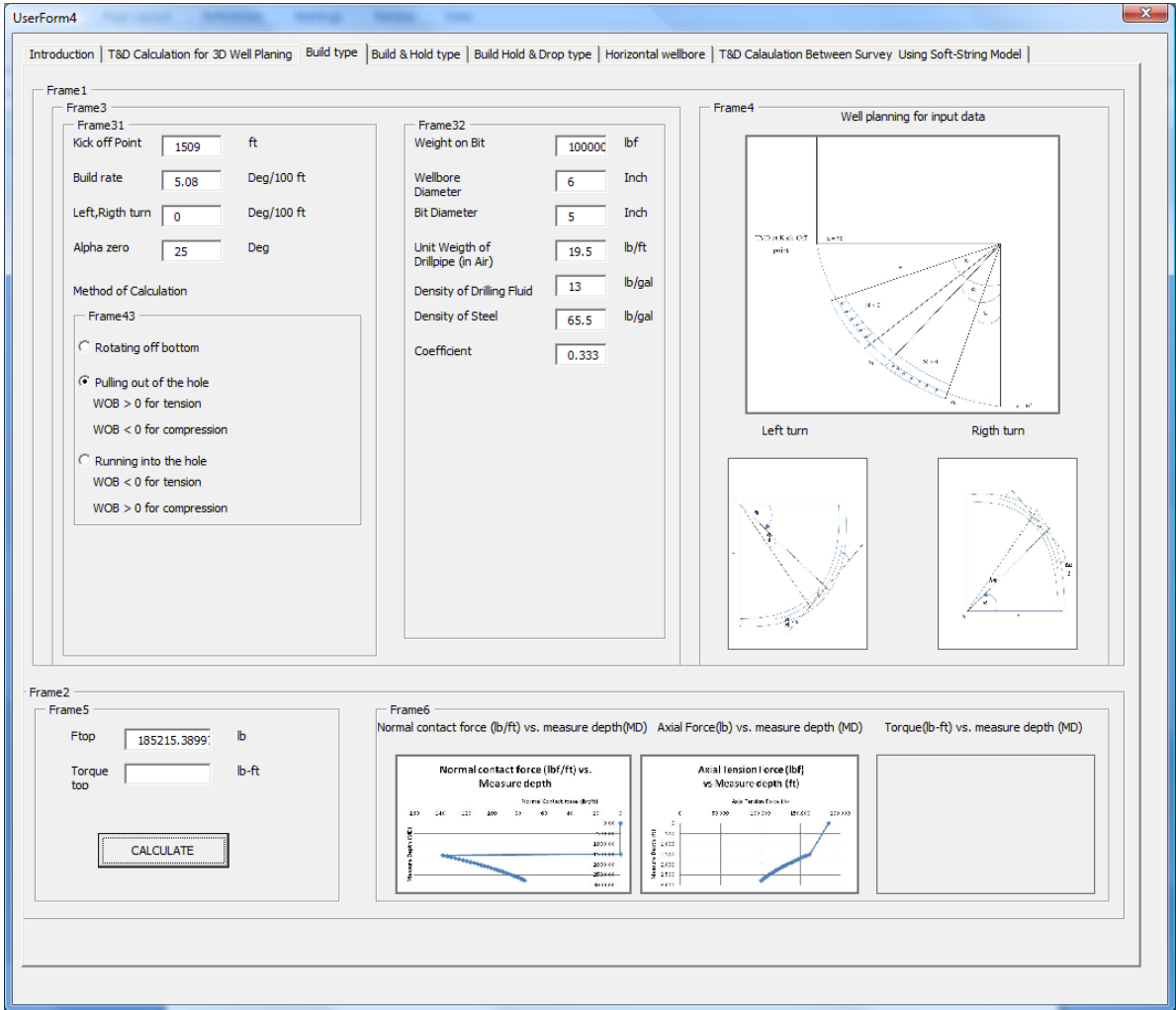


Fig. B.5—Result user form of Appendix B example.

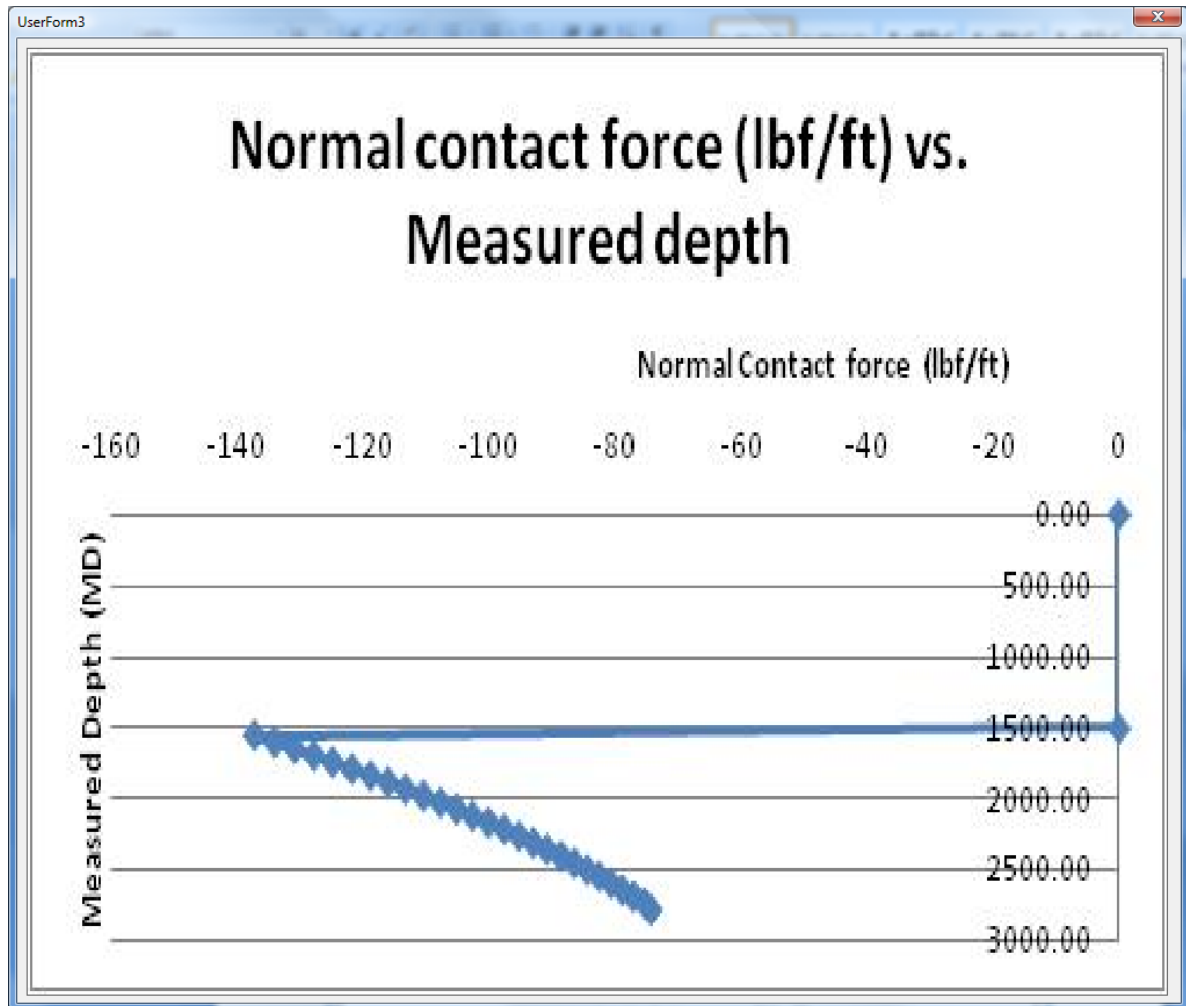


Fig. B.6—Normal contact force (lb/ft) versus measured depth (ft).

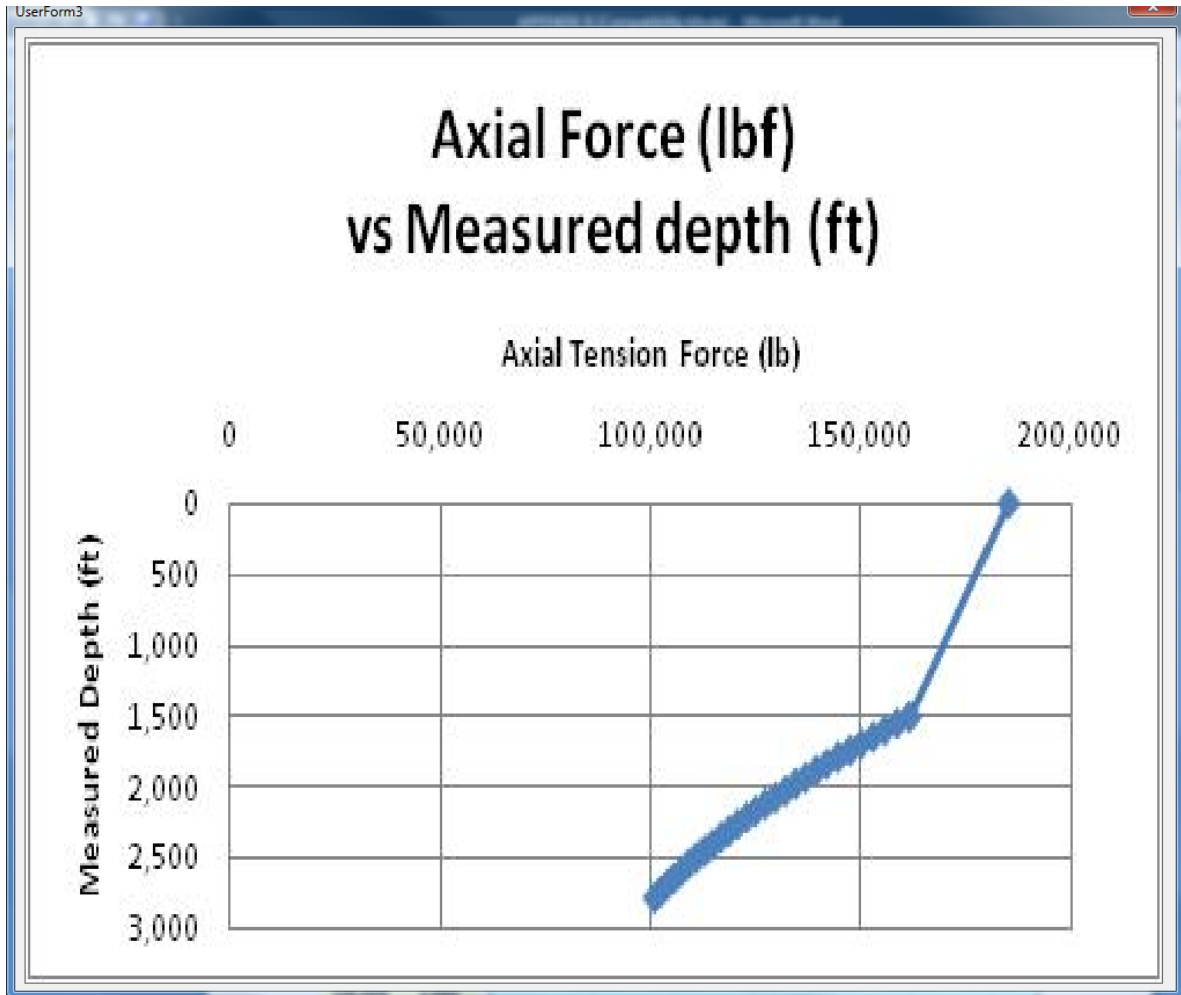


Fig. B.7—Axial tension force (lb) versus measured depth (ft) ( $F > 0$  referred to tensile force).

## **APPENDIX C**

### **COMPARISON BETWEEN WU AND JUVKAM-WOLD'S EQUATIONS AND NUMERICAL METHODS WHILE PULLING OUT OF THE HOLE**

In this appendix will show a comparison between Wu and Juvkam-Wold's (1991) equation and numerical method while running into the hole with  $F_{eoc} = 17,000$  lbf (tension); Extended reach well with final  $I = 65$  deg, BUR = 5.08 deg./100 ft,  $\mu = 0.333$ ,  $I_{KOP} = 0$ ,  $T_{KOP} = 1,509$  ft; Mud wt = 9.6 ppg, Pipe wt = 16.6 lb/ft in air and Density of steel = 65.5 ppg

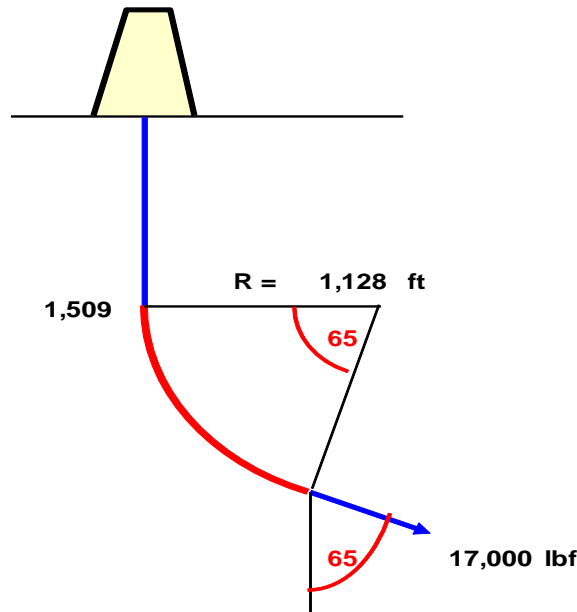


Fig. C.1–Wellbore Schematic for example in Appendix C (Juvkam-Wold, 2007).

$\alpha_0 = 25^\circ/180$ ,  $\alpha_2 = \pi/2$ ,  $W_e = 16.6 (1 - 9.6/65.5) = 14.18$  lb/ft,  $R = 18,000/(\pi 5.08) = 1,128$  ft

From **Eq. 2.46**,  $N_{EOC} = W_e \cos a_0 - F(a_0)/R$

$$N_{EOC} = 14.18 \cos 25 - 17,000/1,128$$

$$= -2.23 \text{ lbf/ft (upside contact)}$$

$$W_e R = 14.18 \text{ lb/ft} * 1,128 \text{ ft} = 15,979 \text{ lbf}$$

From **Eq. 7.15**,  $A = 9,579$  lbf

From **Eq. 7.16**,  $B = -12,789$  lbf

From Eq. 7.14

$$F_{c,KOP} = (-17,000 + 9,579\sin 25^\circ - 12,787\cos 25^\circ) \exp(-0.333 (\frac{D}{2} - 25 \frac{D}{180})) - 9,579\sin 90^\circ - 12,789\cos 90^\circ$$

$$F_{KOP} = 26,400 \text{ lbf (tension)}$$

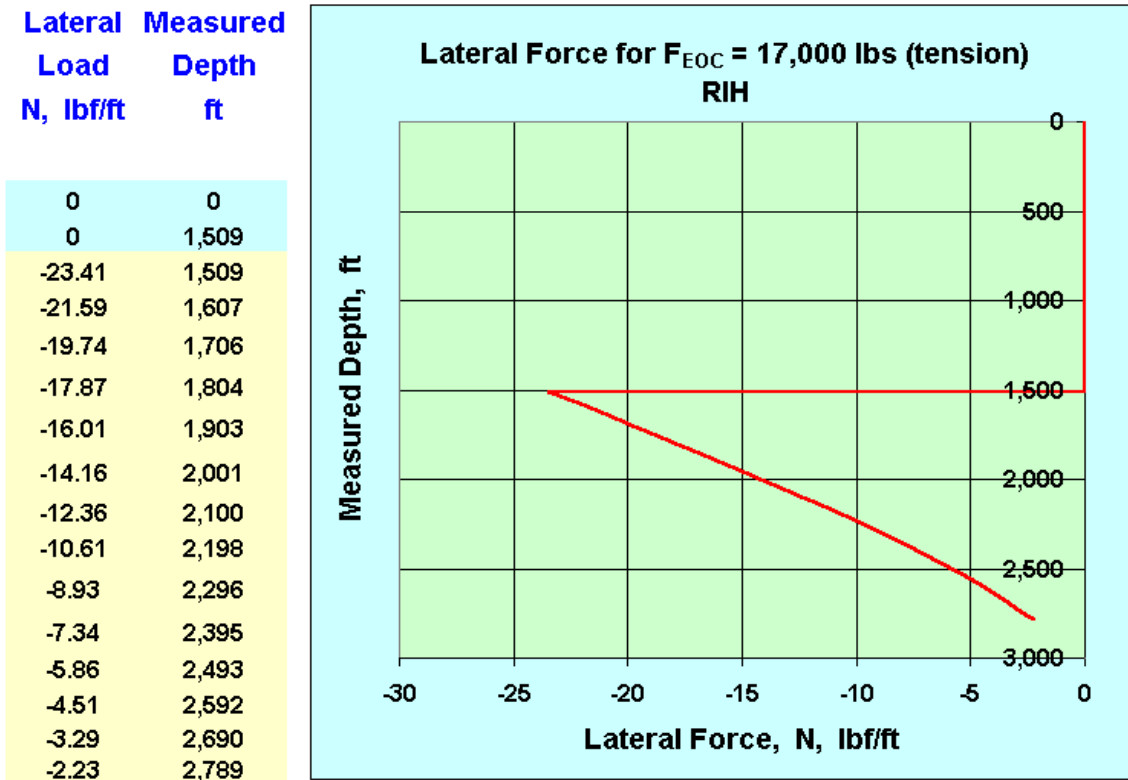


Fig. C.2–Normal contact force (lb/ft) versus measure depth (ft) for this example using Wu and Juvkam-Wold’s (1991) method (Juvkam-Wold, 2007).

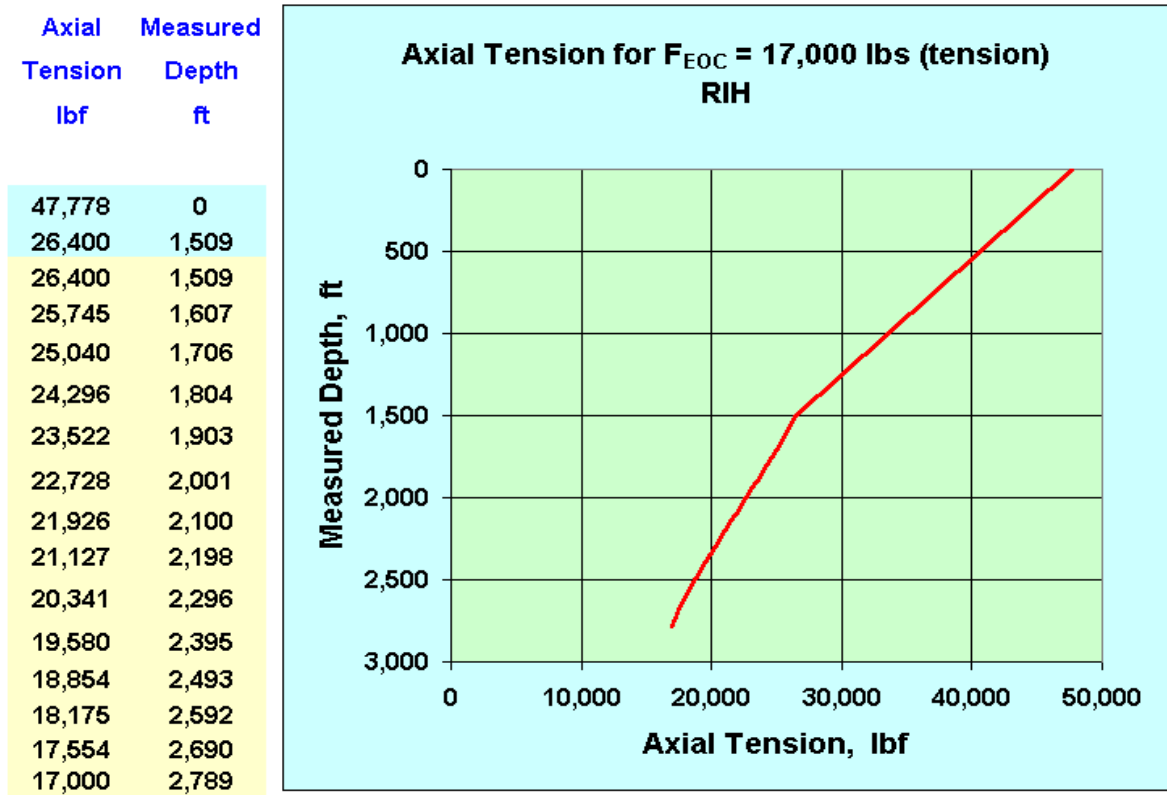


Fig. C.3–Axial tension plot for this example using Wu and Juvkam-Wold’s (1991) method (Juvkam-Wold, 2007).

In this section will be numerical analysis method.

UserForm4

Introduction | T&D Calculation for 3D Well Planning | Build type | Build & Hold type | Build Hold & Drop type | Horizontal wellbore | T&D Calculation Between Survey Using Soft-String Model

Frame 1

Frame 31

Kick off Point  ft

Build rate  Deg/100 ft

Left, Righth turn  Deg/100 ft

Alpha zero  Deg

Method of Calculation

Frame 43

Rotating off bottom

Pulling out of the hole  
WOB > 0 for tension  
WOB < 0 for compression

Running into the hole  
WOB < 0 for tension  
WOB > 0 for compression

Frame 32

Weight on Bit  lbf

Wellbore Diameter  Inch

Bit Diameter  Inch

Unit Weight of Drillpipe (in Air)  lb/ft

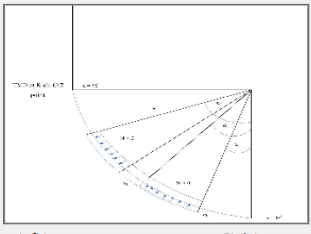
Density of Drilling Fluid  lb/gal


Density of Steel  lb/gal

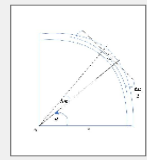
Coefficient

Frame 4

Well planning for input data



Left turn 

Righth turn 

Frame 2

Frame 5

F<sub>top</sub>  lb

Torque  lb-ft

Frame 6

Normal contact force (lb/ft) vs. measure depth (MD)

Axial Force (lb) vs. measure depth (MD)

Torque (lb-ft) vs. measure depth (MD)

Fig. C.4–User form of Appendix C example.



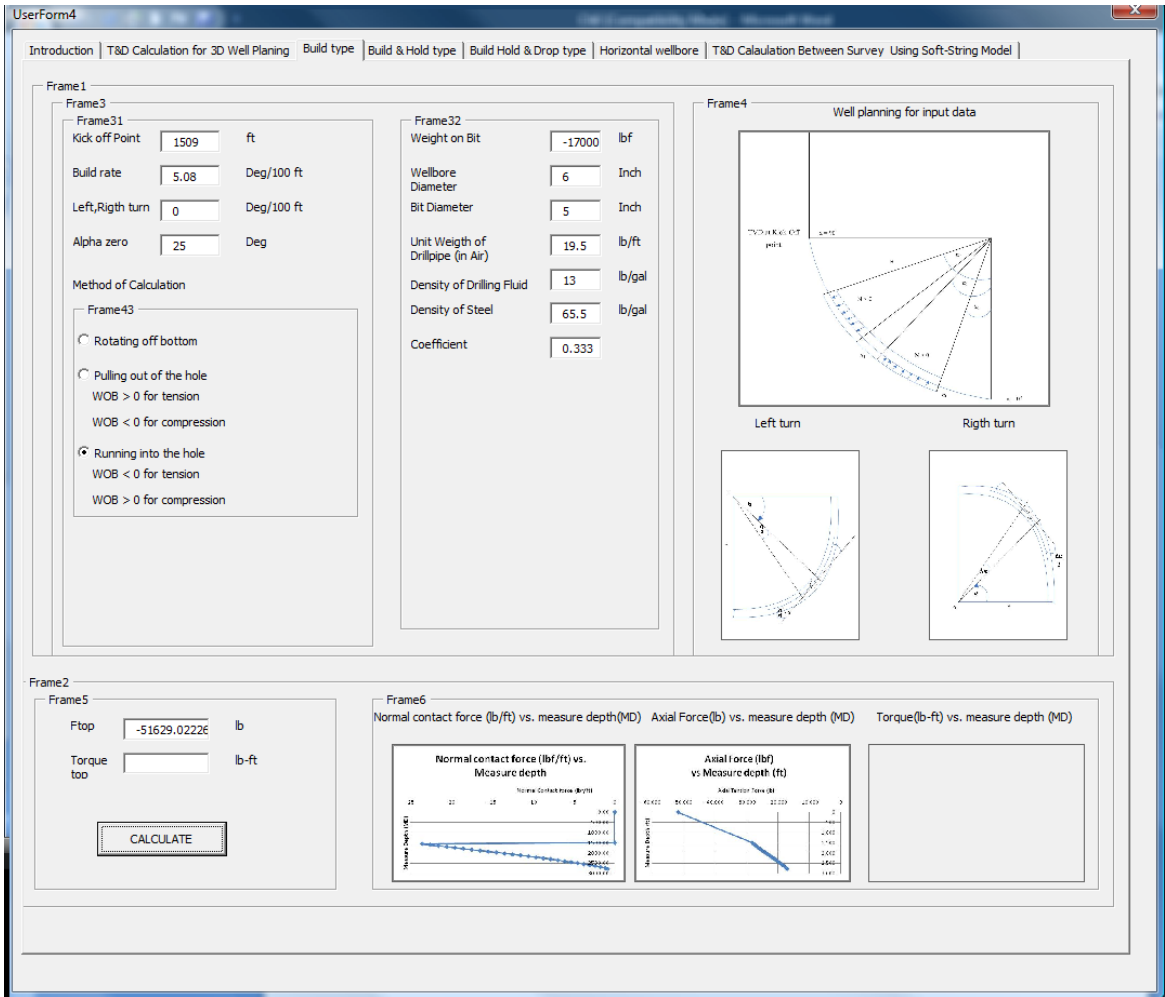


Fig. C.5—Result user form of Appendix C example.

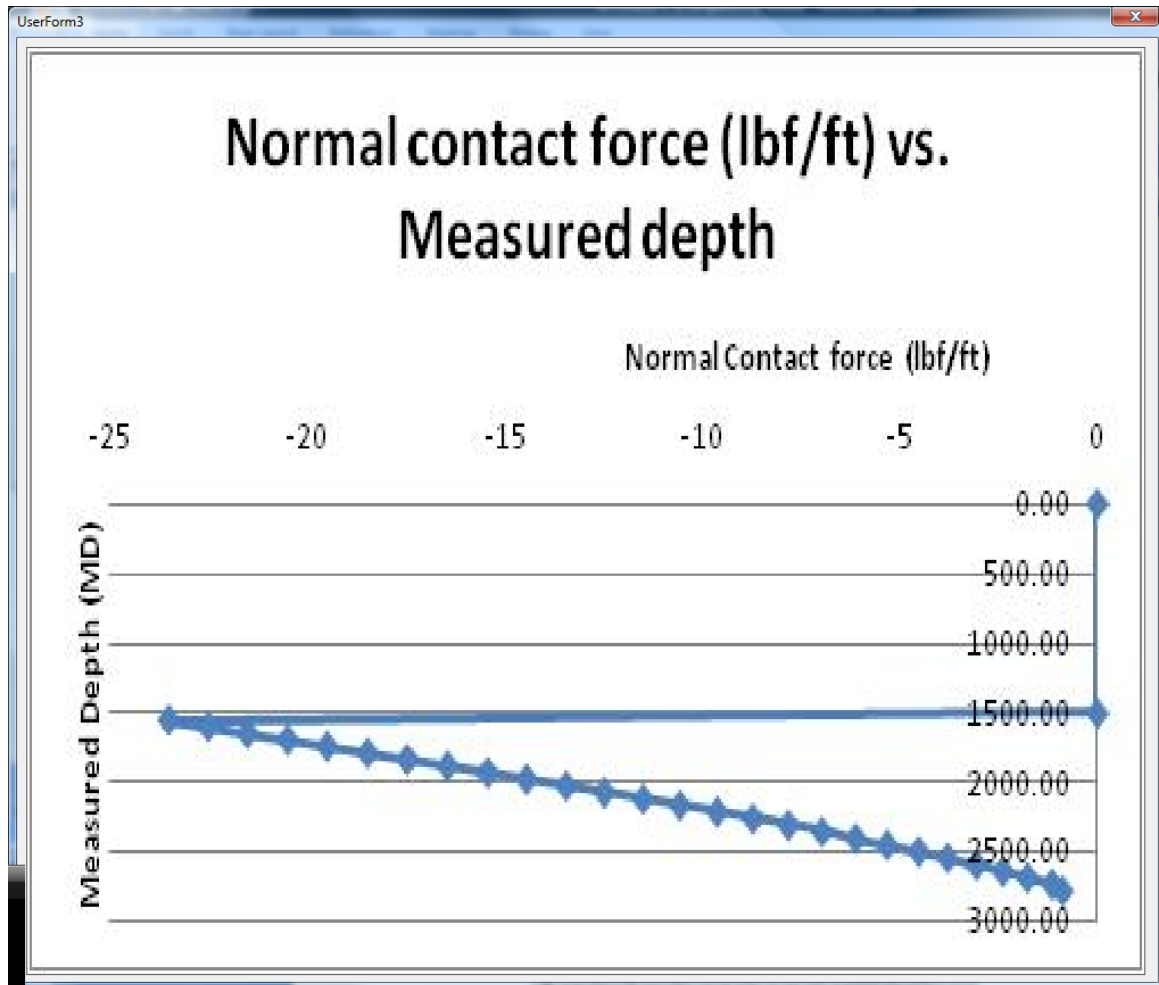


Fig. C.6—Normal contact force (lb/ft) versus measured depth (ft).

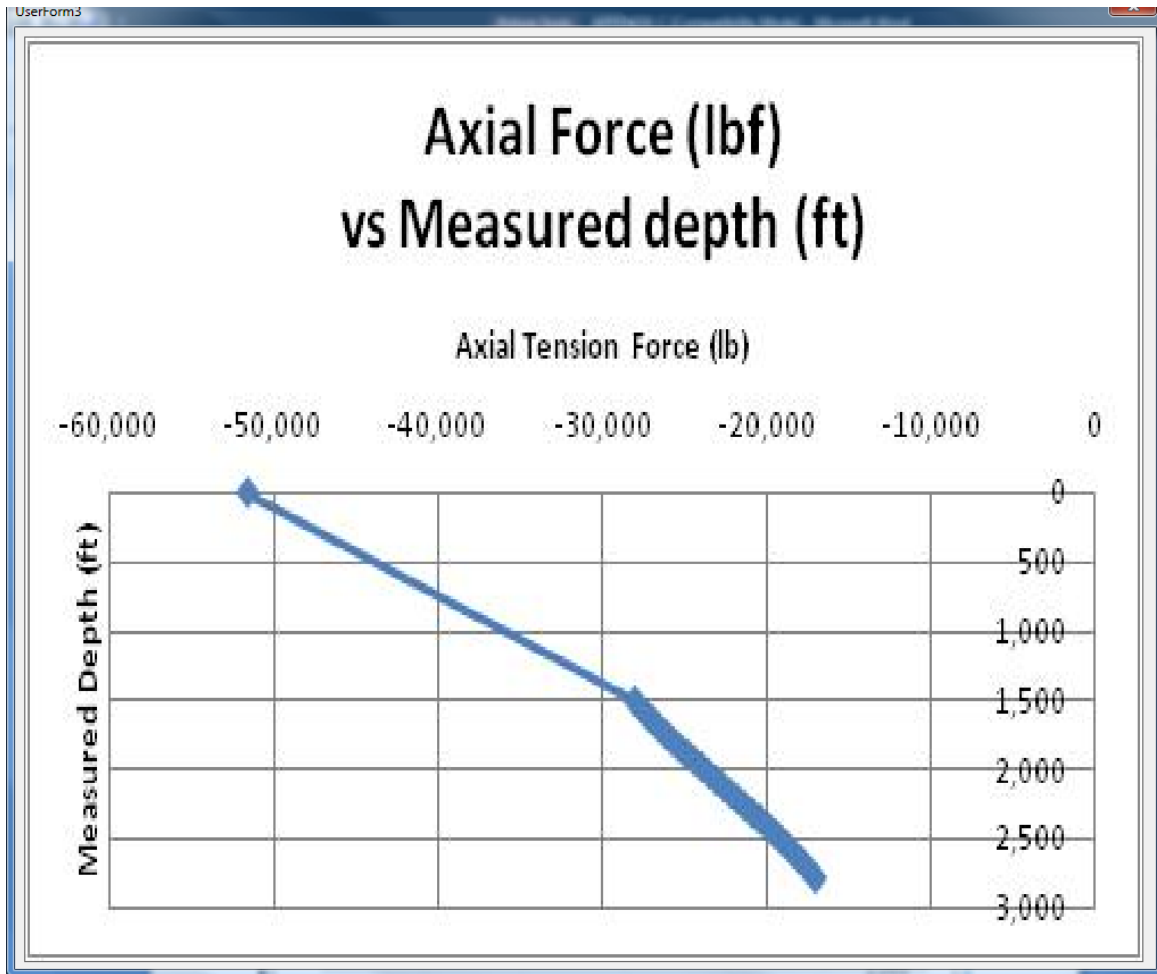


Fig. C.7–Axial force (lb) versus measured depth (ft) ( $F < 0$  referred to tensile force).

**APPENDIX D****COMPARISON BETWEEN WU AND JUVKAM-WOLD'S EQUATIONS AND  
NUMERICAL METHODS WHILE RUNNING INTO THE HOLE WITH  
COMPRESSIVE FORCE**

In this appendix will show a comparison between Wu and Juvkam-Wold's (1991) equation and numerical method while running into the hole with  $F_{\text{eoc}} = 3,000$  lbf (compression). Extended reach well with final  $I = 65$  deg, BUR = 5.08 deg./100 ft,  $\mu = 0.333$ ,  $I_{\text{KOP}} = 0$ ,  $T_{\text{KOP}} = 1,509$  ft. Mud wt = 9.6 ppg, Pipe wt = 16.6 lb/ft in air and Density of steel = 65.5 ppg

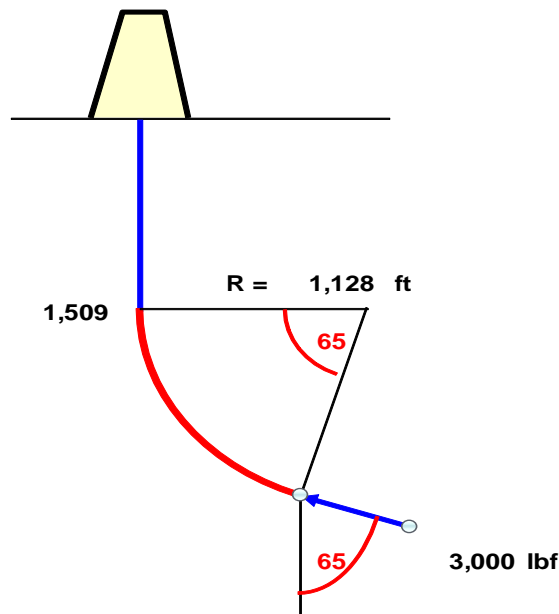


Fig. D.1—Wellbore schematic for example in Appendix D (Juvkam-Wold, 2007).

$\alpha_0 = 25^\circ/180$ ,  $\alpha_2 = 90^\circ/2$ ,  $W_e = 16.6 (1 - 9.6/65.5) = 14.18$  lb/ft,  $R = 18,000 / (5.08) = 1,128$  ft

From **Eq. 2.46**,  $N_{\text{EOC}} = W_e \cos \alpha_0 - F(a_0)/R$

$$\begin{aligned} N_{\text{EOC}} &= 14.17 \cos 25 + (+3,000)/1,128 \\ &= 15.50 \text{ lbf/ft (downside contact)} \end{aligned}$$

By trial and error it is found that, when inclination angle = 15.4 deg. ( $\alpha_1 = 74.6^\circ$ )  $N = 0$ , and contact changes to upside

$$W_e R = 14.18 \text{ lb/ft} * 1,128 \text{ ft} = 15,979 \text{ lbf}$$

$$\text{From Eq. 7.15, } A = 9,579 \text{ lbf}$$

$$\text{From Eq. 7.16, } B = -12,789 \text{ lbf}$$

Using Wu and Juvkam-Wold's (1991) equation between  $\alpha_0$  and  $\alpha_1$  (25 to 74.6 deg.):

$$F_c(\alpha_1) = [F_c(\alpha_0) - A \sin \alpha_0 + B \cos \alpha_0] \exp(\mu(\alpha_1 - \alpha_0)) + A \sin \alpha_1 - B \cos \alpha_1$$

$$F_c(\alpha_1) = -4,230 \text{ lbf,}$$

$$N(\alpha_1) = 14.17 \cos 74.6 + (-4,230)/1,128 = 0.01 \text{ lbf}$$

Now using Wu and Juvkam-Wold's (1991) equation between  $\alpha_1$  and  $\alpha_2$  (74.6 and 90 deg.):

$$F_c(\alpha_2) = [F_c(\alpha_1) + A \sin \alpha_1 + B \cos \alpha_1] \exp(-\mu(\alpha_2 - \alpha_1)) + A \sin \alpha_2 - B \cos \alpha_2$$

$$F_c(\alpha_2) = (-8,108) \quad (\text{in compression})$$

$$F_{KOP} = 8,108 \text{ lbf} \quad (\text{in tension})$$

From Wu and Juvkam-Wold's (1991) equation

$$F_d = F_c(\alpha_2) - F_c(\alpha_0) - W_e R(\cos \alpha_2 - \cos \alpha_0)$$

$$= -8,108 - 3,000 - 15,979 (\cos 90^\circ - \cos 25^\circ)$$

$$F_d = 3,373 \text{ lbf}$$

**Pipe in Compression at EOC**  
**RIH with FEOC = -3,000 lbf**

	Measured Depth	Inclination Angle	Inclination Angle	Angle $\alpha$	Axial Tension	Lateral Load
	ft	deg	radians	radians	lbf	N, lbf/ft
Vertical	0	0	0	1.5708	29,486	0
Vertical - at KOP	1,509	0	0	1.5708	8,108	0
Build Section - at KOP	1,509	0	0	1.5708	8,108	-7.19
Build Section	1,607	5	0.0873	1.4835	6,914	-4.89
Build Section	1,706	10	0.1745	1.3963	5,654	-2.55
<b>Build Section</b>	<b>1,812</b>	<b>15.4</b>	<b>0.2688</b>	<b>1.3020</b>	<b>4,230</b>	<b>0.01</b>
Build Section	1,911	20.4	0.3560	1.2147	2,942	2.33
Build Section	2,001	25	0.4363	1.1345	1,860	4.34
Build Section	2,100	30	0.5236	1.0472	800	6.37
Build Section	2,198	35	0.6109	0.9599	-136	8.25
Build Section	2,296	40	0.6981	0.8727	-943	9.94
Build Section	2,395	45	0.7854	0.7854	-1,620	11.45
Build Section	2,493	50	0.8727	0.6981	-2,164	12.77
Build Section	2,592	55	0.9599	0.6109	-2,575	13.89
Build Section	2,690	60	1.0472	0.5236	-2,853	14.80
Build Section - EOC	2,789	65	1.1345	0.4363	-3,000	15.50

Fig. D.2—Force table for Appendix D example (Juvkam-Wold, 2007).

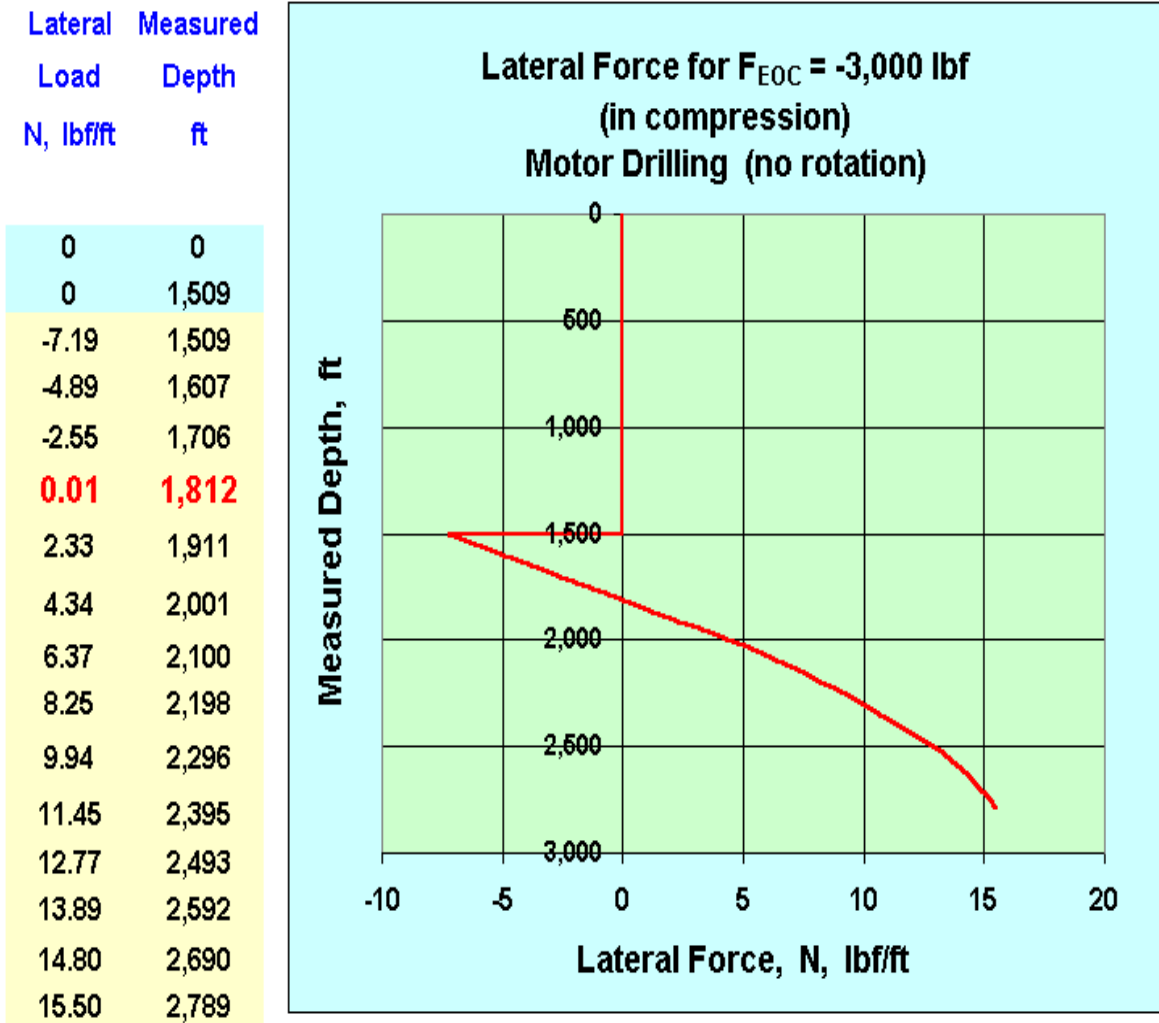


Fig. D.3–Normal contact force (lb/ft) versus measure depth (ft) from Wu and Juvkam-Wold’s (1991) equation (Juvkam-Wold, 2007).



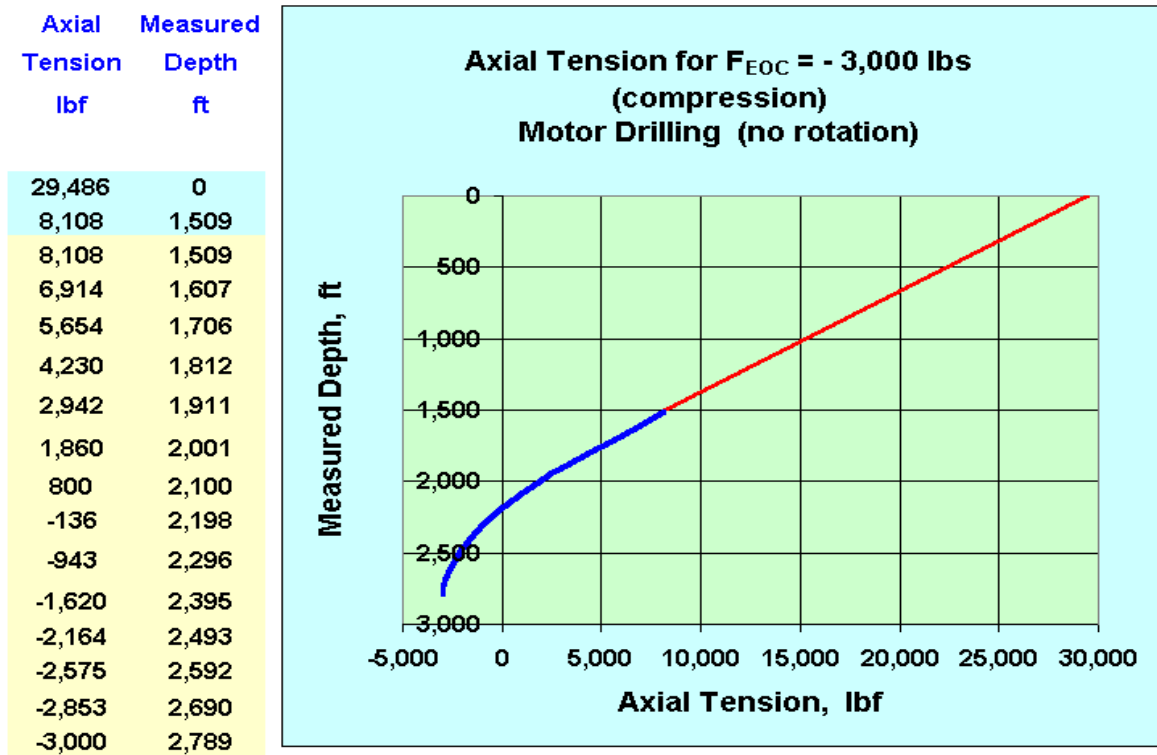


Fig. D.4–Axial tension plot for this example using Wu and Juvkam-Wold’s (1991) method (Juvkam-Wold, 2007).

In this section will be numerical analysis method.

UserForm4

Introduction | T&D Calculation for 3D Well Planing | Build type | Build & Hold type | Build Hold & Drop type | Horizontal wellbore | T&D Calculation Between Survey Using Soft-String Model

Frame1

Frame3

Frame31

Kick off Point  ft

Build rate  Deg/100 ft

Left,Right turn  Deg/100 ft

Alpha zero  Deg

Method of Calculation

Frame43

Rotating off bottom

Pulling out of the hole  
WOB > 0 for tension  
WOB < 0 for compression

Running into the hole  
WOB < 0 for tension  
WOB > 0 for compression

Frame32

Weight on Bit  lbf

Wellbore Diameter  Inch

Bit Diameter  Inch

Unit Weight of Drillpipe (in Air)  lb/ft

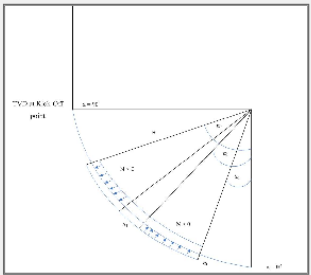
Density of Drilling Fluid  lb/gal

Density of Steel  lb/gal

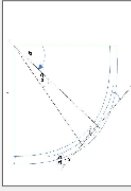
Coefficient

Frame4

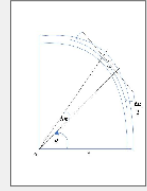
Well planning for input data



Left turn



Right turn



Frame2

Frame5

F<sub>top</sub>  lb

Torque <sub>top</sub>  lb-ft

CALCULATE

Frame6

Normal contact force (lb/ft) vs. measure depth(MD)    Axial Force(lb) vs. measure depth (MD)    Torque(lb-ft) vs. measure depth (MD)

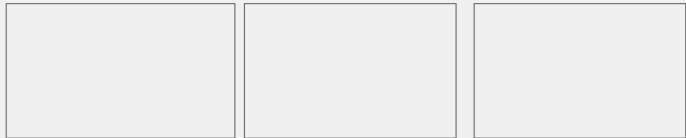


Fig. D.5–User form of Appendix D example.

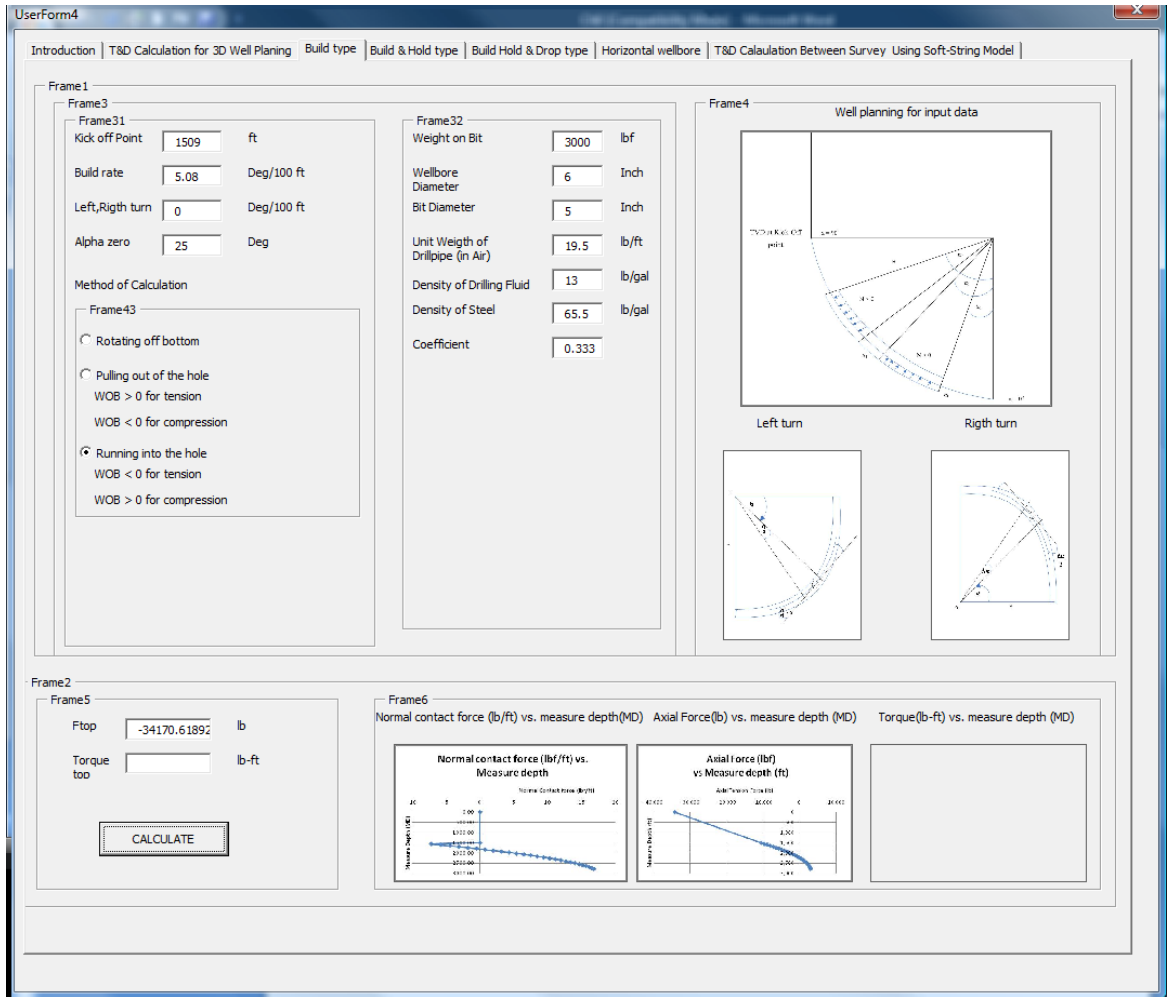


Fig. D.6—Result user form of Appendix D example.

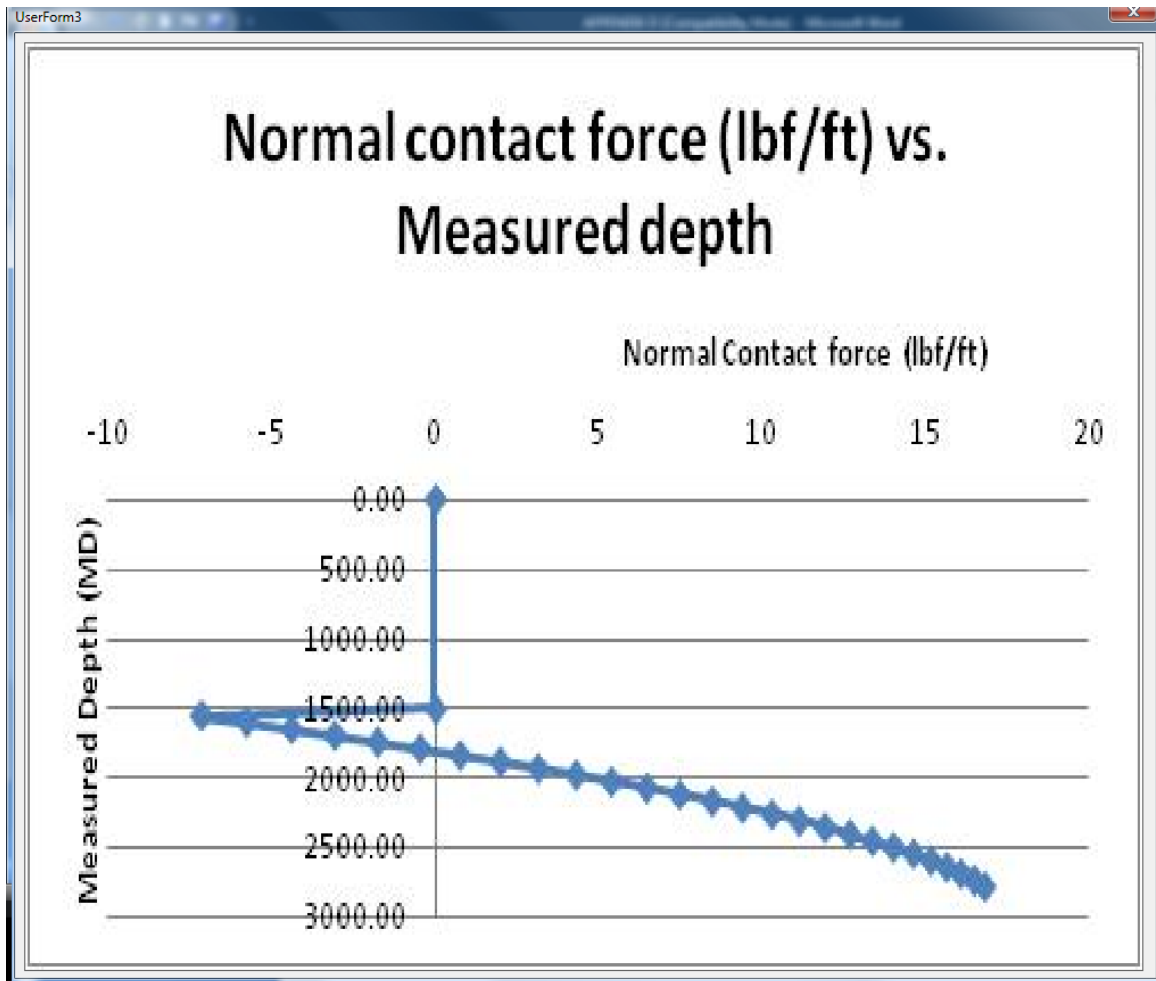


Fig. D.7–Normal contact force (lb/ft) versus measured depth (ft).

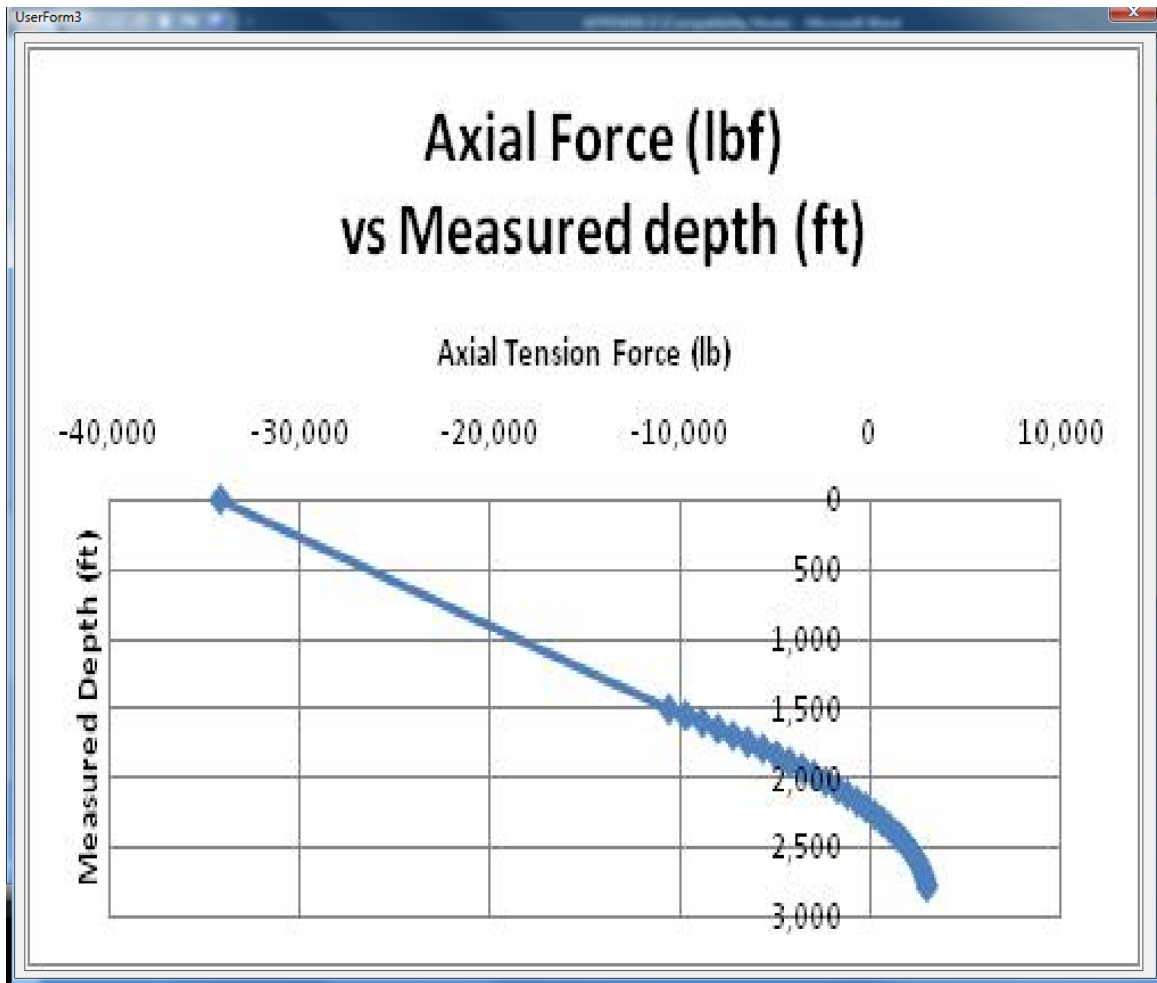


Fig. D.8–Axial force (lb) versus measured depth (ft) ( $F < 0$  referred to tensile force).

## **APPENDIX E**

### **COMPARISON RESULT BETWEEN 2D WELLBORE DESIGN AND 3D WELLBORE DESIGN WHILE RUNNING INTO THE HOLE WITH COMPRESSIVE FORCE**

In this appendix will show a comparison of Hook load ( $F_{kop}$ ) between 2D wellbore trajectory and 3D wellbore trajectory with 10 Deg/100 ft (left/right turn) in build section while running into the hole. By using the same input values as Appendix D.

Extended reach well with final I = 65 deg, BUR = 5.08 deg./100 ft,  $\mu = 0.333$ ,  $I_{KOP} = 0$ ,  $T_{KOP} = 1,509$  ft Mud wt = 9.6 ppg, Pipe wt = 16.6 lb/ft in air, Density of steel = 65.5 ppg and running into the hole with  $F_{coc} = 3,000$  lbf (compression)

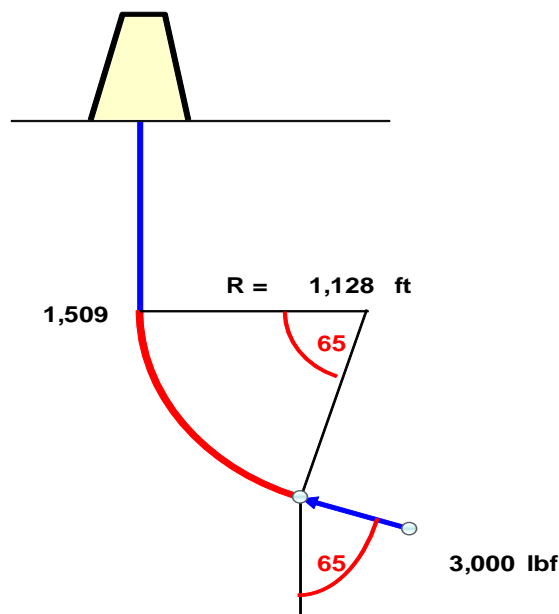


Fig. E.1–Wellbore schematic for example in Appendix E (Juvkam-Wold, 2007).

Using T&D software calculation will give the result same as Appendix D,  $F_{kop} = 34,170$  lb (tension)

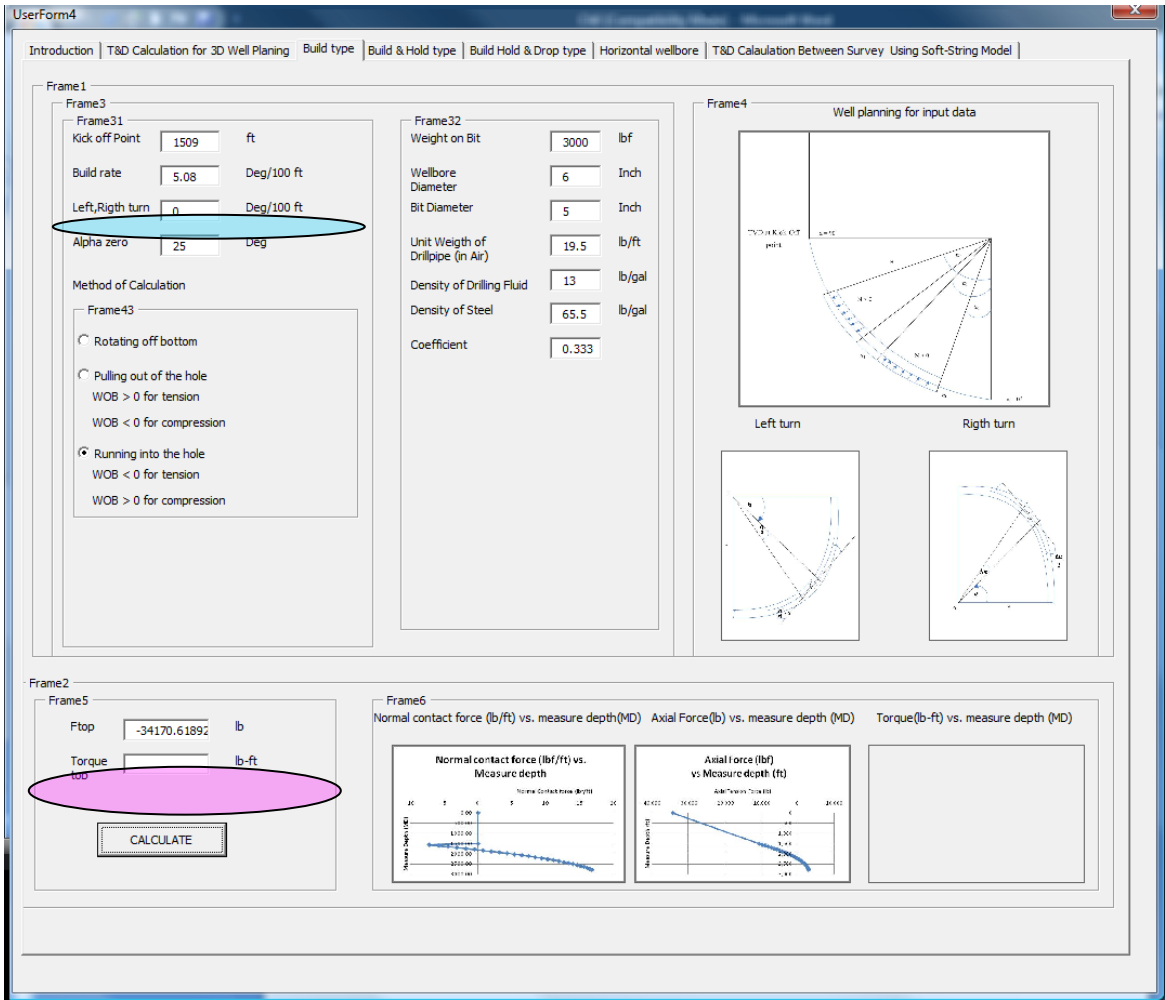


Fig. E.2–Result user form with 2D wellbore trajectory (no left/right turn).



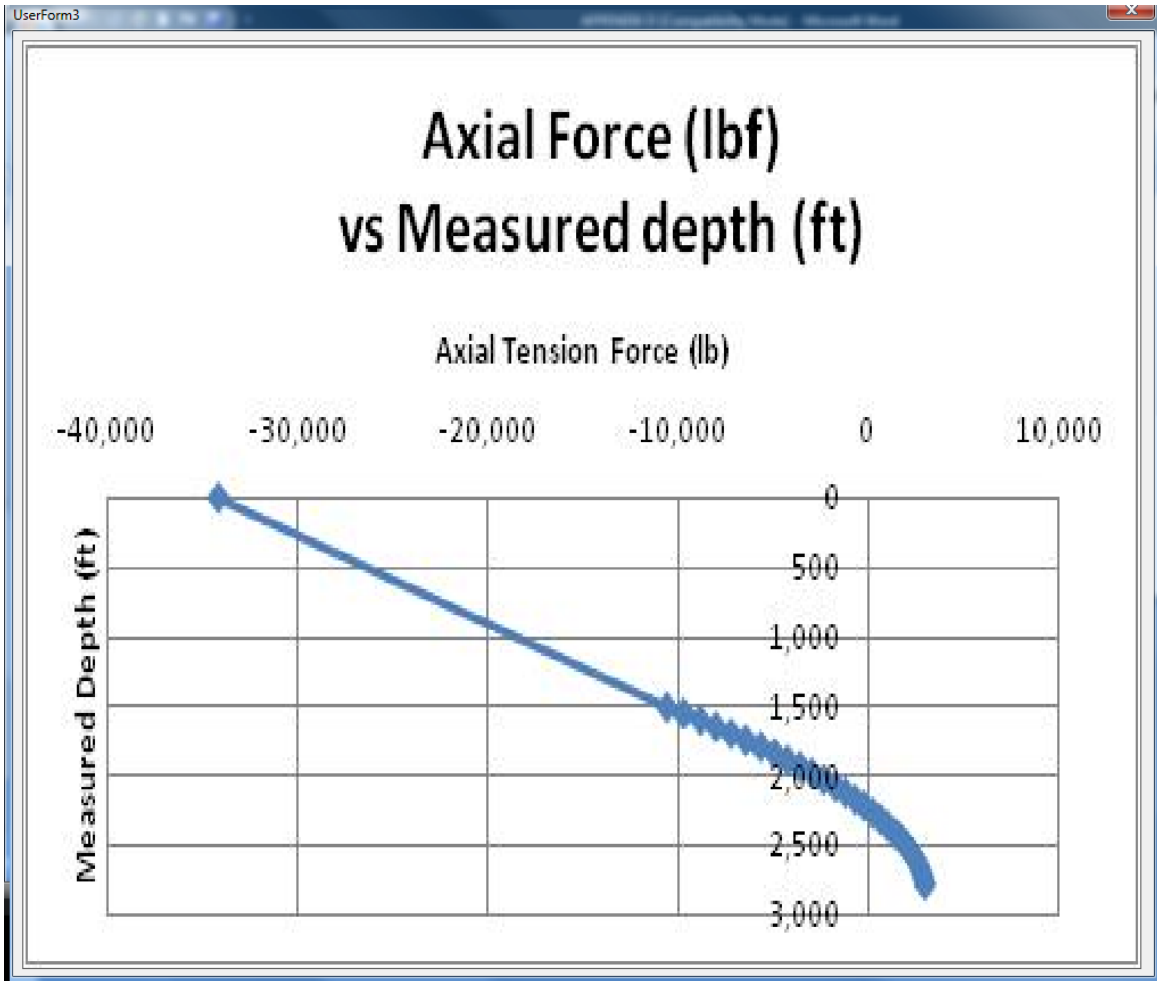


Fig. E.3—Axial force (lb) versus measured depth (ft) ( $F < 0$  referred to tensile force) from 2D wellbore trajectory.

Using T&D software calculation with 10 Deg/100 ft (left/right turn) in build section will give  $F_{kop} = 32,014$  lb (tension)

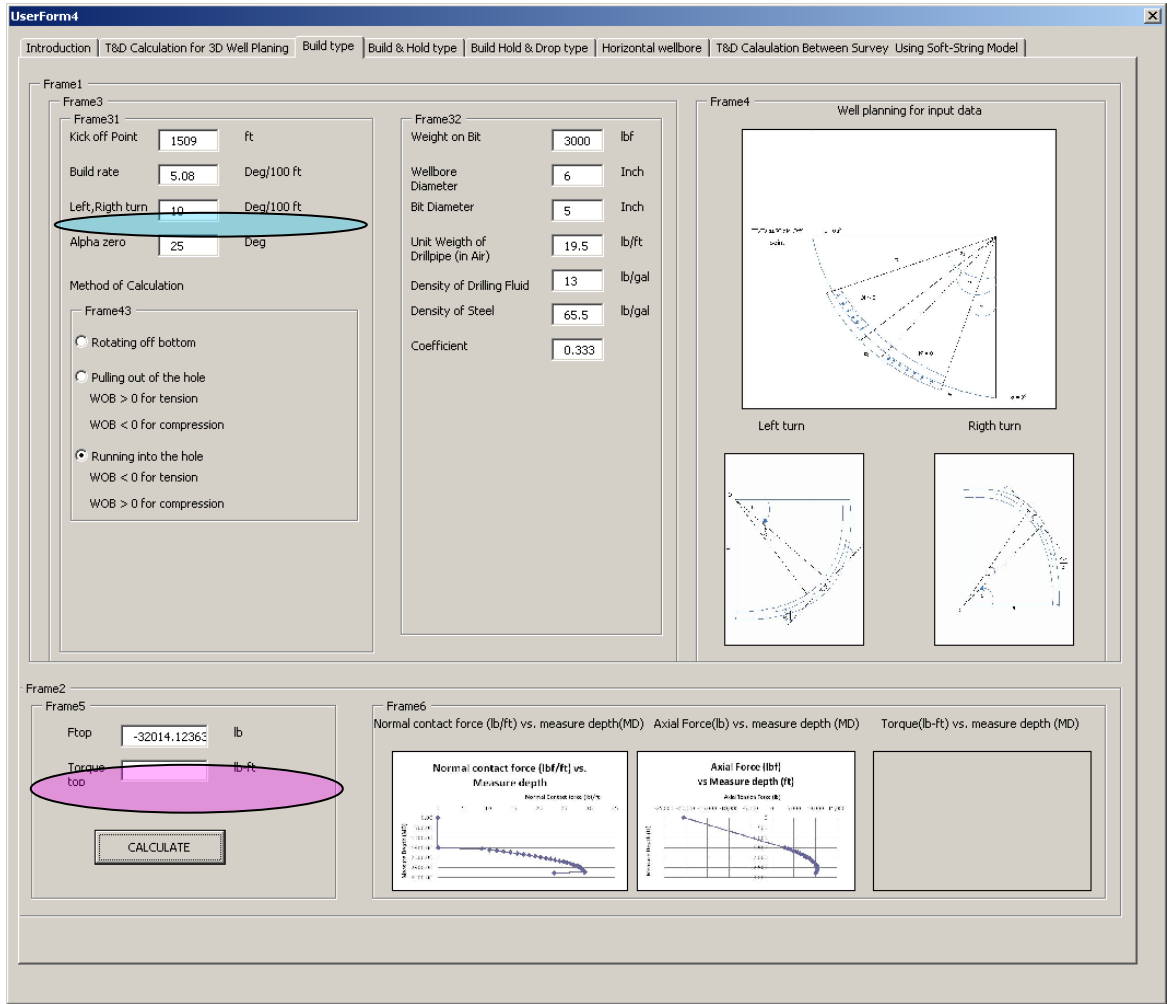


Fig. E.4—Result user form with 3D wellbore trajectory (10 deg/100ft left/right turn).

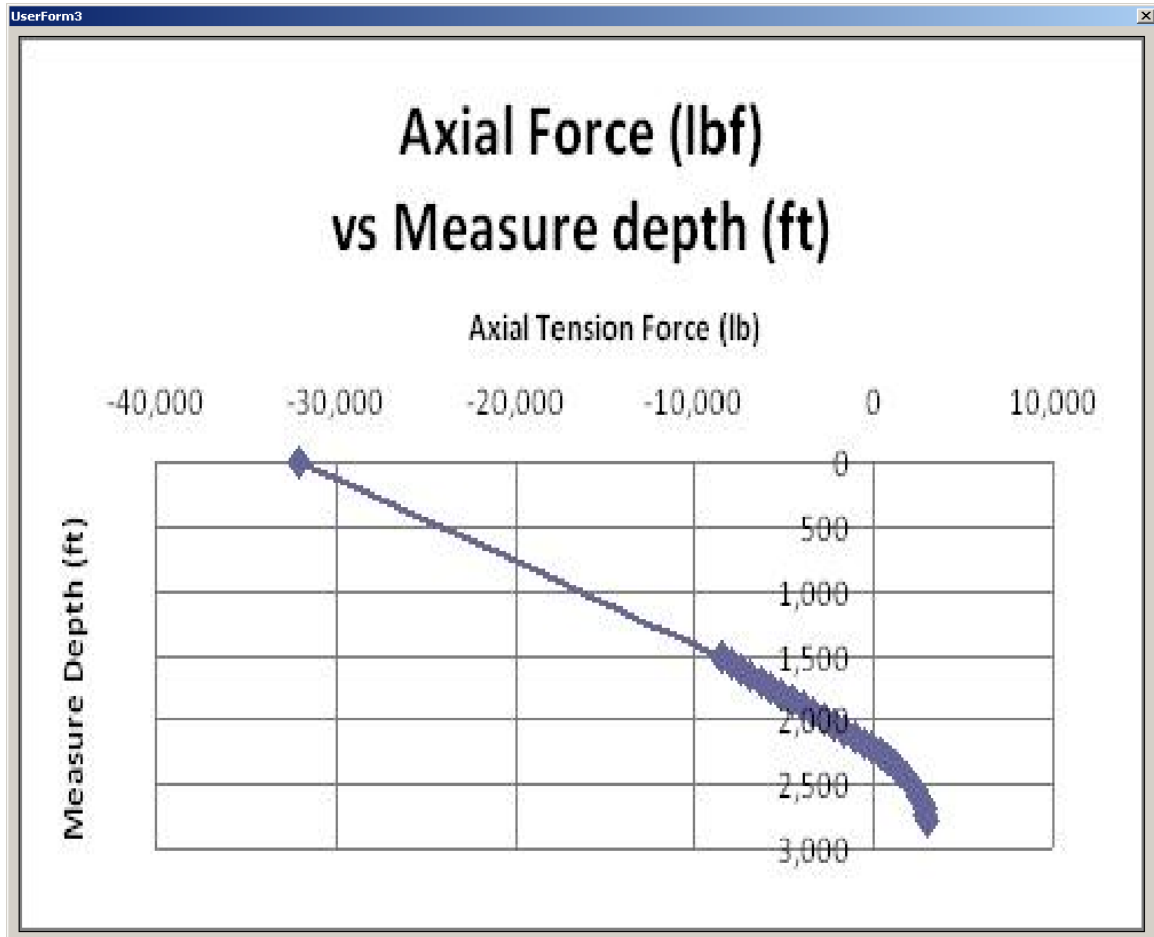


Fig. E.5–Axial force (lb) versus measured depth (ft) ( $F < 0$  referred to tensile force) from 3D wellbore trajectory.

From all the above mentioned, it showed that it will have the different result between 2D wellbore trajectory and 3D wellbore trajectory with 10 Deg/100 ft left/right turn in build section approximately

$$\left( \frac{34,170 - 32,014}{32,014} \right) = 6.73 \% \text{ (based on these well planning and drilling parameters)}$$

It proves that it has a significant different between 2D wellbore trajectory and 3D wellbore trajectory regarding T&D issues.

**APPENDIX F**

**RECOMMENDATIONS**

### **General drilling Recommendations**

Significant progress has been made in the understanding and improvement of tool face control with PDC drill bits. Specifically, the recent papers on reducing torque fluctuations with PDC bits have had a significant impact on utilization of these bits on steerable motor systems. Also field data and early lab tests showed that short aggressive gauge bits yield poorer quality boreholes in terms of instantaneous or local dogleg severity and caliper measurements, than longer full diameter gauge bits. This has been adopted in some areas by some investigators and resisted by others. However, there is a current trend to look at hole quality more critically and to recognize that there are bit designs and system parameters that affect the results.

These oscillation can significantly affect: 1) torque and drag while drilling, limiting the reach of many wells and causing significant tool failures, 2) log quality, particularly showing up in high resolution image logs causing to bottom, the caliper log may not show a problem but the net drift diameter of the hole over a long section can be less than casing diameter. To avoid tortuosity effect we should use rotary steerable system to prevent this effect.

### **Rotary Steerable Tools**

Rotary steerable tools were introduced to the oil and gas industry in the early 1990's. Two basic types emerged; "push-the-bit" and "point-the-bit". Pushing the bit refers to exerting the lateral side force on the bit as it drills ahead. Pointing the bit involves bending the assembly so that the bit is pointed toward the intended direction while

drilling. Point-the-bit is generally acknowledged as being superior; resulting in smoother wellbores with increased dogleg capability (Maidla, Haci, Cluchey, Alexander, and Warren 2005).

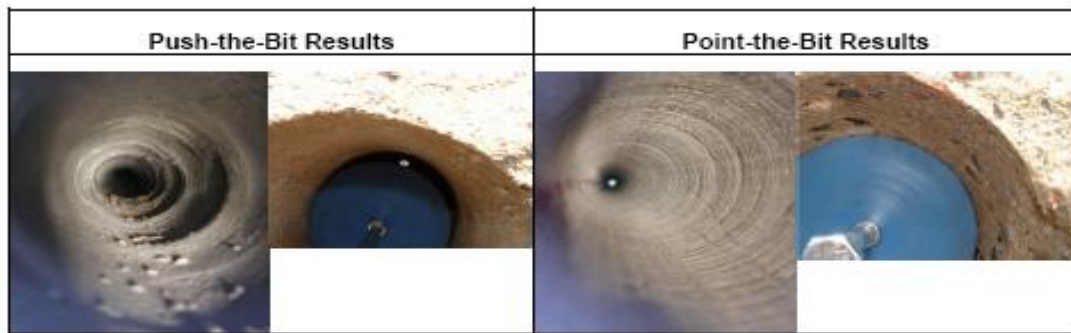


Fig. F.1—Comparison between push-the-bit results and point-the-bit-results (Logging While Drilling 2008).

Tool development was driven by the engineering opportunity and economic advantages that could be obtained by steering the wellbore while continuously rotating the drillstring. Operator demand was driven by the need to drill increasingly difficult well profiles, some of which would not be possible using conventional steering systems. These are some of the advantages to using rotary steerable drilling:

- Eliminates the time spent aligning toolface; the rotary steerable tool controls it automatically.
- 50% increased rate of penetration while using the rotary drilling over the use of sliding with a motor.
- Improves hole cleaning, resulting in more consistent ECD's than when obtained by using the sliding and rotating with a motor.

- Drag, which can cause shocks, vibration, and stick-slip, is reduced compared to sliding. This results in a more consistent weight-on-bit and reduces stress on drilling equipment.
- There is less chance of the drillstring becoming stuck if it's moving most of the time.
- Deviation rates are more consistent as there is no change in mode between steering and not steering to produce the required rate.
- PDC bits with more aggressive cutter angles can be used and optimized for ROP performance, rather than a balance between ROP performance and ability to control toolface while using a motor.
- Wellbore profiles are generally smoother, with no transition ledges resulting from changes between rotating and sliding modes.
- Increases and improves quality of LWD data due to continuous rotation. Slide sections would have to be reamed back over to obtain the same results.
- Reduces chance of wet trips and resulting in slower tripping speeds which are associated with mud motor draining.

## Bottom Hole Assembly (BHA) Configuration

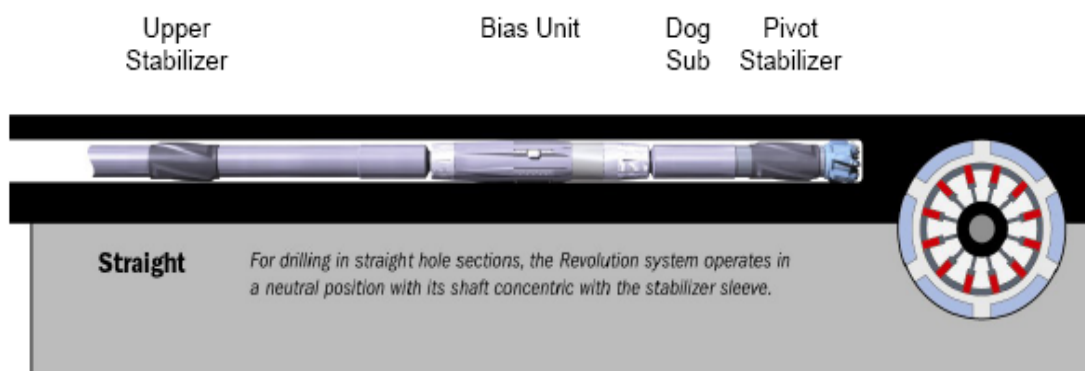


Fig. F.2—The standard BHA configuration (Logging While Drilling 2008).

The upper stabilizer, bias unit sleeve, pivot stabilizer and dog sub are all true gauge or very close to it. Experience and testing have shown that this is the optimum configuration for maximizing directional performance with the tool. The tool is capable of generating doglegs of up to 12 degrees/100 ft or more with this setup. At 90 degrees inclination, tests have also shown that with zero deflection the tool tends to hold an angle or build slightly. Obviously, this is formation dependent and therefore varies to some degree from well to well.

To build an angle at 6 degrees/100 ft with the tool with little or no turn, a 0 deg toolface and 50–60% deflection should be initially selected (a general guide). Monitor the resulting surveys, then adjust the setting accordingly to obtain the required dogleg and counteract any turn. Be aware that the formation changes can have a significant impact on tool response. The assembly achieves the build by deflecting the bias unit sleeve upwards and internal shaft downwards, which in turn pushes the collar above the pivot



stabilizer downwards. The pivot stabilizer pivots and points the dog sub and bit upwards to build an angle.



Fig. F.3—Illustrates deflection in the bottom hole assembly (Logging While Drilling 2008).

To drill in any other direction, change the toolface. To generate different doglegs, change the deflection. The tool does take some time to react in changing the settings, normally only a few minutes (Gaynor et al. 2001).

### **Techniques for Solving T&D Problems**

This section has pointed out to the readers of what is the advantage for using torque and drag 3D calculation for the new technology, especially multilateral wellbore with the tables shown a list of generic torque and drag reduction techniques. The first table (**Table F.1**), listing of generic torque and drag reduction technique, and the second table (**Table F.2**) will be advantages/disadvantages of torque and drag reduction techniques.

**Table F.1–Listing of generic T&D reduction techniques (Aston et al. 1998)**

Application	Deployment		Method	Typical Performance (friction reduction)
	Cased Hole	Open Hole		
Drilling				
DDPs: Rotating	YES		Reduces coefficient of friction	0-15% (Based on surface torque)
DPPs: Non Rotating (NR)	YES		Reduces Torque Radius	0-30% (Based on surface torque)
SUBS: Bearing / Roller Tools	YES	YES	Single or combined effect of Bearing, NR Sleeve or Roller Assembly	0-40% (Based on surface torque)
SUBS: Hole Cleaning	YES	YES	Helix Section stirs up cuttings to assist hole cleaning	0-25% (Based on surface torque)
Specialized Drillpipe	YES	YES	Bladed Pipe assists hole cleaning and dynamics	Field Data not available/analyzed
Lubricants(Including "Cocktail")	YES	YES	Reduces Coefficient of friction	0-50% (Based on surface torque)
Specialized DP + Bearing Sub + Lubricants	YES	YES	Combined (See above)	60% (Miller-based on the surface torque)
DPPs (NR) + Lubricants	YES	YES	Combined (See above)	27% (Niakuk - based on surface torque)
<b>CASING AND COMPLETION RUNNING</b>				
Centralizers: solid NR	YES		Reduces Torque Radius and Improves Standoff	0-30% (Based on rotary Friction Factor)
Centralizers: Roller Tools	YES		As above plus Roller Assembly	0-40% (Based on Torque and Drag per joint)
Lubricants (Single)	YES	YES	Reduces Coefficient of Friction	0-15% (Based on axial and rotary Friction Factor)
<b>COILED TUBING ACCESS</b>				
CT Straightener			Reduce drag from residual bend	0-10% (Based on axial Friction Factor)
Lubricants (Single)	YES	YES	Reduces Coefficient of friction	0-15% (Based on axial Friction Factor)
Lubricants + CT Straightener	YES	YES	Combined (See above)	35% (Wytch Farm - Based on axial friction factor)

**Table F.2–Advantages and disadvantages of T&D reduction techniques (Aston et al. 1998)**

Techniques	Advantage	Disadvantage
Rotating Drillpipe Protectors	<p>Casing wear reduced.                      Reduce pipe fatigue by creating a gradual bend around sharp doglegs.                      Relatively cheap to use.</p> <p>Easy to handle / install.                      Helps reduce differential sticking due to increased stand-off and reduced sidewall contact.</p>	<p>If overstressed, possibility of falling off, getting stuck in the BOP</p> <p>ram cavities and plugging surface equipment                      Need to be routinely and correctly inspected                      Average lifespan is comparatively low.                      Not recommended for open hole, thus limiting extended bit runs.                      Can increase annular pressure loss, reducing hole cleaning                      Efficiency.</p>
Non-Rotating Drillpipe Protectors	<p>Higher torque reductions and longer wear life than rotating DPPs.                      Possible higher penetration rates due to improved torque transmission to the bit.                      Reduced casing wear problems.                      Reduced fatigue effects around doglegs                      Relatively easy to handle and install.                      Can help with differential sticking problems.</p>	<p>Can cause drillpipe wear, especially with abrasive muds.                      Possible slippage or loss of clamping collars in hole.                      Can cause increases in ECD                      Cannot be run in open hole.                      Regular inspection required.</p>
Subs – Bearing based or Roller Tools	<p>Higher torque reduction than NRDPPs.                      Can be used in open and cased hole.                      Can help with differential sticking problems and casing wear.                      Can withstand higher contact loads than NRDPPs.</p>	<p>Some handling issues due to size and weight and increased string length (derrick height).                      Can be expensive on a unit basis compared to other mechanical Tools.                      Requires the correct connections</p>

**Table F.2–Continued**

Techniques	Techniques	Techniques
		Failure of tool could result in costly fishing or sidetrack operation. Fatigue or stress histories not logged. Can increase pressure loss in annulus
Specialized  Drillpipe (DP)	Improved hole cleaning leading to faster trips, faster casing  Smoother drilling, reduction in torque variation. Reduces casing wear, less wall contact. Easy to handle on surface. Designed for open hole. Helps reduce differential sticking. Requires minimum maintenance	Rental can be high. Failure can lead to expensive milling, fishing or sidetrack Operations
Centralizers,  Solid Non-Rotating	Simple design, can be used in open and cased hole Increases stand off reducing the risk of differential sticking. Some designs can improve the quality of the cement job by Creating turbulence. Some Alloys wear resistant so stand off is maintained longer in ERD wells	More expensive than other types of centralizers. Many bed into soft, unconsolidated formations or uting beds.  Limited effectiveness in washed out sections.
Centralizer, Roller  Tools	Can be used in open and cased hole Reduced casing running drags particularly in cased hole section Shaped roller pods designed to generate swirl	Roller damage can occur under high impact loads.  Otherwise as for Centralizers Solid, Non-Rotating

**Table F.2–Continued**

Techniques	Techniques	Techniques
Coiled Tubing Straightener	<p>Reduced drag can extend operating window for CT operations.</p> <p>Easier to make up a completion string under the injector head.</p> <p>Simple, low maintenance, easy to use device</p>	<p>Increased consumption of CT string due to fatigue.</p> <p>Increase rig height.</p>
Lubricants	<p>Can reduce Torque and Drag in both cased and open hole for a wide range of operations.</p> <p>Lower risk in terms of implications of failure than some Mechanical devices.</p> <p>Combinations of lubricants or “cocktails” can produce high levels of torque reduction.</p>	<p>Need to be screened for chemical, temperature, environmental compatibility and formation damage.</p> <p>Can be expensive.</p> <p>Issues of particle recovery with some solid lubricants.</p>

**VITA**

**RUKTAI ACE PRURAPARK**  
6501 S. Fiddler's Green Circle, STE 480  
Greenwood Village, CO 80111

**EDUCATION:** B.Eng., Chemical Engineering  
Chulalongkorn University  
Thailand, B.E., 2004

M.Eng., Petroleum Engineering  
Texas A&M University, 2005

Ph.D., Petroleum Engineering  
Texas A&M University, 2009